Aalto-yliopisto
Aalto-universitetet
Aalto University

Master's Programme in Chemical and Metallurgical Engineering

Simulation-Based Model Optimization for a Center Launder Retrofit

Flotation performance evaluation using HSC Sim software

Aino Saikkonen

Master's thesis
2025

Aalto-yliopisto
Aalto-universitetet
Aalto University

Author Aino Saikkonen

Title of thesis Simulation-Based Model Optimization for a Center Launder Retrofit

Programme Master's Programme in Chemical and Metallurgical Engineering

Major Sustainable Metallurgical Engineering

Thesis supervisor Prof. Rodrigo Serna Guerrero

Thesis advisor BSc Honours Michelle Ball

Collaborative partner Metso Oyj

Date 30.10.2025 **Number of pages** 111+3 **Language** English

Abstract

Effective froth management is crucial to ensure high recovery of metals and operational profitability. In recent decades the size of the operational flotation cells has increased significantly, with cell volumes exceeding 600 m^3. This significant increase in flotation cell volumes has increased the flotation surface parameters, which have been seen to negatively affect sufficient froth management by destabilizing the froth layer and decreasing the probability of particles to be collected. These challenges led to the need for different launder and crowder arrangements to improve froth collection and movement towards the launder lip.

One of the leading flotation launder configurations, the center launder, has enabled significant improvements in the recovery of valuable metals by enhancing froth management in many operations worldwide. This thesis aims to model how consistently the simulation can reproduce results, and how accurately the observed recovery improvements after the center launder upgrade can be simulated using HSC software. Additionally, a center launder upgrade has been observed to positively impact electricity and water consumption as well as CO_2 emissions. To further quantify these impacts and assess the overall environmental benefits, HSC was applied to carry out a Life Cycle Assessment (LCA), alongside metallurgical performance modelling.

The methodology for the research work was created to replicate real-world process conditions as closely as possible, using previous case studies as a reference. The simulation results indicate a clear correlation between the changes in simulated and measured recoveries as the feed characteristics vary. Moreover, the estimated overall recovery improvements after the center launder installation follow a similar trend to the calculated improvements, although with certain limitations.

Overall, drawing final conclusions about the reliability of the results is difficult, as it would require further testing of the methodology in practice. However, this thesis provides a very good foundation for the future development of the model, helping to understand its limitations and approach to modelling.

Keywords minerals processing, flotation, froth management, center launder, HSC Sim, LCA

Aalto-yliopisto
Aalto-universitetet
Aalto University

Tekijä Aino Saikkonen

Työn nimi Simulointipohjainen mallin optimointi center launder -retrofitille

Koulutusohjelma Kemian ja Metallurgian DI-ohjelma

Pääaine Kestävä Metallurgia

Vastuuopettaja/valvoja Prof. Rodrigo Serna Guerrero

Työn ohjaaja BSc Honours Michelle Ball

Yhteistyötaho Metso Oyj

Päivämäärä 30.10.2025 **Sivumäärä** 111+3 **Kieli** Englanti

Tiivistelmä

Tehokas vaahdonhallinta on ratkaisevan tärkeää metallien korkean talteenoton ja prosessin kannattavuuden varmistamiseksi. Viime vuosikymmeninä vaahdotuskennojen koko on kasvanut merkittävästi, ja niiden tilavuudet ylittävät nykyään jopa 600 m³. Tämä on johtanut vaahdotuskennojen pinta-alaparametrien kasvuun, minkä on havaittu vaikeuttavan vaahdonhallintaa heikentämällä vaahtokerroksen vakautta ja pienentämällä partikkelien talteenoton todennäköisyyttä. Näiden haasteiden seurauksena on kehitetty erilaisia vaahdonhallinnan ratkaisuja, joiden avulla vaahtoa voidaan kerätä ja ohjata tehokkaammin.

Yksi johtavista vaahdonhallinan ratkaisuista, center launder, on mahdollistanut merkittäviä arvometallien talteenoton parannuksia monissa prosesseissa ympäri maailman. Tämän työn tavoitteena on arvioida kuinka johdonmukaisesti simulointi pystyy toistamaan havaittuja parannuksia, sekä analysoida sitä, kuinka tarkasti center launderin asennuksen jälkeen havaitut talteenoton parannukset voidaan mallintaa HSC-ohjelmistolla. Lisäksi, center launderin on havaittu vaikuttavan positiivisesti niin sähkön- ja vedenkulutukseen kuin CO_2-päästöihinkin. Näin ollen, metallurgisen suorituskyvyn arvioimisen lisäksi, HSC-ohjelmistoa käytettiin elinkaarianalyysin suorittamiseen ympäristöhyötyjen tarkemmaksi arvioimiseksi.

Metodologia tutkimukselle luotiin jäljittelemään todellisia prosessiolosuhteita mahdollisimman tarkasti aiempia tutkimuksia hyödyntäen. Toteutettujen simulointien perusteella tulokset osoittavat selkeää korrelaatiota simuloitujen talteenottoprosenttien ja mitattujen tulosten välillä syötteen ominaisuuksien vaihdellessa. Lisäksi arvioidut kokonaisparannukset talteenotossa asennuksen jälkeen noudattavat samankaltaista trendiä kuin lasketut parannukset, joskin tietyin rajoittein.

Kaiken kaikkiaan lopullisten johtopäätösten tekeminen tulosten luotettavuudesta on kuitenkin haastavaa, sillä käytetty metodologia vaatisi vielä lisää käytännön testausta. Tämä diplomityö tarjoaa kuitenkin erittäin hyvän perustan mallin jatkokehitykselle, auttaen ymmärtämään sen rajoituksia ja mallinnuslähestymistapaa.

Avainsanat mineraalien prosessointi, vaahdotus, vaahdon hallinta, center launder, HSC Sim, LCA

Table of contents

Preface and acknowledgements

This master's thesis was conducted in collaboration with Metso. I am very grateful for the opportunity to carry out this thesis project and to gain valuable insights from the field that I can apply in my future career.

I would especially like to thank my thesis advisor, Michelle Ball, for her insightful guidance, constructive feedback, and continuous support throughout the process. Finally, I would like to thank my friends and family for their encouragement during this journey.

Otaniemi, 30. October 2025
Aino Saikkonen

Symbols and abbreviations

Symbols

A	Empirically measured constant for flow regime
A_{Ff}	Ratio of the froth area to the pulp cross sectional area
A_{pulp}	Pulp cross-sectional area
b	Time correction factor
c	Concentration of floating particles
c	Assay in concentrate
C_{PB}	Plateau border drag coefficient
D_{32}	Sauter mean diameter of the bubble
D_{axial}	Axial dispersion coefficient
D_b	Diameter of bubble
d_{bo}	Diameter of overflowing bubble
D_p/ d_p	Diameter of particle
f	Assay in feed
f_0	Fraction of material detaching the coalescence
f_{crit}	Critical froth loading factor
f_{in}	Interface froth loading factor
g	Gravitational acceleration
$g_b(x)$	Air flux through the froth surface due to the bubble breakage
$g_f(x)$	Froth flux across the pulp interface
H_f / h	Froth height
J_b	Bubble bursting flux
J_g	Superficial gas velocity
Jl	Volumetric liquid flux
k	Flotation rate constant
k_{max}	Maximum flotation rate constant
n	Empirically measured constant for flow regime
P	Overall collision probability
P_a	Probability of particle attachment
P_c	Collision probability
P_d	Probability of particle detachment
Pe	Peclet number
R	Recovery
R_c	Collection recovery
R_f	Froth recovery
R_G	Total recovery
R_w	Water recovery
R_∞	Infinite recovery
r_{bo}	Radius of overflowing bubble
r_{in}	Inner bubble size radius
r_{out}	Outer bubble size radius
R	Recovery

RI	Ultimate recovery
S_b	Bubble surface area flux
τ	Residence time
t	Time
t	Assay in tailings
T	Throughput
U	Uptime
v_{set}	Settling velocity
Q_W	Liquid flowrate entering the cell
w	Weir height
ϕ	Solids volume fraction
μ	Liquid viscosity
ρ_l	Liquid density
ρ_s	Solid density
k_λ	Lambda prefactor
α	Air recovery / froth stability parameter

Abbreviations

CL	Center launder
CL	Froth crowding level
EF	Emission factor
EI	Energy intensity
Ent	Entrainment factor
FC	Flotation cell
FCR	Froth carry rate
FRT	Froth residence time
FSA	Froth surface area
FTD	Froth transport distance
GLO	Global
IL	Internal launder
IL+R	Internal + radial launder
LCA	Life Cycle Assessment
LCI	Life Cycle Inventory
LCIA	Life Cycle Impact Assessment
LL	Lip length
P50	50% passing size
P80	80% passing size
pH	Hydrogen ion concentration
RC	Rougher concentrate
RoW	Rest of the world
RSD	Relative standard deviation
SG	Specific gravity
T	Throughput
TSA	Area at the bottom of the cell
U	Uptime

1 Introduction

The demand for metals has significantly increased, and the demand of them is expected to continue increasing throughout the 21st century, with the growth rate of copper being one of the highest (Watari et al., 2021). At the same time, ore head grades are constantly decreasing (Northey et al., 2014), making it necessary to focus on improving production performance to meet global needs. Balancing the need to produce more minerals for use in areas such as transportation, clean energy, and infrastructure, while at the same time supporting decarbonization and aligning with global climate change targets, will require greater attention in the future (Morita et al., 2025). This situation highlights the importance for metallurgical process development to meet global needs in a sustainable way, taking into account the carrying capacity and limited resources of the Earth.

Minerals processing circuit is a large entity, consisting of many different parts seamlessly integrated together. To ensure high performance production, all parts of the process need to be optimized and taken into account. Flotation is one of the key components of minerals processing circuit, being the most high-volume separation process (Quintanilla et al., 2020). Therefore, even small increases or decreases in recovery rates can significantly affect the overall profitability of the operation, making the proper optimization of the flotation process especially important.

During the last decades, due to the increased production needs and aim for simplified operations, the size of the operative mechanical flotation cells has been in exponential increase, nowadays reaching the cell volumes up to 630 m^3 (Lopez-Pacheco, A., 2021). Increased cell volumes did not come up only as a beneficial way to meet the production needs, but also facing challenges related to management of increased froth surface areas (Liu et al., 2022). To ensure the effective froth zone optimization, development of different crowder and launder design showed their importance.

The initial solutions to manage increasing froth surface areas were provided by Coleman (2009), and Brito-Prada and Cilliers (2012), after which finding the optimal launder design to meet the flotation needs has been continuously under development. After many new launder designs, center launder was developed in the beginning of 2020s, with the current amount of center launder installations over 150 all around the world. This efficient center launder design enhances both metallurgical and operational performance by improving concentrate flow and process controllability.

Froth flotation challenges and the effects of different launder designs have been researched for many years. This thesis focuses specifically on froth management challenges, excluding other flotation-related issues such as mixing effectiveness or reagent usage. The simulation part aims to optimize the performance of the rougher flotation circuit through a center launder

upgrade, investigating how accurately improvements in the recovery rates of valuable metals can be estimated.

The research work in this thesis was conducted using HSC Sim 10 software due to its ability to model flotation operations with different launder designs and to visualize the differences between them. By utilizing real process data, this thesis aims to simulate actual operating conditions and compare the simulated results with measured improvements during the upgrade assessment periods. To assess the reliability of the simulation results, the conducted simulations also include an evaluation of critical parameters from the simulation perspective, which may impact the gained results.

The data used in this research originates from real industrial operations and was measured during center launder upgrade assessments at the Bagdad, Constancia, and Kennecott sites. Consequently, these case studies provide valuable and representative insights that are directly comparable to real industrial conditions. Whereas further research will be required to optimize the software and validate the final results, the findings of this thesis provide a solid foundation for understanding how HSC Sim can be applied to estimate performance improvements after a center launder retrofit, while also outlining the required operational information and potential challenges in obtaining reliable results.

To gain a broader understanding of the impact of the center launder upgrade on the entire minerals processing circuit and its potential contribution to decarbonization, the research presented in this thesis includes a sustainability assessment using Life Cycle Assessment (LCA). In addition, potential CO_2 emission reductions resulting from the retrofit were calculated to complement the analysis and enable comparison of the outcomes. The conducted LCA evaluates the effects on water usage, overall energy consumption, and the global warming potential associated with reduced CO_2 emissions.

2 Literature review

The literature review of this thesis provides a comprehensive overview of froth flotation within the broader context of the minerals processing circuit, outlining its future trends and highlighting key aspects related to performance optimization. The structure of the review is divided into three chapters, progressing from an overview of the minerals processing circuit to a more detailed examination of froth flotation and froth management in mechanical flotation cells. Aim of this review section is therefore to clarify the relationship between effective froth management and the overall performance of the entire minerals processing operation.

2.1 The future of minerals processing field

Metals are a crucial part of building modern society, including technology, buildings, and infrastructure. The significant increase in the number of publications in recent years highlights the importance and focus on the sustainable use of Earth's raw materials, particularly in response to the growing demand for major metals such as nickel, lead, copper, zinc, aluminium, iron, and steel (Northey et al., 2014; Elshkaki et al., 2018; Watari et al., 2021). Various studies indicate that the demand for these metals will significantly increase throughout the 21st century, with the highest growth projected for aluminium at 215% by 2100, and copper and nickel at 140% (Watari et al., 2021). To meet the long-term demand for metals, the industry needs to support metal circularity and sustainable production of them.

Based on earlier research on historical copper ore grades by Mudd and Weng (2012) and Mudd et al. (2013), the future copper ore grade is estimated to decrease below 0.2% by the end of the 21st century (Northey et al., 2014). As the need for metals continues to rise and ore grades gradually decrease, the mining industry faces the challenge of increasing production capacity (Magdalena et al., 2023). This increasing production capacity negatively impacts the environment by increasing energy consumption and ore deposition (Aramendia et al., 2023; Harmsen et al., 2013).

On the other hand, as the demand for metals rapidly increases, solutions to optimize current process performance to recover more valuable minerals in the same operating time, increase production uptime, and reduce the loss of valuable minerals to tailings are required (Memary et al., 2012). To address this issue, many companies have developed new and more efficient upgrade solutions to sustain more efficient production and increase the recovery rate of valuable minerals, while minimising the overall plant footprint. These solutions include various automation software to better optimize production, and mechanical upgrades to enhance the recovery of valuable minerals.

2.1.1 Structure and function of a minerals processing circuit

Minerals processing circuit is a large entity, consisting of comminution, classification, concentration, and dewatering stages, and its general configuration is presented in **Figure 1** below. Comminution includes blasting, crushing and grinding, where the aim is to reduce the particle size for the desired range based on the optimum liberation size for the ore (Herbst et al., 2003). After comminution particles goes through the classification, where the particles in desired size range continues the flow through the concentration stage, and larger particles are recirculated back to the milling phase (Mular, 2003). These first stages of the minerals processing circuit are especially crucial to ensure effective production, due to the significant impact of the particle size on the subsequent processing stage, concentration.

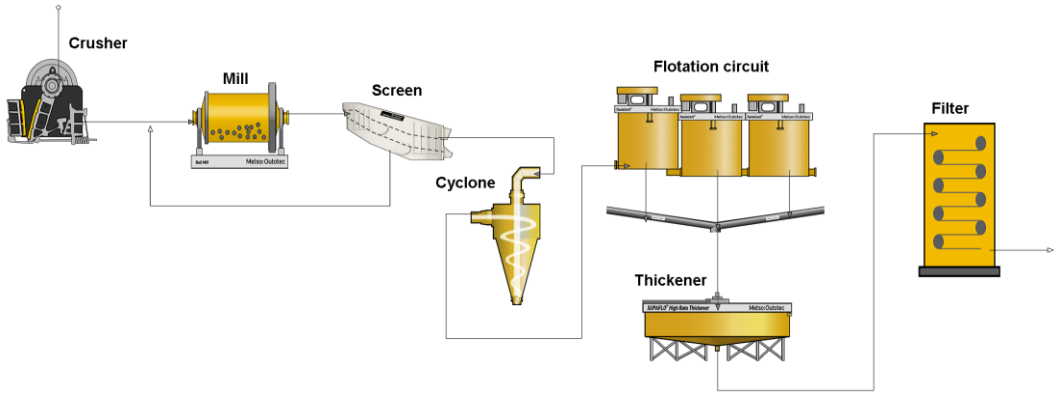

Figure 1. Minerals processing circuit

The concentration process is one of the key components of the whole minerals processing circuit, aiming to recover as much valuable mineral as possible from the ground ore. A typical concentration phase includes the steps of conditioning and flotation. In a conditioning step, the ground ore is mixed with water and reagents before being transferred to the next liberation step called flotation, while the purpose of the flotation circuit is to separate the particles with valuable minerals from the non-valuable gangue material. Therefore, the optimization of the correct particle size (Markovic et al., 2008), as well as the reagents used have a significant impact on the circuit performance, directly affecting the recovery of valuable metals. (Wills & Finch, 2016)

When moving from flotation to the dewatering stage the slurry stream has been separated to the concentrate stream, including as much valuables as possible, and to the tailings stream, where the amount of valuable minerals is aimed to be minimal. The typical dewatering stage includes thickeners and filters, which are used to decrease the water content of the concentrate, to ensure more effective recovery of valuable metals in next processing circuits (Dahlström, 2003), or of the tailings that will be sent to tailings dams.

2.1.2 Sustainable optimization of minerals processing circuits

Currently, the mining industry is responsible for approximately 1.7% of global greenhouse gas emissions, with projections indicating a potential increase to as much as 8% over the next 35 years (Aramendia et al., 2023). Given the significant increase in production needs, the transition toward decarbonization and the development of innovations to reduce environmental impact are becoming increasingly critical and have been under development for many years (Morita et al., 2025).

To adapt to the changing process conditions, like declining ore grades, the use of metallurgical balances is crucial in terms of optimizing the mineral processing circuits, and by controlling the operations to effectively measure the performance (Richardson & Morrison, 2003). The impact of declining ore grades can also be seen to negatively affect decarbonization by increasing the use of explosives and diesel at mine sites, producing more waste in the form of tailings, and increasing the consumption of energy and freshwater in minerals processing circuits (Memary et al., 2012).

These challenges were also highlighted in research and simulations using HSC software, which studied the energy increase effects in both comminution and flotation stages. As decreasing ore grades require higher throughputs to meet metal demand, the need for increased milling capacity and additional flotation cells raises the initial energy demand of the process. Additionally, the need to transport more ore will further increase both energy consumption and produced CO_2 emissions. (Magdalena et al., 2023)

To meet the demands of sustainable production among increasing metal production, technological improvements are essential (Northey et al., 2014). Aim of these technological innovations is to increase the process performance and therefore the profitability of the process (Yianatos & Vallejos, 2024). Through effective process optimization enabled by digitalization, the performance of existing mineral processing operations can be significantly improved by reducing energy consumption, enhancing product quality, and optimizing material flows to better adapt the processing circuit. Furthermore, digital tools facilitate real-time monitoring and data-driven decision-making, allowing greater flexibility and environmental responsibility across the entire production system. (Pavloudakis et al., 2024)

2.2 Froth flotation

As described in the previous section, flotation circuit is a key component in terms of minerals processing circuit. The flotation technique has been used in industrial operations for over hundred years and seen as the most important innovation in the whole mining industry. The main advantages of using flotation in mining operations is the cost-effectiveness of the process to separate valuable minerals from gangue material based on the

hydrodynamics of the particles (Wills & Finch, 2016; Prakash et al., 2018). However, in addition to the hydrophobicity of the particles, the technique is highly dependent on the added reagents and chemicals, aiming to create efficient froth layer on top of the cell (Jera and Bhondayi, 2021). (Kortelainen, J., 2019)

Depending on the used flotation technique, direct or reverse flotation, the process is based on the collection of hydrophobic minerals attached to the upcoming air bubbles, (Gorain, 2007). The difference in these two processes is that direct flotation aims to attach the valuable minerals with the air bubbles, whereas the reverse flotation aims to attach the gangue particles to improve the concentrate grade. (Wang et al., 2014)

Flotation performance can be described in terms of the achieved metal recovery, which is calculated from the amount of valuable metal in the feed, concentrate, and tailings. The higher the recovery, the more metal is separated into the concentrate and, correspondingly, less valuable metal is lost to the tailings. This concept is expressed in Equation 1, where R represents metal recovery as a percentage, F and C denote the mass flow of feed and concentrate, respectively, while f and c represent the metal grade in the feed and concentrate, respectively.

$$R = \frac{C \cdot c}{F \cdot f} \cdot 100\% \qquad 1$$

Three main variables in flotation process can be described as follows: surface chemistry, type of the flotation machine, and the operating conditions of the cell (Gorain, 2007). All these three variables influence flotation kinetics, while the impact of operational conditions is affected by factors like variations in ore grade, particle size, and feed flow rate (Çilek, 2004). The kinetic model for flotation was first introduced by Zuniga (1935) in Chile based on Equation 2. Since then, the adjustment for kinetic model calculations have been made to better describe flotation performance.

$$\frac{dC}{dt} = -CK, \qquad 2$$

where K describes the flotation rate constant and C(t) the concentration of floating particles remaining in the flotation cell up to the flotation time t (Bu et al., 2016). The kinetics of the flotation circuit can be determined based on many different equations, but the most widely used is the first order kinetic model, which is described in Equation 3 below.

$$R = RI(1 - e^{-k(t+b)}), \qquad 3$$

where R describes the recovery at time t (min), RI is the ultimate recovery, k is the rate constant, and b is the time correction factor (Çilek, 2004).

To ensure effective flotation performance, it is crucial to ensure optimal use of flotation reagents, like collectors, frothers, activators, extenders, depressants, deactivators, flocculants, and dispersants. The role of collectors is to make valuable particles hydrophobic and therefore enhance the attachment of them with the upcoming air bubbles. As well as collectors, frothers are also surfactants, aiming to reduce bubble rise velocity, and enhance the formation of froth and preservation of small bubbles. The reduced bubble size increases the total volume of the bubbles, and the reduced velocity of bubble rise increases the residence time, therefore improving the flotation kinetics. (Wills & Finch, 2016)

As previously mentioned, all aspects of froth flotation influence flotation kinetics and, consequently, the overall performance of the flotation process. The primary factors include particle and bubble concentrations, bubble–particle collision rates, and the stability and efficiency of particle attachment (Wills & Finch, 2016). Achieving effective flotation performance requires a thorough understanding of particle transport and residence time. This knowledge is essential for the optimal selection of flotation reagents and operational parameters, and it can be assessed through batch testing using laboratory-scale flotation cells.

This section introduces the design of mechanical flotation cells and flotation circuits. It addresses challenges associated with flotation operations, such as the increasing size of flotation cells, and examines their impact on overall process performance. Additionally, it explores strategies for managing these challenges effectively.

2.2.1 Design of mechanical flotation cells

The industry utilizes various types of flotation cells, including mechanical, pneumatic, and column cells, as well as froth separators. Among these, mechanical flotation cells are the most widely used in the minerals processing field. Mechanical flotation cells were originally discovered in 1901 by Alcide Froment, introducing oil into the process to facilitate the attachment of bubbles to particles. Following this initial discovery, several variations of the original design were developed, and around 1915, the first subaerated flotation machine was introduced in the industry. (Gorain, 2007)

Mechanical flotation cells consist of several components that are optimized to maximize cell performance. The main components are the vessel and the mixing mechanism, ensuring proper mixing of the solid-liquid suspension. Effective mixing promotes the dispersion of air bubbles, creating an environment conducive to the attachment of bubbles to hydrophobic particles. The specific design of the mixing mechanism therefore depends on the type of cell and typically includes an impeller and a diffuser, each having their

own distinct function. The impeller suspends the solids and disperses air into fine bubbles, enhancing microturbulence and promoting efficient bubble-particle collisions. The diffuser, also called the stator, surrounds the impeller with multiple blades and reduces vortex formation, thereby maintaining stability within the cell. (Gorain et al., 2000)

Whereas the main responsibility of the flotation cell mechanism is to ensure effective bubble-particle collision, the optimization of air entry also plays a crucial role in the design of an optimal cell structure. Based on the dependency between bubble surface area flux and the first-order rate constant, the optimal air supply of the cell can be designed. (Gorain et al., 2000)

There are two different models, based on which the optimal introduction of air can be designed: the forced air entry mode and the self-induced air entry mode. In the forced air mode, air is supplied using a blower, and the impeller is positioned near the bottom of the cell, with air being introduced through the shaft. In contrast, in the self-induced mode, the air enters the cell by vortexing, and the impeller is located closer to the midpoint of the cell, drawing the air through the space between the standpipe and the shaft. (Gorain et al., 2000)

Three hydrodynamic zones of mechanical flotation cell are: turbulent zone, quiescent zone, and froth zone, as described in **Figure 2** below. Each of these three zones having their own role in ensuring the effectiveness of flotation performance.

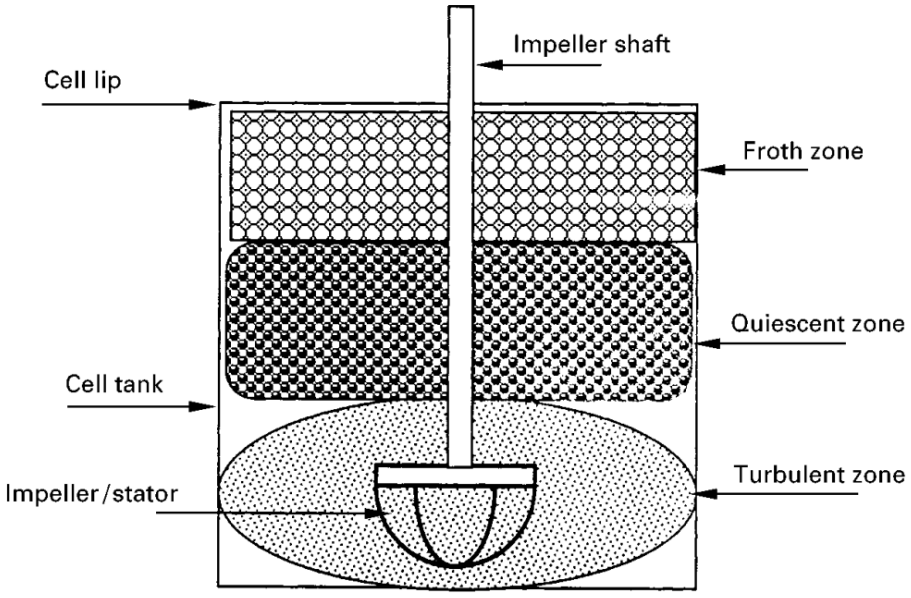

Figure 2. Three hydrodynamic zone of mechanical flotation cell, adapted from Gorain et al. (2000)

The turbulent zone of a mechanical flotation cell, close to the impeller, is responsible for efficient bubble-particle interaction, ensuring the effective collection of particles on the surface of the bubbles. In the middle of the flotation

cell is the hydrodynamic zone called the quiescent zone, which aims to reduce the number of gangue particles attached to the bubble surface. The froth zone, located at the top of the flotation cell, aims therefore to further enhance the restraint of gangue material and thereby improve the concentrate grade. (Gorain et al., 2000)

The selected type of the mechanical flotation cells depends on many factors, like needed capacity and type of the processed ore. The model of the cells can be either rectangular, truncated rectangular, or U-shaped, whereas the design of impeller can vary based on the used cell type (Fuerstenau & Somasundaran, 2003). Difference in cell design, including the impeller speed, the volume flow rate of introduced air, and the plant operational conditions, affect air dispersion within the cell, thereby influencing bubble size, gas holdup, and superficial gas velocity. (Gorain, 2007). As all of these factors affect the hydrodynamic zones of the flotation cell, to ensure optimal recovery, the cells must be designed by considering the hydrodynamic conditions of the cell.

To design and optimize the selection of correct flotation cells, it is important to take into account the concept of bubble surface area flux, describing the gas dispersion properties (Gorain, 2007). The bubble surface area flux (S_b) can be described by using the Equation 4 (Wills & Finch, 2016).

$$S_b = \frac{6\,J_g}{D_{32}}, \qquad 4$$

where J_g describes the superficial gas velocity and D_{32} means the Sauter mean diameter of the bubble, on the other hand meaning volume-to-surface mean bubble diameter.

2.2.2 Design principles and process of flotation circuits

As previously discussed, the flotation circuit is a well-defined entity and customized for the needs of each specific site. However, the typical design of flotation circuits across different sites generally consists of several flotation cells arranged as flotation banks (Gorain et al., 2000), including at least the stages of rougher, scavenger, and cleaner flotation, as well as the regrinding stage. Rougher, scavenger, and cleaner flotation banks are connected in series to maximize the circuit performance, with each flotation bank having its own role in the process. This typical design is shown in **Figure 3** below.

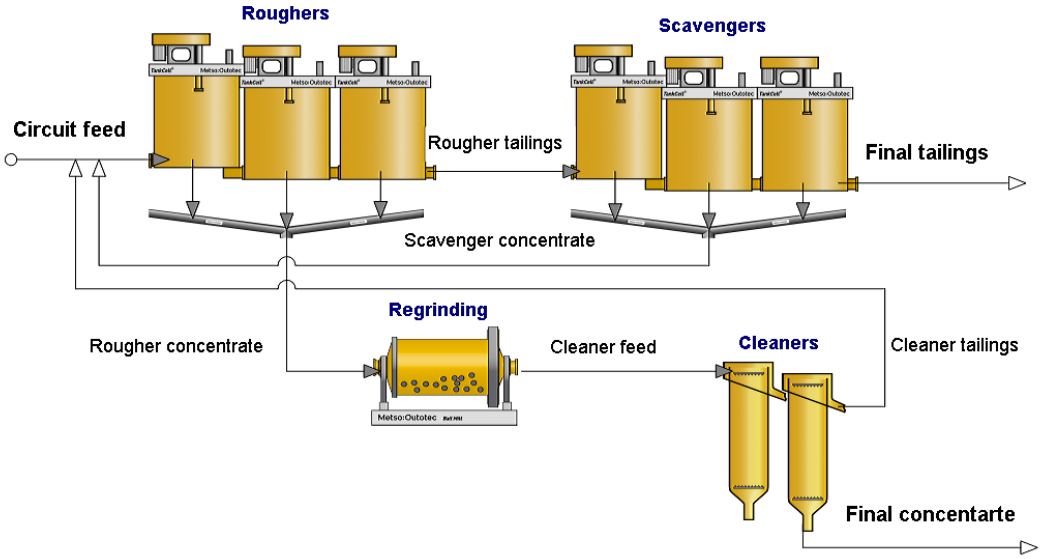

Figure 3. Typical flotation circuit design

The first stage of the flotation circuit is the rougher flotation circuit. This is where the new feed is introduced to the circuit along with recycled slurry from the scavenger concentrate and cleaner tailings (Fuerstenau & Somasundaran, 2003). The recycling of the cleaner tailings stream, as well as the scavenger concentrate aims to recover as much valuable minerals as possible (Loveday and Brouckaert, 1995). The rougher flotation circuit has also proved to have the highest effect on the gained amount of recovery from the whole concentration circuit (Radmehr et al., 2018).

After that, the collected rougher flotation concentrate is fed into the cleaner stage, either directly or through the regrinding stage (Fuerstenau & Somasundaran, 2003). The cleaner stage typically consists of several flotation columns, compared to the rougher circuit which usually consists of mechanical flotation cells. In the cleaner stage, the aim is to maximize the grade of the concentrate, as the cleaner flotation concentrate forms the final concentrate of the circuit. On the other hand, as the cleaner tailings stream may still contain a significant amount of valuables, it is recirculated into the circuit to minimize the loss of valuable minerals. (Bergh & Yianatos, 2011).

Flotation circuit designs always vary between different sites, as all operations are dealing with different ore types and head grades, as well as different environmental conditions. Therefore, the decision of circuit design is influenced by many factors and tailored specifically for each operation. When making the decisions about the type, number, and size of the used flotation cells, there are two important factors to consider. These two factors are the required residence time and the amount of concentrate being able to recover within a given froth surface area, which are influenced by the flotation

kinetics, characteristics of ore type, grade and particle size, as well as the used reagent concentration (Coleman, 2009). (Loveday and Brouckaert, 1995)

The design phase of the flotation circuit starts with conducting the batch testing based on the mineral composition of the ore. The batch tests show the needed residence time to achieve the desired recovery, measured based on the flotation kinetics. With the defined residence time and the volumetric flow rate of the slurry through the processing stage, the needed flotation bank volume can be defined (Loveday and Brouckaert, 1995). To ensure effective production, the type and amount of used reagents during the flotation process also need to be very well defined, as the correct pH and use of reagents directly affect surface properties (Fuerstenau, & Somasundaran, 2003).

In addition to that, it is also important to pay attention to environmental and economic aspects during the design phase. These considerations include how the handling of waste is organized, how much fresh water the circuit uses, and how the water is recycled, as well as how to minimize the negative impact on the environment. From an economic point of view, it is important to consider how profitable the operation is and how it can be improved to maximize the recovery of valuable minerals, thereby increasing the profitability of the entire operation.

Overall, the design of the flotation circuit affects highly on the gained recovery and needs therefore to be well defined and designed. Based on the previous research, it has been shown that for example the number of stages in the concentration circuit influences the overall recovery of the circuit. (Radmehr et al., 2018). To ensure high overall recovery of the flotation concentrator, it is especially important to focus on the size fractions of the feed, as particle size will affect the required amount of reagent and the necessary residence time. Therefore, to enhance the overall recovery of the circuit, effective classification and adaptation of the regrinding circuit are beneficial, since recovering valuable minerals becomes more difficult when the slurry contains a wide range of particle size fractions (Pease et al., 2006).

2.2.3 Current challenges in froth flotation

Designing and efficient optimization of the froth flotation circuits has become increasingly challenging, due to the high demand of low-grade ore bodies (Yianatos & Vallejos, 2024; Gorain, 2013). The declining ore grades, coupled with economic, safety, and environmental challenges, necessitate the development of new technologies and chemicals to ensure effective production in the future. However, developing new reagents and chemical compounds is a lengthy and costly process, with extended development and implementation periods, posing significant challenges for optimizing and selecting flotation reagents. (Nagaraj & Farinato, 2016)

The decreased ore grades have also affected the liberation of valuable minerals, as the ore is required to be ground to smaller particle sizes, which

increase the presence of fine and ultrafine particles. On the other hand, as the environmental aspects require more focus on sustainability challenges (Nagaraj & Farinato, 2016), the energy savings on the mills have led to the coarser grind sizes, also decreasing the potential of recovery of valuable minerals by affecting the attachment of particles and bubbles. The collision probability of particles can be described based on the Equation 5 below. (Bilal et al., 2022)

$$P_c = A\left(\frac{D_p}{D_b}\right)^n, \qquad 5$$

where D_p represents the diameter of the particle, D_b represents the diameter of the bubble, and A and n are empirically measured constants for flow regime. Based on this equation, the relation of particle and bubble dimensions affects collision probability and therefore overall collision probability (P) presented in Equation 6 (Bilal et al., 2022).

$$P = P_c * P_a * (1 - P_d), \qquad 6$$

where P_a and P_d represents probability of particle attachment and detachment, respectively. The lower collision probability of fine particles occurs due to the lower momentum of them, making them more prone to follow fluid streamlines rather than collide with the upcoming air bubbles. Coarse particles are therefore more prone to increase the turbulency of the flow, due to their small specific surface area, decreasing the collision strength between the particles and bubbles. (Bilal et al., 2022)

At the same time, the need to process higher throughputs to meet the global needs and adapt to the declining ore grades has resulted in an increase of the size of the operational flotation cells (Liu et al. 2022; Lopez-Pacheco 2021), with current cell volumes reaching up to 600 m^3(Vallejos et al., 2023). However, this significant increase in cell size has introduced several challenges for both operational efficiency and metallurgical performance, mainly due to the larger surface area (Mesa & Brito-Parada, 2019). The trend of increasing cell sizes over the past years is illustrated in **Figure 4** below (Wills & Finch, 2016; Dreyer, 1976; Lynch et al.,2007; Hassanzadeh et al., 2022).

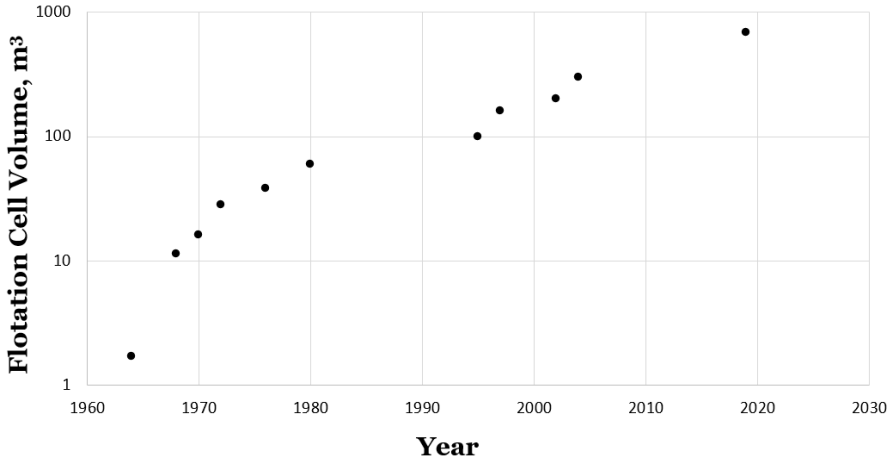

Figure 4. Flotation cell size evolution

As can be seen in the **Figure 4**, the size of the flotation cells has increased ten times over the past four decades (Mesa & Brito-Parada, 2019). This increase in flotation cell sizes has posed challenges related to efficient froth management due to the increased froth surface parameters (Brito-Parada et al., 2020; Vallejos et al., 2020). Previous research has shown that both longer transport distance and larger froth surface area negatively affect froth stability, and therefore hinder the collection of itby crowding (Corona-Arroyo et al., 2021). The ratio between froth crowding and cell surface parameters can be described by Equation 7 below.

$$CL = 100\left(\frac{TSA-FSA}{TSA}\right), \qquad 7$$

where FSA represents the froth surface area at the top of the cell, and TSA represents the area at the bottom of the cell. Based on this equation, a larger froth surface area affects directly by decreasing the level of froth crowding, and the collection potential of valuable minerals.

The lack of froth crowding impacted by the larger froth surface areas leads to challenges in avoiding stagnant froth zones on top of the cell, which therefore decreases the froth stability (Brito-Prada et al., 2020). The lack of froth stability can result in bubble bursting, causing a loss of valuable minerals to the tailings (Farrokhpay, 2011), whereas ensuring effective production with larger cell sizes requires understanding on how the increased cell volume and surface parameters influence flotation scale-up factors. This was first studied by Mesa and Brito-Prada in 2019, after which the challenges were further discussed by for example Yianatos and Vallejos in 2024. These studies highlight that accurately predicting scale-up factors becomes more difficult, because conventional models do not account for froth transport characteristics and the effects of cell size.

2.2.4 Optimization of flotation circuit performance

To ensure high operational profitability, it is important to maximize the flotation performance, as the amount of collected minerals as a concentrate directly effect on the gained profit. The process begins with efficient suspension of mineral particles and air in the turbulent zone, after which the responsibility for high flotation recovery moves to the performance of the froth zone.

Optimizing flotation is a complex process influenced by numerous variables (Quintanilla et al., 2020). These include feed composition, air and wash water flow rates, reagent dosages, pH, conductivity, ore mineralogy and distribution, particle size distribution, as well as slurry levels. Operational parameters like airflow rate, freshwater usage, and froth bed thickness are also carefully controlled to maintain optimal conditions at each stage of the flotation circuit (Bergh & Yianatos, 2011).

Among all these factors, mineral surface chemistry has the most crucial role in ensuring the optimal conditions for bubble-particle attachment, after which the development of the attachment probabilities can be developed by optimizing the operational parameters of the cell (Gorain, 2007). To understand the mineralogical composition of the processed ore, as well as the particle size distribution of the feed, is especially important when optimizing the use of correct flotation reagents and flotation rate (Nagaraj & Farinato, 2016; Yianatos et al., 2012).

From an operational parameter perspective, the height of the froth bed has been shown to affect the concentrate grade. Based on the conducted research by Wang et al. in 2014, the increase in froth bed thickness decreases the rate of particle entrainment, as the higher froth layer will increase the froth retention time and therefore providing more time for the entrained gangue particles to drop back. Generally, this phenomenon can be linked to the decrease in gangue particle recovery, as the higher froth bed decrease the entrainment of water, and therefore the amount of unwanted gangue particles to the final concentrate (Yianatos et al., 2008).

One important part of the flotation operational optimization is the correct optimization of the froth surface area of the cell, as the stable froth zone is crucial in a sense to prevent particle drop-back and ensure the effective froth flow to the launder (Corona-Arroyo et al., 2021). The optimization of the froth surface area can be enhanced, for example, by installing the physical froth flow modifiers to optimize the froth geometry by decreasing the surface area and froth transport distance, as well as to improve the froth movement towards the launder (Jera and Bhondayi, 2021).

In addition to physical froth flow modifiers, the type and concentration of the frother used, as well as the quality of process water strongly affects on the froth surface performance (Heath and Runge, 2019). The concentration of dissolved cations can influence the stabilization of the froth phase, whereas the amount of water fed to the cell effects on the mobility of the froth.

Therefore, the use of either potable or plant water will depend on the site conditions and process requirements.

To better control the flotation operation performance, the implementation of advanced control systems into the existing operations can be used to minimize the costs, predict the operational effectiveness and develop the performance (Quintanilla et al., 2020). These control systems can be used to control several variables including froth depth, level of the pulp, grade of the concentrate, as well as the flow rates, number of solids, and mass pull of minerals.

2.3 Froth management

Optimizing the froth zone in flotation cells is particularly important, as it directly affects the recovery of valuable minerals. Effective froth zone management enhances froth transportation and eliminates stagnant froth zones, thereby improving the overall metallurgical performance of the cell (Brito-Parada et al., 2020).

The research work of this thesis focuses on froth management in large-scale operational flotation cells, whereas the topic has been examined in greater detail. This section of the literature review introduces froth phase modelling and discusses the significance of froth zone performance, presenting strategies to improve froth management.

2.3.1 Froth phase modelling

Modelling of the froth transfer process can be described with four sub-processes presented below (Mathe et al., 1998):

1. True flotation: Selective transfer of target material to the froth based on the bubble-particle attachment
2. Entrainment: Non-selective transfer of material to the froth based on the bubble-particle attachment
3. Drop back: Selective and non-selective process, where rather gangue, or valuable minerals will drop back to the slurry phase
4. Froth transfer: The movement of material from froth to the concentrate based on the mechanical and hydraulic forces

One of the froth modelling models is a Laplace equation (Equation 8), which can describe the froth flow, froth residence time and bubble velocity distribution, as well as the streamlines of bubble (Jera and Bhondayi, 2021). Based on this model, it has been recognized that bubbles upcoming close to the concentrate weir are having a way shorter residence time compared to the froth regions back to the cell. This has been seen to effect on the gained concentrate

grade and the recovery, whereas the longer residence time decrease the recovery, and shorter residence time therefore decrease the concentrate grade.

$$\frac{\partial^2 \emptyset}{\partial x^2} + \frac{\partial^2 \emptyset}{\partial z^2} = 0 \qquad 8$$

Another used model to represent the froth phase is the two-stage tractable model, by dividing the froth area into different zones, having different type of flow regime (Jera and Bhondayi, 2021). Based on the different flow regimes described in two-stage tractable model, the optimization of the froth zone is important in a sense of minimizing the dead zones and improving the froth movement and collection as a concentrate. These three flow regimes are described as below and visualized in the **Figure 5** below, where w and h represent the height of the concentrate weir and the height of the froth phase, respectively, $g_f(x)$ denotes the froth flux across the pulp interface, $g_b(x)$ the air flux through the froth, and α the froth stability parameter.

Three flow regimes:

1. Called dead zone, where all the bubbles reaching the surface area are breaking, and the valuable minerals are falling back to the bottom of the cell.
2. Part of the entering bubbles are breaking up, and the particles are lost, whereas most of the bubbles are collected as a concentrate.
3. All the entering bubbles are collected as a concentrate.

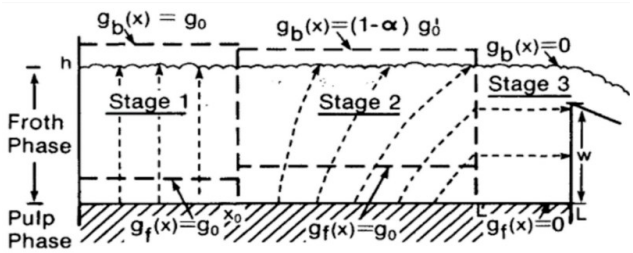

Figure 5. The flotation two-stage tractable model, adapted from Jera and Bhondayi, 2021

2.3.2 Importance of froth zone performance

The performance of the froth layer can be described based on the froth phase sub-processes: bubble coalescence, drainage of the liquid, and reattachment and detachment of the particles and bubbles (Jera and Bhondayi, 2021). These froth phase sub-processes are mainly dependent on froth mobility and froth stability, whereas the froth stability is mainly affected on proper gas distribution, properties of the particles, as well as the chemical conditions. Therefore, the addition of correct flotation chemicals, ensuring the optimized

gas distribution and for example the size and the number of particles are all crucial elements to ensure efficient froth management.

Managing the stable froth layer is especially important, as it contributes to determining both recovery and grade of the concentrate (Jera and Bhondayi, 2021). One of the key factors in the case of stable froth layer is the presence of particles, since flotation performance is highly dependent on both particle size and the amount of them in the flotation feed, by affecting on the mobility and movement of the froth (Heath and Runge, 2019). It has been shown that the stability of froth layer decreases with decreasing number of particles (Tsatouhas et al., 2005), as well as with the lack of fine particles (Grau et al., 2019).

The optimal particle size depends on the processed ore, but based on the several research, the curve of the recovery of particles as a function of particle size remains similar. This curve in **Figure 6** below is commonly considered to resemble the shape of an elephant, showing the decrease in mineral recovery rates with ultrafine and coarse particle sizes (Anzoom et al., 2024).

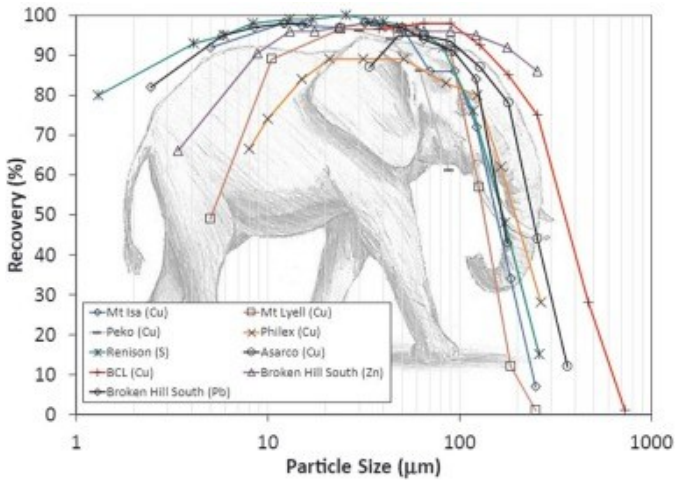

Figure 6. Recovery as a function of particle size, adapted from Lynch et al., 1981

The decrease in the recovery rates of ultrafine and coarse particles represented in **Figure 6** above can be explained based on ineffective attachment properties between bubble particles. Based on the earlier research it has been also obtained, that smaller bubble size tends to increase the viscosity of the froth (Li et al., 2018), whereas the higher viscosity affects negatively on the mobility of the froth (Heath and Runge, 2019). Coarser particle size therefore increases the probability for particle drop-back, due to the detachment of particles and bubbles because of the turbulence (Anzoom et al., 2023).

Differences in froth stability can be observed along a bank of flotation cells, since the fast floating particles are recovered first in the beginning of the flotation row, and therefore the stability of the froth typically decreases in the end of the row (Tsatouhas et al., 2005). To better optimize the

performance of the cell, the froth mobility can be optimized by changing the flow rates of water or superficial gas, as well as the concentration of used reagents (Heath and Runge, 2019). The concentration of frother affects the size of the produced air bubbles, therefore increasing the amount and the bubble surface area (Wills and Finch, 2016).

Additionally, to ensure efficient froth mobility, different physical froth flow modifiers have been developed, including launders, crowders, froth paddles, and froth scrapers (Jera and Bhondayi, 2021). The purpose of these designs is to improve froth flow towards the launder lip and to enhance froth stability by eliminating the stagnant froth zones on top of the cells. Due to the decreased froth stability at the end of the row, the installation of these physical froth modifiers is typically concentrated in that area.

2.3.3 Froth zone performance optimization

This thesis focuses on modelling froth management performance by implementing a circular froth launder design, center launder, on top of the flotation cell. Consequently, the optimization of chemical usage, air distribution, or feed characteristics is beyond the scope of this work. The main emphasis in froth zone optimization is therefore placed on refining froth surface parameters in large operational flotation cells.

Increasing size of the flotation cells increases the need for proper froth zone optimization, as the bigger cell sizes decrease the froth stability and movement towards the launder (Brito-Parada et al., 2020). As it can be seen from the **Figure 7** below, the increased cell volumes effect on both, froth transport distance and froth surface area, by increasing them respectively.

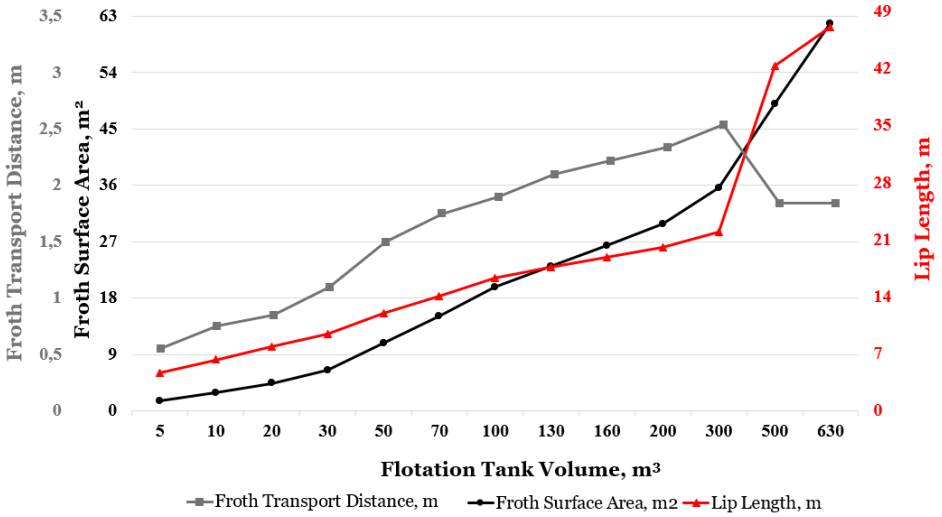

Figure 7. FTD, FSA, and LL as a function of cell volume

After reaching the cell sizes larger than 300 m^3, it was not beneficial anymore to continue processing with current launder installation due to the increased surface parameters. Therefore, the flotation cells larger than 300 m^3 have been already equipped with double internal launders, which can be seen from the **Figure 7** by a clearly increased lip length, and drastically reduced froth transport distance.

When discussing optimal froth zone performance, the significance of high froth recovery, optimized froth carry rate, and efficient lip loading becomes crucial (Jera and Bhondayi, 2021). Froth carry rate (FCR) can be used to measure the performance of the froth zone, as it measures the amount of dry concentrate removed from the unit surface area of the flotation cell within a certain time (Equation 9). Lip loading (LL) therefore measures the amount of dry concentrate recovered per unit length of the launder lip within a certain time (Equation 10).

$$FCR = \frac{Solids\ in\ product\ (tonnes\ per\ hours)}{Froth\ surface\ area\ (m^2)} \qquad 9$$

$$LL = \frac{Solids\ in\ product\ (tonnes\ per\ hours)}{Lip\ length\ (m)} \qquad 10$$

Based on the equations 9 and 10 presented above, by changing the froth surface parameters, froth surface area and lip length, both froth carry rate and lip loading of the flotation cells can be optimized. The general FCR values for mechanical flotation cells based on the cell duties can be defined as presented in **Table 1** (Jera and Bhondayi, 2021).

Table 1. General values for froth carry rates based on cell duty

	Rougher	**Scavenger**	**Cleaner**
FCR (t/m^2h)	0.8-1.5	0.3-0.8	1.0-2.0

These design values for froth carry rate presented in **Table 1** above are used for a whole bank of flotation cells, and the individual values for each cell are differentially defined (Jera and Bhondayi, 2021). Both of these parameters, froth carry rate and lip loading, are needed to be optimized, in a sense of high-performing flotation circuit. Too high or low solids percentage in a froth phase will lead to the unwanted situation, negatively affecting on froth stability and the gained overall recovery (Heath and Runge, 2019). Therefore, specifically defined values of FCR and LL for each individual cell in a flotation bank are important.

There are many different factors, depending on the operational parameters affecting on the selection of optimal froth carry rate. These include the type of floated mineral, particle density and size, and the grade of the processed ore. Additionally, since the flotation feed typically contains both fast

and slow floating particles, metal recovery varies across different cells in a flotation bank, which must be considered when optimizing individual cells. After optimizing the FCR for each individual cells in a flotation bank, lip loading of the cell can be defined and calculated to be at least less than 1.5 t/m/h. (Heath and Runge, 2019)

Typically, the recovery of first cells in a flotation bank recover about 70-80% of the metal, whereas the last cells are responsible for the rest 20-30% of the metal's recovery. To optimize the high flow of fast-floating minerals for the first cells of the flotation bank, the feed can be also splitted for first two cells, therefore increasing the probability of particles to be recovered. Additionally, to improve the performance of the last cells with lower flow, the froth surface parameters of each cells need to be optimized, for example, by using different launder and crowder arrangements to improve forth mobility. (Heath and Runge, 2019)

2.3.4 Journey of different launder arrangements

As previously discussed, the increasing volume of flotation cells leads to a larger cell diameter, whereas the cells may better address challenges related to froth movement and drainage, thereby enhancing froth flow (Jera and Bhondayi, 2021). To overcome the challenges related to proper froth management, new designs were needed to enhance the froth management. The initial launder installation into operational flotation cells were introduced by Hoover (1910). After the significant increase in cell sizes of operational flotation cells, the advanced launder configurations were needed to improve the froth management.

New launder and crowder configurations to improve froth management in large operational flotation cells were first introduced by Coleman (2009), and Brito-Prada and Cilliers (2012), after which the evaluation of their performance in operations continued (Brito-Parada et al., 2020; Corona-Arroyo et al., 2021; Liu et al., 2022, Bermudez et la., 2021, Bermudez et al., 2022).

Launder designs are tailored specifically for each operation, whether greenfield or brownfield, by retrofitting existing flotation cells during plant shutdowns. The configuration of them is optimized to enhance the concentrate flow out of the flotation cell, similarly by minimizing the need of air supply therefore leading to the savings in operational costs (Coleman, 2009). Within a same flotation bank, there might also be different launder configuration depending on the expected mass recovery for each specific cell design (Jera and Bhondayi, 2021).

There are many different launder designs, including transversal, internal, external, radial, hexagonal, and center launders. The configuration of each design differs, and therefore their selection depends on the design and duty of the cell, aiming to maximize the collection surface area (Jera and

Bhondayi, 2021). Visualizations of these different launder designs are presented in **Figure 8** below.

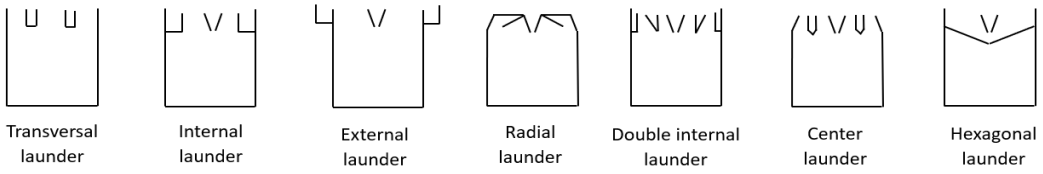

Figure 8. Different launder arrangements

The design of launder arrangements can be divided into internal and external launder designs, where all the designs including transversal, peripheral internal, radial, double internal, and center launder can all be categorized into the internal launder designs. In general, the designs of internal landers have effect on froth residence time (FRT) by reducing the froth transport distance, froth volume, and by improving the froth movement, whereas the effect of external launders on froth recovery and froth carry rates are minimal (Jera and Bhondayi, 2021).

Transverse launder configuration divides the froth surface area into segments with two transverse launders, aiming to reduce the froth transport distance. Internal and external peripheral launder designs are installed either inside or outside the flotation cell wall, whereas the external design provides larger froth surface area, and internal design reduces froth transport distance by similarly enhancing the lip loading. In the applications, where the additional lip length is needed, depending on the cell size, different number of radial launders can be installed on top of the cell in addition to internal or external peripheral launder.

The design of external hexagonal launders therefore allows the maximized froth surface area with an increased lip length, allowing the honeycomb design of the cells in a flotation bank. Double internal launder design divides the froth surface area into two sections therefore decreasing the froth transport distance. Compared to the center launder design, in the double internal launder design, the direction of the froth flow towards the launder is same, whereas the center launder design allows froth flow from both directions towards the center launder, with an enhanced froth crowding from both directions.

The effect of launder design for measured froth carry rate as a function of flotation cell size can be described in **Figure 9** below. Based on that figure, the flotation cell equipped with center launder upgrade provides the highest FCR, whereas the external launder the lowest.

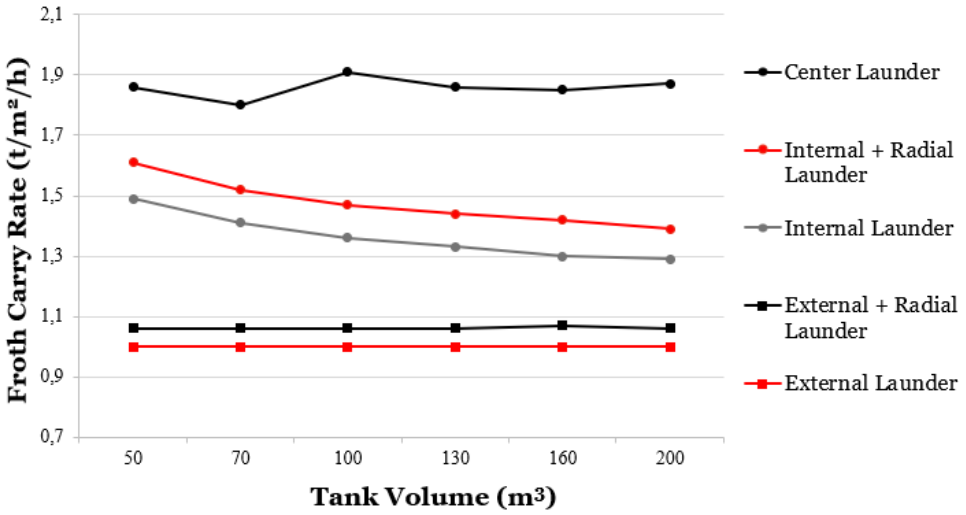

Figure 9. Froth carry rate as a function of cell size and launder design

2.3.5 Center launder: innovative design in large flotation cells

Following the overview of various launder designs, this section focuses on the center launder design. After many other launder designs, the center launder was designed to enhance the froth management of large flotation cells. It consists of three key components: outer crowder, center launder, and froth cone crowder in the middle of the cell. Both, the outer crowder inside the cell wall and the froth cone crowder in the middle of the cell, are directing the froth from both directions towards the concentric center launder. **Figure 10** below illustrates this three-dimensional structure of center launder arrangement.

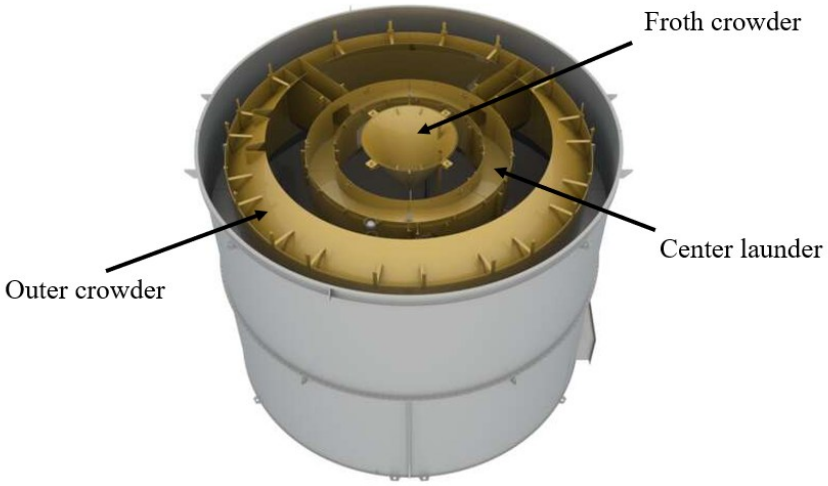

Figure 10. Center launder arrangement

The center launder upgrades have been installed in many operations around the world, showing the significant improvements on process performance by enhancing both, operational and metallurgical performance. This arrangement divides the froth surface area of the cell into two sections, therefore shortening the froth transport distance and decreasing the froth surface area. Decreased FTD together with decreased FSA have been seen to improve the concentrate overflow over the launder lip, therefore improving the recovery of valuable metals (Bermudez et al., 2021).

Because of the decreased froth transport distance, the recovery increases have been measured to be higher with coarser particles, attributed to the higher probability of them to reach the launder lip (Liu et al., 2022). Smaller FSA has also been noticed to eliminate the stagnant froth zones on top of the cell (Seaman et al., 2021), which are leading to decrease the recovery rates (Brito-Parada et al., 2020).

Based on the accomplished center launder installations, the upgrade has resulted in decreased operational airflow rates, as well as increased froth bed thicknesses. The thicker froth layers have been observed to positively impact the controllability of the operation (Bermudez et al., 2022), while overall, increased froth bed thicknesses have seen to improve the grade of the concentrate by increasing the restrain of gangue particles (Heath & Runge, 2019). In addition to the enhanced controllability of the operation, the reduced airflow rates have also led to the saving in blower's energy consumptions (Bermudez et al., 2022).

3 Case study evaluations

Center launder upgrades have been successfully installed in many operations around the world. The evaluation of the upgrade performance has been studied in several cases, providing very consistent results by improving both operational and metallurgical performance of the operation. This thesis evaluates upgrade solutions implemented at the Bagdad, Constancia, and Kennecott operations. The Bagdad and Constancia cases were used to develop and calibrate the simulation methodology, while the Kennecott case was applied as a validation case to assess the reliability of the methodology. This section presents the operational conditions and performance results of all three case studies.

3.1 Bagdad operation

The Bagdad copper and molybdenum concentrator, located in United States, has been in operation since 1942. Since then, the concentration plant has been upgraded several times to increase the production capacity. Nowadays, the concentrator plant is operating with five grinding lines, with a throughput of about 90,000 t/d, and the fed ore consists mainly of chalcopyrite and molybdenite. The rougher circuit of the operation consist of two parallel lines, Line A and Line B, both equipped with six TankCell® e300 flotation cells. The illustration describing the arrangement of these lines is provided in **Figure 11** below.

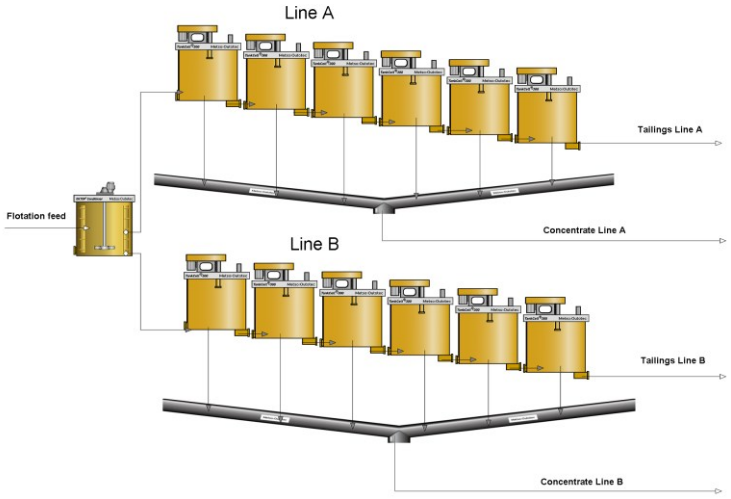

Figure 11. Bagdad rougher flotation circuit

Like described in **Figure 11** above, the feed is split into two streams for both parallel lines from the distribution box. The total mass flow of milled ore and the grade of copper and molybdenum in the feed before the distribution box

have been measured, but there are not any flowmeters installed in feed streams of parallel lines. However, due to the same distribution box for both parallel rougher lines, the distribution difference is considered to be negligible, and therefore the feed is assumed to be equivalent for both lines A and B.

During the retrofit installation conducted in April 2021, the last three 300 m³ flotation cells in Line A were upgraded with center launders, replacing the original internal launder design. Measurements were taken after the installation, allowing evaluation of performance improvements of the upgraded line compared to the baseline.

3.1.1 Bagdad data collection and assessment

The effect on center launder upgrade on rougher line performance was determined based on collected 12-hour shift composite samples. The performance was calculated then based on the chemical assays of the samples taken for feed, tailings, and concentrate streams by using automated on-line sampling devices and by balancing the results using HSC Chemistry® software. The samples were taken from all streams, including feed, concentrate, and tailings, and the gained recovery was calculated based on the equation 11, where c, f and t represent the assays in concentrate, feed, and tailing respectively.

$$R = \frac{c(f-t)}{f(c-t)} \qquad 11$$

The net recovery gain was then determined based on the recovery difference between the parallel lines. To minimize the errors and variations, the operating conditions of the plant were stabilized before sampling, and the ore feed rate was controlled to stay steady. In addition, levels of the pulp and froth, pH, and the density of the rougher feed were strictly controlled to stay within the target range. After stabilizing the operating conditions, the composite sample was collected by taking in total four measurements, during one hour, in 15 minutes intervals to collect the composite sample. After the collection, the composite samples were filtered, dried, and assayed in standard manner.

3.2 Constancia operation

Hudbay's Constancia Mining operation is located in southeastern Andes of Peru. The primary metal of the operation is copper, with molybdenum, gold, and silver being secondary metals. Current throughput of the operation is about 90 000 t/d, operating with two grinding lines, and the mineralogical composition of the ground ore mainly consists of chalcopyrite, molybdenite, pyrite, and bornite, with quartz as a gangue mineral.

The bulk flotation circuit of the operation consists of copper and molybdenum flotation circuit. The rougher flotation circuit of the operation consists of two parallel rougher lines, Line 1 and Line 2, with each rougher line equipped with 7 TankCell® e300 flotation cells, resulting in a total of 14 cells in the rougher circuit. The illustration of bulk flotation circuit operation in Constancia is described in **Figure 12** below.

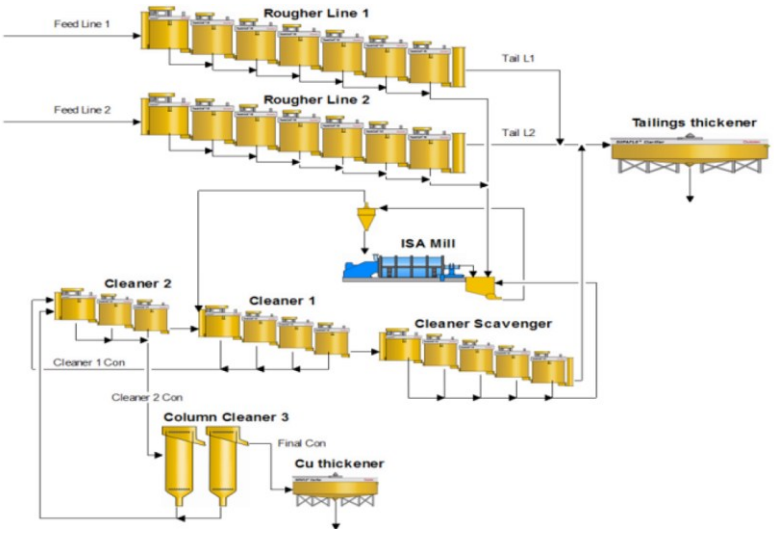

Figure 12. Constancia flotation circuit

Based on the earlier studies conducted, the main challenge in Constancia operation was identified to be the low froth carry rate in the last cells of the operating rougher flotation circuit. To enhance the current operation performance, Constancia decided to upgrade the last three of the 300 m^3 flotation cells with center launders, replacing the existing radial launders. The upgrade was conducted for both parallel lines, with Line 1 being upgraded in June 2019 and Line 2 in November 2019.

3.2.1 Constancia data collection and assessment

The assessment of the results is conducted based on the chemical assays of the 12-hour shift composite samples. The feed and tailings streams analysis samples were collected separately from both operational lines, whereas the concentrate stream was analysed as a combined concentrate sample from both operational lines by using MSA3 /140H metallurgical automated online sampling devices. The shift composite samples were assayed for elements including Cu, Au, Ag, Mo, CuS, Fe, Zn, and Pb.

Collected samples were balanced by using the method of LaGrange multipliers for all streams, including feed, tailing, and concentrate. Based on the balanced results the recovery was calculated based on the Equation 11. Errors and uncertainties were taken into account by excluding the data points that

the mill was not in operation, or the operating time of the rougher line was less than 75 percent during that shift. The excluded data accounts for approximately 4 percent of the total amount of data points collected.

The estimated uncertainty in the taken samples, expressed as the relative error of each metal in the feed, concentrate, and tailings streams, was applied as described in **Table 2** below. Compared to the measurements taken from the feed and tailings, the relative error was set higher for the concentrate stream because the measurement was conducted only for the combined concentrate streams of Line 1 and Line 2, not separately for each line.

Table 2. Relative errors of streams by metal

Stream	Tonnage	Cu	Ag	Au	Mo	Zn	Pb
Feed	0 %	5 %	10 %	8 %	5 %	5 %	5 %
Concentrate	5 %	10 %	20 %	15 %	10 %	10 %	10 %
Tailings	5 %	3 %	6 %	5 %	3 %	3 %	3 %

The net recovery gain of copper and molybdenum were calculated based on the Equation 12 by comparing the measured recoveries of both lines before and after the upgrade.

$$R_{total} = \left(R_{L1,After} - R_{L2,After}\right) - \left(R_{L1,Before} - R_{L2,Before}\right), \quad 12$$

where R_{total} represents the gained net recovery improvement, $R_{L1,Before}$ and $R_{L1,After}$ represent the recoveries of upgraded Line 1, both before and after the upgrade, whereas $R_{L2,Before}$ and $R_{L2,After}$ represent the recoveries of baseline 2 similarly.

In addition to chemical assays, the measurements also included the evaluation of froth bed thickness, and the airflow rates used. However, the focus of these measurements was on the last three cells of the parallel rougher lines to highlight the differences between non-retrofitted cells and the retrofitted cell with a center launder.

3.3 Validation case operation

This results validation case was selected to be the center launder retrofit evaluation conducted in Kennecott Copperton concentrator located in the United States. This case study was selected due to the similar operational conditions compared to Bagdad and Constancia, but also due to the available data measured before the launder retrofit installation. The operation has a throughput of about 150,000 t/d, and the feed consists mainly of chalcopyrite and molybdenite, with quartz occurring as the principal gangue mineral. Kennecott concentrator has two parallel lines, Row 7 and Row 8, both of which

consisting of five TankCell® e300 flotation cells. The design of this flotation circuit has presented in **Figure 13** below.

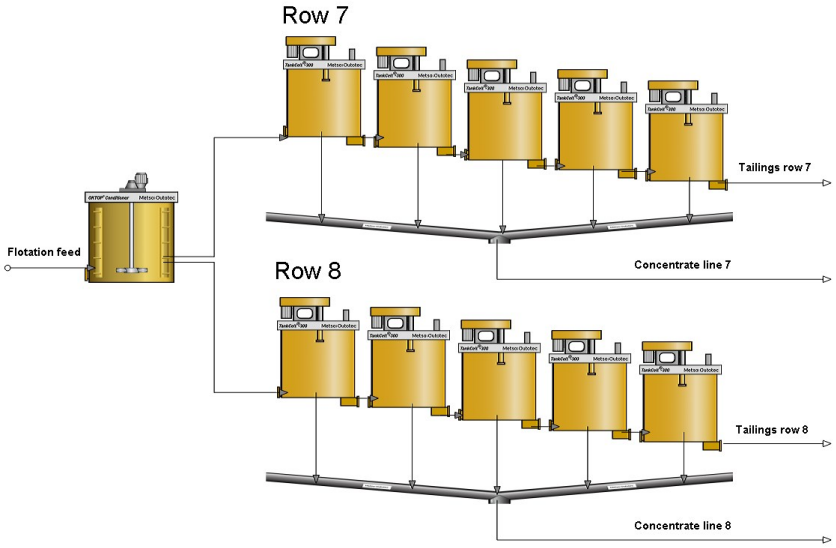

Figure 13. Kennecott flotation circuit

The first two cells from both operational lines work as roughers, and the last three cells as scavengers. Additionally, as described in **Figure 13** above, after the conditioning the flotation feed is split into two lines, while concentrate and tailings streams are collected as combined streams from both lines. Due to the parallel design of lines, the changes in operation can be assumed to affect both lines equally.

During the conducted launder retrofit in October 2020, the internal radial launders of the last three cells from the Row 8 were replaced with center launders. The evaluation between the lines was conducted both before and after the retrofit in order to measure the performance improvements of the upgraded line compared to the base line.

3.3.1 Validation case data collection and assessment

Like in the previous cases presented, the sampling was carried out by taking 12-hour shift composite samples using automatic metallurgical samplers. These samples were taken from both rows and included measurements of copper and molybdenum head grades in feed and tailings, respectively. Each sample was collected individually, and due to the limited data regarding mass flow rates, the recovery of copper and molybdenum was calculated using the two-product formula presented in Equation 13 below.

$$R = \frac{(f-t)}{f} \qquad 13$$

Due to the parallel design of the lines, operational changes were assumed to affect both lines similarly, and the mass flow rates between the sampling points can be considered approximately constant. Furthermore, as the calculated recoveries were considered only to determine the recovery differences between the lines, the relative error can be assumed to affect both parallel lines similarly. Due to these assumptions, the model can be applied to provide a reliable estimate of metal recovery, as individual variations in mass flow are effectively mitigated.

However, because of the inherent noise in the operational parameters during the evaluation period, a direct comparison of metallurgical performance before and after the retrofit was not possible. Therefore, the net recovery gain of these metals was calculated based on the relative difference between the lines before and after the installation, in a similar manner to the Constancia case, using the equation 14 presented below.

$$R_{total} = \left(R_{R8,After} - R_{R7,After}\right) - \left(R_{R8,Before} - R_{R7,Before}\right), \quad 14$$

where R_{total} represents the gained net recovery improvement, $R_{R8,Before}$ and $R_{R8,After}$ represent the recoveries of upgraded Row 8 before and after the upgrade; and $R_{R7,Before}$ and $R_{R7,After}$ represent the recoveries of the baseline Row 7, similarly. Before calculating the total net recovery gains, the collected shift data points were filtered according to certain criteria, including the absence of taken assays, recovery difference greater than ±40% between the lines, or the other tests being conducted simultaneously.

3.4 Measured results from the case studies

Case studies presented in this study, provide highly consistent data regarding the gained improvements after center launder retrofit. These significant improvements not only enhanced the operational effectiveness of the process, but also profitability. Return on investment for upgrade conducted in Constancia was calculated to be only six months, whereas in Bagdad case study only two months (Bermudez et al. 2021; Liu et al. 2022).

3.4.1 Metallurgical improvements

In all cases, the metallurgical improvements were calculated as an improvement of copper and molybdenum recoveries. For Constancia and Kennecott, the net recovery improvements were calculated using Equations 12 and 14, respectively, while for Bagdad they were determined from the difference between the recoveries defined by Equation 11. Because the ore type and operational parameters are similar in all three cases: Constancia, Bagdad, and

Kennecott, the measured recovery improvements are comparable with each other. The obtained improvements are presented in **Table 3** below.

Table 3. Recovery improvements after center launder installations

Net recovery improvement	Constancia	Bagdad	Kennecott
Cu	0.70 %	0.93 %	0.74 %
Mo	1.40 %	3.15 %	0.82 %

Based on these significant recovery improvements presented in **Table 3**, all the results can be seen to follow a similar trend, particularly in terms of copper recovery. In the case of Bagdad, the copper recovery was studied additionally based on the cumulative recovery analysis through whole rougher flotation line, and by analysing the rougher concentrate size by size. Based on the results from cumulative down-the-bank sampling, the final copper recovery was increased by a significant 2.3%. These results are shown in **Figure 14** below.

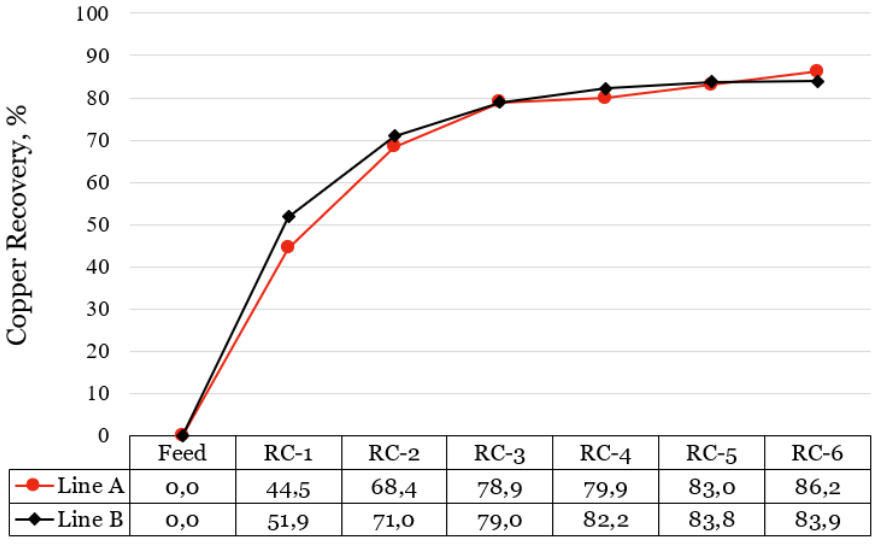

	Feed	RC-1	RC-2	RC-3	RC-4	RC-5	RC-6
Line A	0,0	44,5	68,4	78,9	79,9	83,0	86,2
Line B	0,0	51,9	71,0	79,0	82,2	83,8	83,9

Figure 14. Cumulative copper recovery in Bagdad

The results from size-by-size analysis represent the difference in recoveries between different particle size fractions. Based on the results, the most significant recovery improvements can be achieved with coarse particle fractions (+106 µm and +300 µm), whereas the recovery of fine particles tend to be more stable before and after the center launder installation. This can be explained by the typically higher tendency of coarse particles to drop back to the pulp phase (Anzoom et al., 2023), while the improved froth surface parameters introduced by the center launder upgrade mitigate this effect. These results are represented in the **Figure 15**.

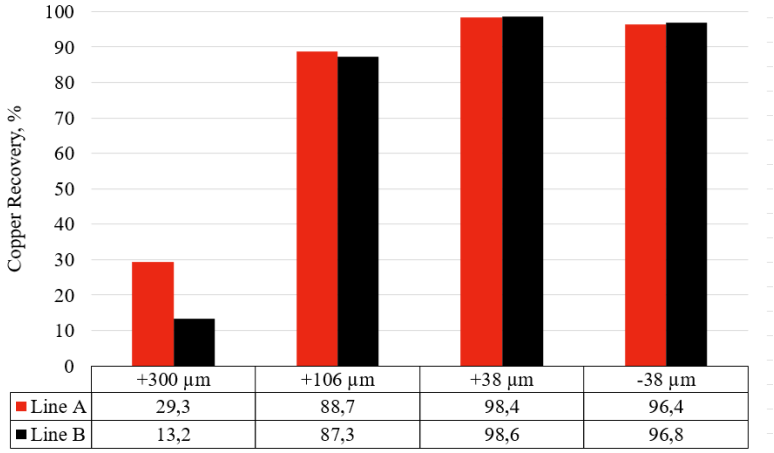

Figure 15. Rougher concentrate size-by-size analysis in Bagdad

3.4.2 Operational improvements

The operational improvements of the upgrade were measured based on the decreased froth surface area and reduced froth transport distance. These results describing the gained improvements after center launder retrofit are provided in **Table 4**, **Table 5**, and **Table 6** below.

Table 4. Operational improvements in Constancia

Constancia	Before	After	Improvement
Reduction in FSA, m^2	33.1	19.2	-42 %
Reduction in FTD, m	2.6	0.8	-69 %

Table 5. Operational improvements in Bagdad

Bagdad	Before	After	Improvement
Reduction in FSA, m^2	37.5	23.4	-38 %
Reduction in FTD, m	3.0	0.9	-72 %

Table 6. Operational improvements in Kennecott

Kennecott	Before	After	Improvement
Reduction in FSA, m^2	37.3	23.3	-38 %
Reduction in FTD, m	2.9	0.9	-71 %

In the cases of Constancia and Kennecott, before the installation of center launders the cells were equipped with radial launders, whereas the cells in Bagdad were equipped only with peripheral internal launders. Despite the different designs, the reductions in froth surface parameters were found to align closely with each other, especially between Kennecott and Bagdad, even though the initial launder designs were different. Based on the results presented above, the froth surface area was decreased by an average of 39%, whereas the froth transport distance was reduced by an average of about of

71%. The significant reduction in froth surface area increases froth crowding, consequently enhancing the probability of valuable particles being recovered as concentrate.

Sample collection and analysis during the upgrade periods at Constancia and Kennecott included measurements of operating airflow rates as well as froth layer thicknesses. Based on the improved results, the required airflow rate was significantly lower after the center launder installation compared to the previous situation. The decreased airflow rate can be seen to have a positive impact on the energy efficiency of the process by reducing the energy consumption of the blower. This trend is presented in **Figure 16** for Constancia and in **Figure 17** for Kennecott, showing the airflow rate in Nm^3/h for the last three flotation cells in the upgraded line, both before and after the retrofit installation. The installation period is indicated in these figures by a black dotted line, with the calculated average values also highlighted using dotted lines.

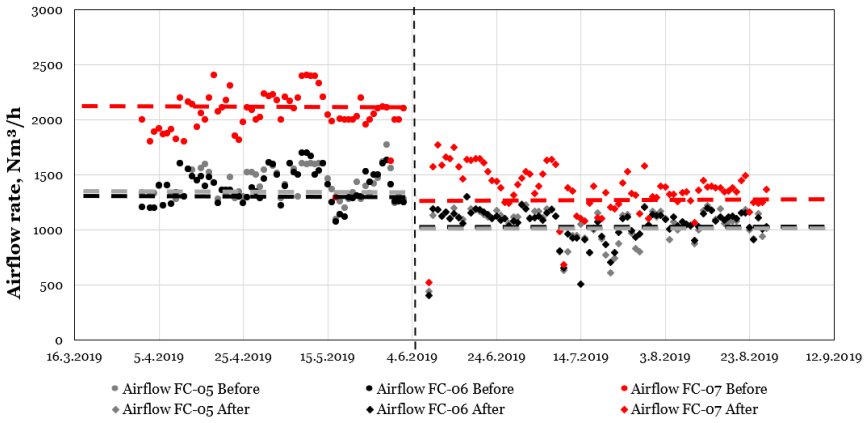

Figure 16. Airflow rate in the last three cells of Line 1 before and after the center launder retrofit in the Constancia operation

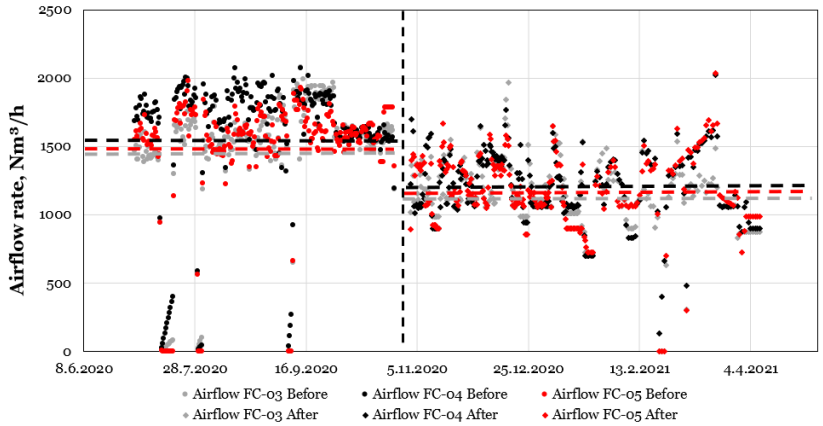

Figure 17. Airflow rate in the last three cells of Row 8 before and after the center launder retrofit in the Kennecott operation

In addition to the decreased airflow rates observed after the center launder installation, the retrofit allows operation with higher froth bed thicknesses due to the reduced froth surface area. Higher froth layer thickness is believed to improve the selectivity of the process by limiting the collection of gangue material, while also enhancing the stability of the current flotation process. This increase in froth levels is presented in **Figure 18** for Constancia and **Figure 19** for Kennecott, respectively.

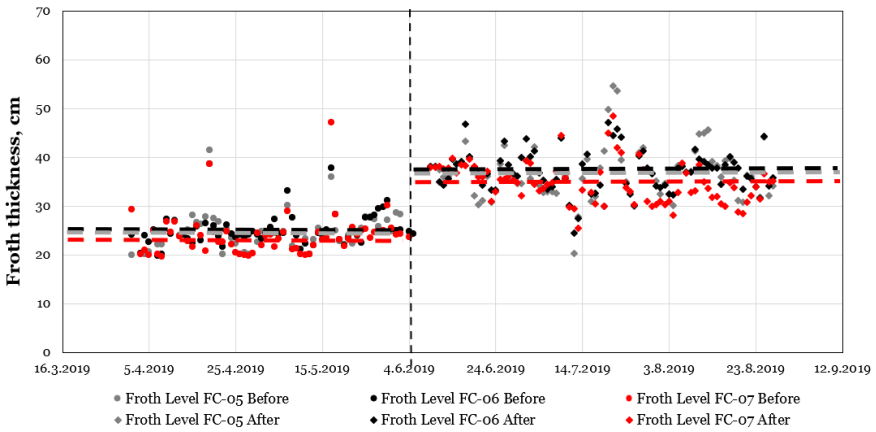

Figure 18. Froth thickness in the last three cells of the Line 1 before and after the center launder retrofit in the Constancia operation

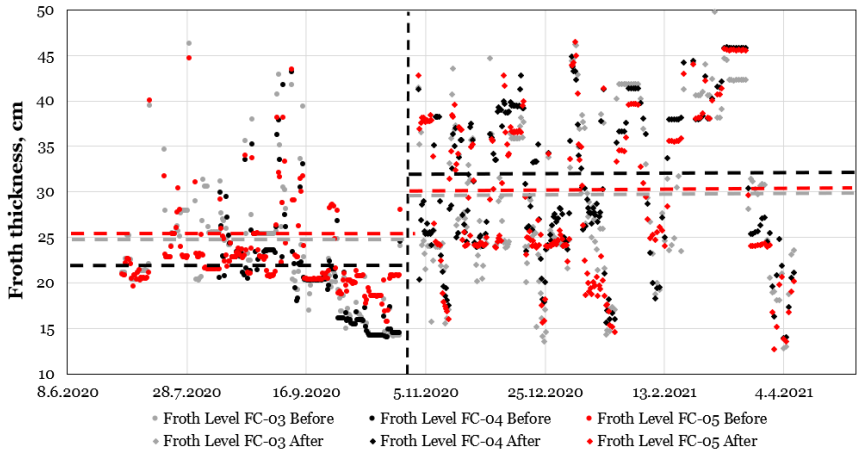

Figure 19. Froth thickness in the last three cells of Row 8 before and after the center launder retrofit in the Kennecott operation

Based on these results, the overall trend of increased froth levels and decreased airflow rates is clear from the calculated averages. However, as shown in the graphs above, there is still considerable variation in the measured airflow rates and froth levels. This variation does not directly correlate with disturbances in process conditions, but may, for example, result from the smaller froth surface area, which makes the froth layer more sensitive to feed fluctuations.

4 Methodology

HSC Sim 10 software can be used to visualize real-world process conditions and assess the impact of changes in process parameters on overall performance. The software incorporates a wide range of variables, including the mineralogy and particle size distribution of the processed ore, flotation cell design parameters, and other operational conditions within the circuit.

In this study, HSC Sim was used to model the process changes following the center launder installations at the Bagdad, Kennecott, and Constancia mines, where the center launder upgrade installation has been conducted during 2019, 2020, and 2021, respectively. The simulations were based on measured data from these sites and aimed to replicate the operating conditions and performance improvements observed after the retrofits. As the Kennecott case was used as a validation case, the simulation methodology was first developed based on information collected from Bagdad and Constancia and then validated using Kennecott as an example.

4.1 Applied simulation methodology

Based on the simulation results, this thesis aims to identify the most reliable methodology for evaluating performance improvements following a center launder retrofit by analysing the key variables and parameters involved. This section presents detailed information about the applied methods and the HSC Sim calculation model used in the evaluation.

4.1.1 Simulation model selection

HSC includes two types of calculation models: static and dynamic simulation models. The static simulation model calculates the equilibrium state under specific process conditions without considering time, whereas the dynamic model visualizes time-dependent process behaviour. Therefore, the static model is well-suited for modelling specific process areas and understanding mass balance relationships, while the dynamic model is more appropriate for broader-scale simulations involving time-dependent changes.

This thesis applies the static simulation model, as the objective is to understand the equilibrium state after the center launder installation in order to evaluate the resulting recovery improvements. The static model also allows for adjusting the number of iteration rounds, which can be optimized to achieve the most reliable outcome. In this simulation work conducted, the used amount of iteration rounds has selected to be 50.

4.1.2 Simulation setup

Because of the simulations were created to duplicate the real process conditions, the simulated flotation circuits were created based on the operational conditions in each site. In the Constancia operation, both rougher lines, Line 1 and Line 2, are fed separately, and the feed characterization for each line is analysed independently. However, the tailings and concentrate streams are first collected separately from each line, after which the concentrates from both lines are combined, and the final concentrate of the circuit is analysed as this combined stream. In this case, the simulation phase was conducted to study both the correlation between measured and simulated recovery changes across the operational lines after the retrofit installation, and the recovery improvement on Line 1 compared to the base scenario.

The Bagdad operation includes two parallel rougher lines, with the flotation feed being split after the conditioner. The fed flotation feed consists of both scavenger tailings and fresh feed, which is diluted with water. The combined tailings and concentrate streams from both lines are analysed separately before the next processing steps. Because of the split flotation feed for Line A and B, the characterization of it has been assumed to be equivalent in both parallel lines at each timepoint, and therefore the estimated recovery improvements can be simulated based on the base scenario (Line B) and the upgraded scenario (Line A). In addition to estimating the overall recovery improvement based on baseline conditions, as in the Constancia case, HSC Sim was also used to evaluate the correlation between measured and simulated recovery differences across the lines, assessing how well HSC captures the variations in flotation feed and their effect on the final recoveries.

The center launder retrofit at the Kennecott concentrator was used as a validation case, applying the same methodology as used for Constancia and Bagdad. Similar to Bagdad, the operational lines in the Rougher-Scavenger circuit at Kennecott are parallel, and changes in feed are assumed to affect both Row 7 and Row 8 in a similar manner. However, due to the available data prior to the launder installation, the overall recovery improvement was simulated based on the collected shift data prior to the retrofit installation. The simulated correlation between the rows after the retrofit was also analyzed to validate the methodology used at Constancia and Bagdad, and to allow comparison with the previous case experiments.

To ensure accurate optimization of the flotation circuit, it is essential to clearly define the flotation kinetics parameters. For all case studies, the kinetics were controlled based on the measured recoveries in base line scenario without center launders. In this simulation setup, the selected kinetic model is a rectangular distribution, described in equations 15 and 16 below.

$$R = \frac{R_\infty}{b} \sum 1 - \frac{1}{1+\kappa_i \tau^2} \qquad 15$$

$$k_1 = \frac{k_{max}}{b}; k_i > 1 = k_{i-1} + k_1; R_\infty < 100 \quad (16)$$

The key parameters of the model are the maximum flotation rate constant (k_{max}) and infinite recovery (R_∞), where infinite recovery describes the theoretical maximum recovery that could be achieved. The k_{max} for both chalcopyrite and molybdenite has been defined based on the simulated baseline scenario prior to the installation of the center launder upgrade, whereas the infinite recoveries have been selected to remain constant. To ensure comparability between the non-upgraded and upgraded cases, the same kinetic parameters were applied in the simulations for both lines at each time point.

4.2 Recovery model selection

As the effectiveness of the center launder upgrade in improving the recovery of valuable metals is based on the decreased froth surface parameters, the selected calculation model in HSC Sim was Neethling model. This model was selected due to its ability to represent froth-phase phenomena, including froth recovery, entrainment, and water recovery, under steady-state conditions. The options for parameter selection in this model are presented in Appendix A.

The Neethling model incorporates detailed mechanistic descriptions of particle and bubble behaviour in the froth, accounting for parameters such as particle settling velocity, air recovery, and bubble size distribution. These parameters are critical in evaluating the impact of froth transport dynamics on overall flotation performance. The following principles and equations form the basis of the simulation calculations.

The behaviour of particles in the froth is characterized by their settling velocity, which is calculated by using the Equation 17:

$$v_{set} = \frac{(1-\phi)^{4,65}}{2} \frac{\frac{g}{3}(\rho_s - \rho_l){d_p}^2}{18\,\mu}, \quad (17)$$

where ϕ is the solids volume fraction, g is gravitational acceleration, ρ_s and ρ_l are the solid and liquid densities, d_p is the particle diameter, and μ is the liquid viscosity.

Air recovery α is therefore either defined as a fixed input or calculated dynamically based on the superficial gas velocity J_g and the bursting flux J_b, which is given by Equations 18 and 19 below.

$$J_b = J_{b0} + aJ_g + b{J_g}^2 \quad (18)$$

$$\alpha = 1 - \frac{J_b}{J_g} \quad (19)$$

The size of the overflowing bubbles d_{bo} is either user-defined or calculated as a function of froth height H_f, using the Equation 20 below.

$$d_{bo} = d_{32} + (d_{bo\,max} - d_{32}) \frac{Hf}{Hf_{max}} \quad (20)$$

Froth recovery R_f is modelled differently depending on the air recovery regime. When α < 0.5, the recovery is calculated as presented in Equation 21, and when α≥0. 5, the recovery is calculated as presented in Equation 22:

$$R_f = \frac{1 - f_{crit}}{1 - f_{in}} \left(\frac{r_{in}}{r_{bo}}\right)^{f_0} \left(\frac{\alpha(1-\alpha)J_g}{v_{set} A_{Ff}}\right)^{\frac{f_0}{2}}, \quad (21)$$

$$R_f = \frac{1 - f_{crit}}{1 - f_{in}} \left(\frac{r_{in}}{r_{bo}}\right)^{f_0} \left(\frac{J_g}{4\, v_{set} A_{Ff}}\right)^{\frac{f_0}{2}}, \quad (22)$$

where A_{Ff} is the froth-to-pulp area ratio, and f_{crit}, f_{in}, and fo are model-specific parameters. Entrainment is modelled using the axial dispersion coefficient D_{axial}, which is calculated as defined in Equation 23:

$$D_{axial} = \frac{{J_g}^{1.5}}{\sqrt{k_1 \left(\sqrt{3} - \frac{\pi}{2}\right) Pe}}, \quad (23)$$

where *Pe* is Peclet number and $k_1$is defined based on Equation 24:

$$k_1 = \frac{\rho_l g}{3\, C_{PB} \mu}, \quad (24)$$

where C_{PB} is the plateau border drag coefficient. The entrainment factor Ent is then determined based on the air recovery as presented in Equation 25, if α < 0.5, and in Equation 26 if α ≥ 0.5.

$$\text{Ent} = \exp\left(-\frac{v_{set}^{1,5} h_f}{D_{Axial}\sqrt{J_g \alpha(1-\alpha)}}\right) \quad (25)$$

$$\text{Ent} = \exp\left(-\frac{2 v_{set}^{1,5} h_f}{D_{Axial}\sqrt{J_g}}\right) \quad (26)$$

Water recovery Rw is calculated from the volumetric liquid flux Jl, the pulp cross-sectional area A_{pulp}, and the feed water flow rate $Q_{W\ Feed}$ (27).

$$Rw = Jl\ \frac{A_{pulp}}{Q_{W\ Feed}} \tag{27}$$

When α < 0.5, the liquid flux Jl is defined as presented in Equation 28, and when α ≥0.5 as in Equation 29:

$$\mathrm{Jl} = \frac{J_g^2 \lambda}{k_1 A_{Ff}}\ (1-\alpha)\alpha, \tag{28}$$

$$\mathrm{Jl} = \frac{J_g^2 \lambda}{4 k_1 A_{Ff}}, \tag{29}$$

where λ is calculated based on Equation 30 when k_λ is lambda prefactor.

$$\lambda = \frac{k_\lambda}{{r_{bo}}^2} \tag{30}$$

By selecting the correct launder models, modifying the froth surface parameters, as well as the froth layer thickness, the model also allows for the calculation of entrainment and water recovery based on gas flux, dispersion coefficients, and froth geometry, making it particularly suitable for assessing modifications that influence froth structure and flow paths.

4.3 Input data and assumptions

The characterization of the simulation model has been assessed based on the collected shift data from the operations and was used to model the recovery of copper and molybdenum at certain time points in operation. In the case of Bagdad, data collection was conducted only after the retrofit installation, unlike in the Constancia and Kennecott cases, where data was collected both before and after the installation from both lines.

Measured data from Bagdad and Constancia included the total amount of fed ore and the bulk composition of copper and molybdenum in flotation feed, tailings, and concentrate streams. Due to the lack of stream analysers, the shift data collected from Kennecott did not consist of metal grades in the concentrate stream. The operational data were also limited, as the size distribution of flotation feed was measured only at the Constancia mine, while the airflow rates and froth thicknesses were measured only in the cases of Constancia and Kennecott.

Due to the lack of operational data from the case studies, the airflow rate and froth thickness used in the simulation work were assumed based on measurements from Constancia. According to these measurements, the documented airflow rate before the upgrade installation was on average around 25 m^3/min, while the froth level of the cells to be upgraded was 250 mm before the center launder installation. After the center launder installation, the froth thickness of these cells was measured at 350 mm. Although these operational parameters were based on the Constancia case, due to similar operational conditions, the parameters measured at Kennecott appear to align well with these assumptions.

Based on the given elemental compositions for the feed and the assumed mineralogy of the ore, HSC Sim can be used to balance the bulk mineralogy of the ore. Due to the unknown nature of the overall feed mineralogy, assumptions regarding the feed mineralogy have been made based on the provided elemental data and available operational information.

In all cases, the feed mineralogy has been assumed to consist of molybdenite, chalcopyrite, and quartz. Therefore, the defined calculation rules have been set to calculate all copper as coming from chalcopyrite, all molybdenum from molybdenite, and the rest of the fed ore as quartz. Based on these modal rules, the defined elemental bulk composition in the feed can be translated into a mineralogical composition.

To ensure the reliability of measured shift data values and the recoveries based on those, all the selected data point were first balanced with HSC Mass Balance tool, after which the balanced values were used in conducted simulations. These variables are optimized through the stream setup by adjusting the correct solid mass flow (t/h) and the weight percentages of copper and molybdenum. Due to the lack of operational data from Kennecott regarding concentrate grade, mass balancing could not be completed, and therefore, the shift data was used as measured. The used standard deviation table in mass balancing is presented in **Table 7** below.

Table 7. Applied standard deviation rules in mass balance calculations

Stream	Total solids RSD	Cu RSD	Mo RSD
Feed	0	5	5
Concentrate	5	10	10
Tailings	5	3	3

4.4 Sustainability assessment

This section presents the methodologies of two applied calculation models used to assess the environmental impact of the center launder retrofit. In the first research part, sustainability has been assessed based on the Life Cycle Assessment created with HSC Sim, whereas the second part involves the CO_2 reduction potential model based on the recovery improvements achieved.

4.4.1 Methodology of Life Cycle Assessment

Life Cycle Assessment (LCA) is a widely known methodology for evaluating the inputs, outputs, and potential environmental impacts of a product system throughout its life cycle. This methodology is based on the ISO 14040:2006 standard and follows the framework of four phases: Goal and scope definition, inventory analysis, impact assessment, and interpretation. This framework is illustrated in **Figure 20** below.

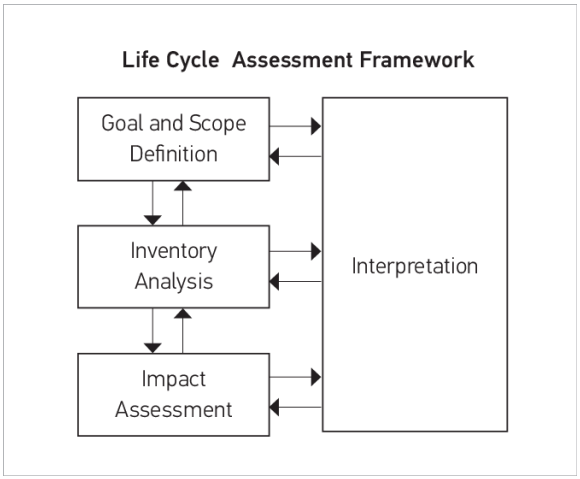

Figure 20. LCA Framework

In overall, the Life Cycle Assessment of minerals processing circuit is dependent on many factors, including applied process technology, metal recovery, type of raw material used, energy efficiency, source of the energy used, location of the site, and recycling rates of the streams in operation. For that reason, the simulation setup of LCA needs to be well defined, and the goal and the scope of the work must be clear. Based on the iterative framework of the process described in **Figure 20** above, the inventory analysis (LCI), as well as the impact assessment (LCIA) must go through several mandatory steps to determine the nature of flows, and selection of impact categories.

Due to the complexity of mineral processing circuits, several of the previously mentioned challenges also arise in conducting a Life Cycle Assessment (LCA) work (Segura-Salazar et al., 2019). First, in many regions, the available LCI databases are insufficient, lacking much of the detailed information required for a comprehensive LCA. Secondly, to obtain a clearer picture of the sustainability of mining operations, the work would also require the adoption of a cradle-to-gate approach, including the management of tailings, process water, and land use. This, in turn, would require extensive operational data, for example on water recirculation streams.

The flotation operation itself requires a lot of water and energy to ensure effective mixing and separation of valuable metals. Based on previous

research, five key components have been identified in the LCA of flotation: ore grade, energy mix, ore mineralogy, production scale, and allocation method (Marmiroli et al., 2022). Furthermore, it has been recommended to use databases such as Ecoinvent and to account for a broader range of variables in impact assessment of mining activities. These include waste generation and energy demand, in addition to incorporating the global warming potential based on produced CO_2 emissions. (Segura-Salazar et al., 2019)

HSC Sim module includes the Life Cycle Assessment tool, which can be used to estimate the environmental impact of a product system throughout its life cycle. Overall, mining is responsible for high emission rates, and Life Cycle Assessment is an efficient way to assess the environmental impact of it (Soto-Vázquez, R, 2025). The assessment of the role of flotation in the context of the LCA of the whole mineral processing plant has not been extensively studied (Marmiroli et al., 2022).

The analysis conducted in this thesis applies the openLCA 2.4.1 software to evaluate the environmental benefits of center launder retrofit in a flotation circuit. The aim is therefore to quantify how improvements in copper recoveries influence the energy consumption in terms of electricity, and the need for process water per functional unit of produced copper in concentrate. Due to the limited amount of data, this study excludes assessing the environmental impact of flotation chemicals, like collectors and frothers. In addition to that, the impact of used materials in a center launder manufacturing has been excluded from this study.

As the aim of the LCA analysis is to focus on the impact of the center launder retrofit, the study takes into account only the environmental impact of the mineral processing circuit up to the rougher flotation, excluding the impact beyond the flotation circuit. It also does not take into account the circulating flows such as used process water or fed ore. Consequently, the simulation cannot provide a comprehensive view of waste generation or water management. Nevertheless, this LCA procedure can serve as an indicator of how increased recovery rates of valuable metals may positively affect CO_2 emissions.

The test work was conducted using hypothetical scenarios in which the number of launder installations was varied. The analysis examined the resulting trends in improvements, as well as water and energy consumption. The LCA simulations conducted followed a methodology similar to that used in the research work studying the effect of center launder installation on the flotation circuit, utilizing both a base case and an upgraded scenario to determine the differences between them. To ensure comparability between the scenarios, operational variables were kept constant throughout the simulations.

This research work has been conducted by using the Ecoinvent database, and the applied impact categories have selected to be global warming potential, the use of water, as well as the use of non-renewable energy resources.

In this study, the inventory results are presented as an equivalent based on copper in the final concentrate in tons per hour. This approach was selected because the aim of this part of the research part is to study the impact of the increased recoveries of copper over a specific timeframe after the center launder installation. Therefore, the calculation considers the normalized amount of CO_2 emissions produced based on the needed amount of feed and electricity, volume of needed water, and required oil assuming that all energy is produced entirely from fossil fuels.

4.4.2 Methodology of the applied CO_2 emission reduction model

The effect of retrofitting mechanical flotation cells in terms of flotation decarbonization has been studied recently, by lowering the energy consumption of the plant per ton of concentrate produced (Bermudez et al., 2023a; Bermudez et al., 2023b). These CO_2 emission reductions have been calculated based on the recovery improvements achieved within a given time frame, considering the energy intensity per ton of processed metal and the emission factor defined for the mine location. The equation for the avoided CO_2 emissions is presented in Equation 31:

$$Avoided\ CO_2 = T \cdot feed - wt\% \cdot rec\% \cdot EI \cdot U \cdot EF, \qquad 31$$

where T is throughput in t/h, feed-wt% is metal grade in feed, rec% is recovery increase of metal after the launder retrofit, EI is energy intensity in GJ per processed ton of copper, U is uptime in hours, and EF is emission factor in tons of CO_2 per produced MW in hour.

This calculation approach has been utilized in the second part of the sustainability assessment to compare the gained results from the simulation, and by giving another perspective on the topic. To ensure comparability between the results, this part of the research work was calculated based on the simulated recovery improvements from the first part of the study, as well as using the same head grade of metal in the feed.

5 Simulation-based research

This section describes the research work conducted to investigate the reliability of HSC in estimating the performance improvements after the center launder retrofit. The simulated setups were first designed to determine the relationship between the selected parameter values and the resulting simulation outputs. Based on these insights gained, case study simulations were then carried out to examine how well the software calculates the gained recovery improvements. In addition to recovery improvement modelling, this section provides detailed descriptions of the Life Cycle Assessments conducted for the circuits.

To model recovery improvements after the launder upgrade, three test scenarios were developed: a center launder retrofit at Constancia, a center launder retrofit at the Bagdad concentrator, and a case example used to validate the applied simulation methodology. In all cases, the base scenario before the center launder installation was modelled using internal launder designs, even if the actual baseline included internal radial launders. This approach was adopted to provide a more realistic representation of surface area reductions and to maintain a consistent methodology across all case studies, as the reduced froth surface parameters were very similar in all cases.

5.1 Effect of different parameters on the simulation results

Understanding the effect of different parameters in flotation circuit modelling is crucial to ensure reliable estimates of expected process improvements. The aim of this research part is to define which of the simulation parameters are affecting the results, how significant their effect is, and which of those are crucial to know when simulating the effect of a center launder retrofit.

The simulation setup was created using hypothetical and simplified data solely to examine their effect during the simulation development phase. This simulation setup is described in **Figure 21** below, consisting of six flotation cells, each with a volume of 300 m^3, and a conditioning unit prior to the cells. Final tailings are collected after the sixth cell, and concentrate is collected as a combined concentrate from all the cells.

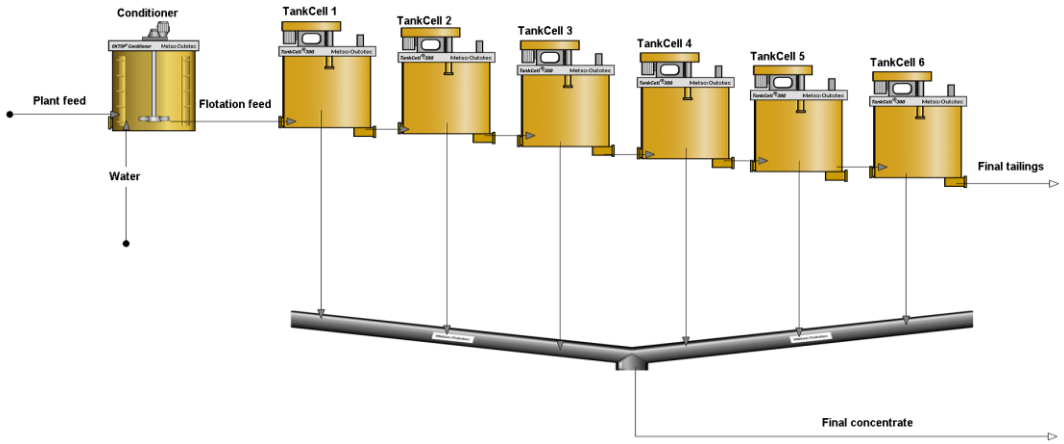

Figure 21. Simulation setup for sensitivity analysis

To ensure reliable test runs, characteristics of the flotation feed have been assumed to be constant over all measurements. All runs were completed using 50 iterations, and the flotation model selected for this trial was the rectangular distribution model. The amount of fed ore has selected to be 2,000 t/h, whereas the selected mineralogy was assumed to consists of chalcopyrite, molybdenite, and quartz. Additionally, the bulk composition is assumed to be 0.3% copper and 0.03% molybdenum, with all copper derived from chalcopyrite and all molybdenum from molybdenite, and the remainder of the feed mineralogy assumed to be quartz.

5.1.1 Effect of flotation slurry parameters

Stream setup selection is responsible for the setup of total flow rate, ore mineralogy, and particle size distribution, described as a structure in **Figure 22** below. The research setup applied in this part aims to define how all these parameter options affect the results obtained.

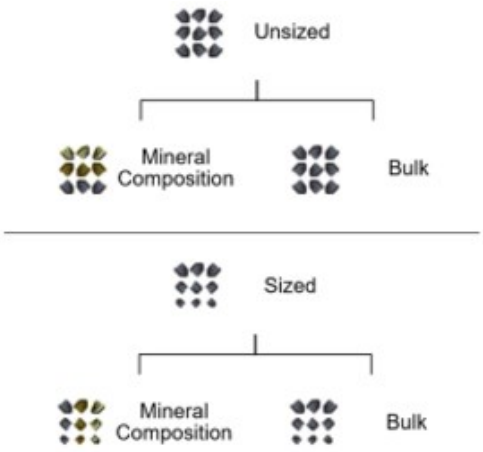

Figure 22. Solids modelling structure in HSC

Stream setup allows for a selection between simulating with a known particle size distribution and with bulk composition. The effect of particle size distribution can be studied by adding a sieve series, after which the size distribution model is selected, and the cumulative passing size of particles is defined. Due to the hypothetical simulation setup, the applied sieve series is a commonly used flotation sieve series consisting of 11 sieve classes from 38 µm to 1,168 µm, and the selected size distribution model is the Rosin–Rammler distribution with an applied 80% passing size.

The first part of the research focuses on the effect of the P80 value for stream setup. To model the effect of PSD, all the other parameters have been kept constant. The selected launder design in all flotation cells is an internal launder, with a froth thickness of 300 mm, a d_{32} bubble size of 1 mm, and a feed solids percentage of 40%. The airflow rate was set to 18 m^3/min in every cell, while the kinetics of different particle size classes were assumed to be equal. The infinite recoveries of chalcopyrite and molybdenite have been set to 90%, and for quartz to 30%. The maximum flotation rate constant (1/min) has therefore been set to 0.9 for chalcopyrite, 0.7 for molybdenite, and 0.01 for quartz. After the parameter setting, the simulation tests are conducted with three different setups, P80 being 150 µm, 175 µm, and 200 µm.

As the flotation kinetics are highly dependent on the specific ore type and mineralogical characteristics, the kinetic values used in this study represent approximate estimates based on reasonable assumptions. These assumptions were based on typical values reported in the literature, indicating recoveries of approximately 90% for molybdenite in pure water (Zhu et al., 2020) and for copper in sulphide ores (Yianatos et al., 2005), while the flotation kinetics of chalcopyrite among sulphide minerals are generally observed to be higher (Tanaka et al., 2021). The kinetics of quartz were therefore assumed to be significantly lower, as it is an unwanted gangue mineral whose apparent recovery is mainly attributed to entrainment.

In addition to studying the impact of different particle size distributions of the flotation feed, simulations have also been conducted to compare the difference between sized and unsized flotation feed. The base scenario used in this simulation is identical to the first measurement, whereas the selected P80 for the sized ore simulation is 175 µm.

One of the key aspects on determining the flotation stream setup is the solids percentage of the flotation feed. For that reason, the conducted simulations included also the comparison of simulation results with different solids percentages of the flotation feed. These simulations were conducted with the unsized feed, by varying the solid percentage of it from 30% to 45% with 5% intervals. All the other operational conditions were kept constant, as defined above.

5.1.2 Effect of flotation cell parameters

This research part was conducted to study how different flotation cell parameters affect the obtained simulation results. The simulation setup was created in a manner similar to that of the previous case in section 5.1.1, with the P80 set to 175 µm in all measurements. The four main parameters investigated are:

- Launder design
- Froth layer thickness
- Airflow rate
- Bubble size

The first measurement was conducted by simulating the flotation line with different launder designs while keeping the feed characteristics constant. The comparison was completed with three different launder designs: internal launder (IL), internal launder and radial launders (IL + R), and center launder (CL). In all cases, the size of the flotation cell was set to be 300 m^3. The calculated froth surface parameters after the selection of each launder model are presented in **Table 8** below.

Table 8. Froth surface parameters depending on the launder design

Variable	IL	IL +R	CL
Net Volume, m^3	**302.93**	**301.89**	**306.61**
Pulp Area, m^2	50.27	50.27	50.27
Froth Surface Area, m^2	**32.00**	**28.55**	**23.5**
Lip Height, m	6.60	6.60	6.60
Lip Length, m	**21.99**	**41.19**	**28.3**
Froth Transport Distance, m	**2.54**	**1.12**	**1.05**
Number of Radial Launders	0	8	0
Rotor Diameter, mm	1750.00	1750.00	1750.00
Rotor Speed, rpm	70.00	70.00	70.00
Power Number	5.90	5.90	5.90
Step to Next Cell, m	0.80	0.80	0.80
Selected Motor, kW	250.00	250.00	250.00

The net volume will change slightly after the launder design, depending on launder size, but the clearest difference can be seen with FSA, LL, and FTD. When comparing the changes in froth surface parameters, it can be observed that the reduction in FSA between the IL and CL designs is 27%, whereas from IL+R to CL the reduction is 18%. In terms of FTD, the reductions can be calculated as 59% and 6%, respectively. Based on these calculations, the simulated scenario of upgrading from an internal launder to a center launder

aligns more closely with the observed reductions presented in **Table 4**, **Table 5**, and **Table 6** in Section 3.4.2.

The base scenario was simulated with internal launder designs in all six flotation cells, after which subsequent test runs were completed by replacing the internal launder designs from the last three cells with both options, radial launders and center launders, as well as by replacing all six internal launders with both options. The second simulation part was conducted to analyse how froth thickness variation affects the final simulation results. The base case scenario was therefore created with the identical setup to the first simulation but using the internal launder designs in all cells and 300 mm froth thickness. The difference in the obtained recovery and grade of the metal in the final concentrate has been simulated by increasing the froth thickness to 350 mm and 400 mm.

The third research part was designed to model the effect of airflow rate on the final recovery of valuable metals. The base case scenario was created with the identical setup to the previous simulations, using the internal launder designs in all cells and 300 mm froth thickness. In the previous simulation, the airflow rate was set to 18 m^3/min in all six flotation cells, whereas this study simulates flotation by using airflow rates of 16 m^3/min, 17 m^3/min, 18 m^3/min, 19 m^3/min, and 20 m^3/min.

The last test focusing on flotation cell parameters was conducted to measure the effect of bubble size. HSC provides an option to define the bubble Sauter diameter in the pulp phase, whereas the overflowing bubble size is simulated as a linear function of froth depth. In the base case scenario of this research, the froth depth was set again to 300 mm and the airflow rate to 18 m^3/min, with the initial d_{32} set at 1 mm. The tests have been conducted by increasing the bubble size from 1 mm to 2 mm in 0.25 mm intervals, and all results for the four scenarios are presented in section 6.1.2.

5.1.3 Effect of flotation kinetics

This part of the research work aims to evaluate the effect of flotation kinetics on the simulation results. The kinetic model used is the rectangular distribution model, and the effects of infinite recovery and maximum flotation rate constant were studied. Kinetics can be adjusted either as bulk kinetics of the mineral or by size class, depending on the defined sieve series.

The base scenario was created in a similar manner to the previous simulations, by setting the froth level to 300 mm, airflow rate per cell to 18 m^3/min, solids percentage in the feed to 40%, and d_{32} to 1 mm. Because this part of the research work was conducted specifically to simulate the effect on kinetic parameters, rather than the effect of particle size distribution, the effect of particle size was not taken into account. Therefore, in this case, the kinetics were selected as bulk values of R_∞ between zero and one hundred, and k_{max} for chalcopyrite, molybdenite, and quartz.

The research work was conducted to model the effect of both R_∞ and k_{max}, focusing on changes in the floatability of chalcopyrite, while keeping the kinetic parameters of both molybdenite and quartz constant. The applied kinetics were defined in a similar manner to the case 5.1.1, while the infinite recoveries were set to 30% for quartz and 90% for molybdenite, and the maximum flotation rate constants to 0.01 and 0.7, respectively. Simulations were conducted for all different combinations of infinite recovery from 80% to 100% in 5% intervals and k_{max} from 0.6 to 1 in 0.1 intervals. The results of the conducted test work are presented in section 6.1.3 in Table 28 and **Figure 39**.

5.2 Center launder retrofit in Bagdad

This section describes the research setups for test simulations aimed at modelling recovery improvements in the Bagdad case. In this case, the simulation work was conducted based on two different research parts, where the first part aimed to model the correlation between the simulated and calculated recovery improvements between the selected datapoints, and the second part aimed to evaluate the simulation accuracy in estimating the gained recovery improvements based solely on the baseline information. Due to the parallel structure of lines, the simulations for both parallel lines, A and B, were conducted by using the similar line structure, described in **Figure 23** below.

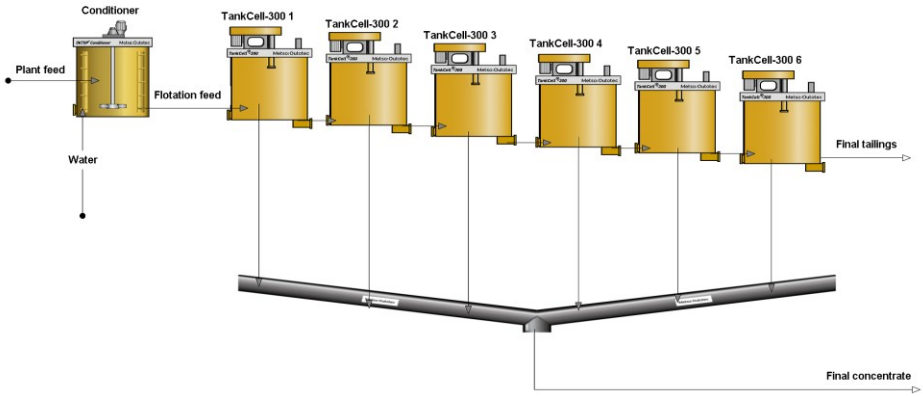

Figure 23. Simulation setup for retrofit analysis in Bagdad

The collected shift data from the operation does not include information about the operational airflow rate, the froth bed thickness, or the bubble size. Therefore, the bubble size (d32) was assumed to be 1 mm, with the airflow rate set to 25 m^3/min in all cells. The froth thickness was assumed to be 400 mm in the first two cells in a row, 300 mm in the third cell, 250 mm in the last three cells in Line B, and 350 mm in the last three cells in Line A after the center launder retrofit installation.

After modelling the flowsheet, the stream setup for the flotation feed was adjusted to match the collected shift data. Due to the limited information about the operational conditions, the selection of datapoints used in the first research part was conducted solely based on the solids flow, and copper and molybdenum head grades in flotation feed. The selection of these three parameters to be controlled aimed to minimize operational variation and stabilize the conditions across the conducted simulation work.

These data points were selected based on their tendency to match the averaged shift data, and the criterion for selecting them was that the solids flow remained within 95–105%, and head grades within 70-130% of the calculated average values over the evaluation period. The selected data points and the variables used at each measurement point are presented in **Table 9**, and the minimum and maximum limits based on the measured average are presented in **Table 10** below.

Table 9. Selected data points for retrofit analysis in Bagdad

Test	Milled ore per line, t/h	Feed grade of Cu, %	Feed grade of Mo, %
1	1695	0.343	0.024
2	1728	0.357	0.023
3	1760	0.392	0.020
4	1712	0.365	0.016
5	1734	0.306	0.018
6	1838	0.383	0.020
7	1802	0.345	0.019
8	1797	0.385	0.023
9	1791	0.331	0.016
10	1739	0.307	0.016
11	1842	0.318	0.021
12	1812	0.311	0.016
13	1847	0.406	0,019
14	1708	0.394	0.025

Table 10. Criteria for data selection in Bagdad case study

	Average	Minimum limit	Maximum limit
Ore feed, t/h	3 564	3 391	3 693
Feed grade of Cu, %	0.360	0.306	0.406
Feed grade of Mo, %	0.022	0.016	0.025

Once the modal rules are defined, the elemental composition of the feed can be converted into a mineralogical composition. Due to the unknown size distribution of the feed, the mineral setup has been defined as a bulk composition. Solids percentage of the feed is also unknown, which is why it was assumed to be 40%.

Due to the equal feed characteristics between these two lines, the flotation kinetics of them were also assumed to be equal at each data point. For these simulations, the infinite recoveries were set at 92% for chalcopyrite, 95% for molybdenite, and 40% for quartz. These assumptions on infinite recoveries were based on the lab tests conducted and the shift data provided from the site.

However, the maximum flotation rate constants were adjusted differently in each simulation setup, based on the balanced recoveries of copper and molybdenum in a base line scenario. The selected setpoint was the balanced metal recovery of Line B, while the controlled variables were the flotation rate constants for chalcopyrite and molybdenite.

The second part of the research was conducted by using the mass balanced average shift data for baseline B. Therefore, the upgraded simulation setup was created with the same feed characteristics and kinetics, in order to estimate improvements under the same conditions. This research work was conducted by using the similar conditions to those in the previous simulation work for Bagdad, and the used solids flowrate was 1781.89 t/h, while the copper and molybdenum grades were 0.360 and 0.022, respectively.

5.3 Center launder retrofit in Constancia

This section describes the simulation-based research conducted to model recovery improvements after the center launder installation at the Constancia mine. As the design of the operational flotation line is identical between both lines, 1 and 2, the simulation flowsheet was created identically for both of them. The applied flowsheet design is presented in **Figure 24** below.

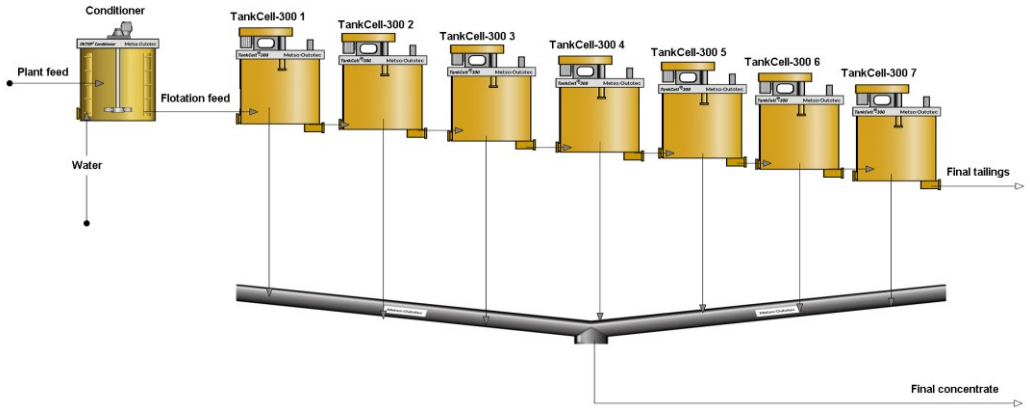

Figure 24. Simulation setup for retrofit analysis in Constancia

This research work includes two parts. The first part was conducted to study how well the calculated recovery improvements, based on the collected composite samples, correlate with the simulated recovery improvements after the launder upgrade. The second part of the simulation work therefore focuses

on evaluating the total recovery improvements of copper and molybdenum based on the Line 1 performance prior to the retrofit.

The collected shift data consists of measured particle size distribution of flotation feed, which have been applied in simulation work to increase the accuracy of results. The selected data points from the shift data and the used variables in the first simulation part at each data point are presented in **Table 11** below. These variables are optimized through the stream setup by adjusting the solid flow (t/h), the weight percentages of copper and molybdenum in flotation feed and measured particle size distribution.

Table 11. Selected data point for retrofit analysis in Constancia

Test	Line 1				Line 2			
	Milled ore, t/h	Cu feed grade, %	Mo feed grade, %	P80, µm	Milled ore, t/h	Cu feed grade, %	Mo feed grade, %	P80, µm
1	1841	0.356	0.018	158	1873	0.343	0.019	149
2	1896	0.322	0.013	148	1908	0.341	0.014	138
3	1874	0.406	0.012	141	1880	0.410	0.013	137
4	1887	0.526	0.014	133	1896	0.526	0.014	141
5	1906	0.362	0.017	156	1857	0.369	0.014	150
6	1892	0.408	0.013	148	1968	0.377	0.012	149
7	1827	0.324	0.013	156	1953	0.373	0.012	158
8	1929	0.467	0.014	141	1908	0.467	0.014	138
9	1922	0.478	0.014	164	1953	0.462	0.013	159
10	1912	0.323	0.014	150	1943	0.332	0.015	144
11	1799	0.334	0.013	139	1891	0.323	0.011	147
12	1794	0.307	0.013	156	1983	0.296	0.018	158
13	1816	0.398	0.015	143	1905	0.378	0.014	139
14	1882	0.459	0.016	164	1998	0.463	0.016	157

These data points are selected based on their tendency to stay within an average range from the taken datapoints over the plant evaluation period, similarly to the Bagdad case study. The criteria for flow were set to remain within 95–105%, and head grades of metals within 70–130%. In addition, the P80 value for the feed was required to remain within 90–110% of the calculated average, with the mill operating 12 hours per 12-hour shift. The allowed variation compared the measured averages were set to be as presented in **Table 12**.

Table 12. Criteria for data selection in Constancia case study

Line	Parameter	Average	Minimum limit	Maximum limit
1	Feed, t/h	1840	1794	1929
1	P80	150	133	164
1	Feed grade of Cu, %	0.412	0.307	0.526
1	Feed grade of Mo, %	0.016	0.012	0.018
2	Feed, t/h	1897	1857	1998
2	P80	148	137	159
2	Feed grade of Cu, %	0.413	0.296	0.526
2	Feed grade of Mo, %	0.016	0.011	0.019

The criteria for the data point selection differ a bit from the Bagdad case study evaluation, due to the different type of data collected. The collected shift data in this case consisted of size distribution for feed, given as a measured p80 value, operational hours of mill during each shift, total ore in tons per hour for both flotation lines, as well as the elemental composition of measured streams. For that reason, also the availability of mill, as well as the P80 have been considered.

As the second part of the simulation work was conducted to study the overall recovery improvement on Line 1, the simulation setup was created based on two flowsheets: Line 1 before the retrofit and Line 1 after the center launder retrofit, by applying the same initial values. The applied data was calculated as an average from the collected datapoints over the evaluation before the launder retrofit. The used solids flowrate was 1897.09 t/h, P80 being 157, while the copper and molybdenum grades were 0.419 and 0.014, respectively.

Even though there is a small variance between two operational lines, in the first simulation part, the flotation kinetics were adjusted based on the Line 2, by controlling the maximum flotation rate constants of copper and molybdenum. In the second part of the study, the kinetics were adjusted based on the averaged data in the baseline scenario and applied respectively in the upgraded scenario. Kinetics of quartz have not been controlled in this research, while the maximum flotation rate constant was set to 0.01 and infinite recovery to 40%. For chalcopyrite and molybdenite, the infinite recoveries were set in a similar manner than for Bagdad simulations to 92% and 95%, respectively due to the lack of kinetic data.

The operational parameters in the flowsheet were defined in a similar manner in both cases and compared to the Bagdad study, whereas the solids percentage for flotation feed was also assumed to stay in 40%, bubble size (d32) in 1 mm, and airflow rate in 25 m^3/min in each cell. As both lines consists of seven flotation cells, the froth thickness was set to the level of 400mm in first three cells, 300mm in third cell, 250mm in the last three cells without center launder installed, and 350mm in Line 1 after the retrofit.

5.4 Center launder retrofit validation

As the aim of this research work is to understand the methodology behind the HSC Sim and create the model to estimate the gained recovery improvements after the center launder installation, the used simulation method in Constancia and Bagdad is validated through a third case study, Kennecott.

The evaluation of this retrofit impact was carried out based on the collected shift analyses from both operational lines, both before and after the installation. In terms of reliable estimation of gained recovery improvements, the operational conditions of mine have to remain constant, including the total solids flow rate, head grades of valuable metals, solids percentage of slurry, as well as the particle size distribution of ore. Based on this assumption, this simulation work was conducted by using the averaged shift data collected from the operation before the launder retrofit, by applying the same feed characteristics and flotation kinetics in both simulations. The considered datapoints before the launder installation were those for which the Proflote system was on. The applied simulation setup is described in **Figure 25.** Simulation setup for retrofit analysis in Kennecott below.

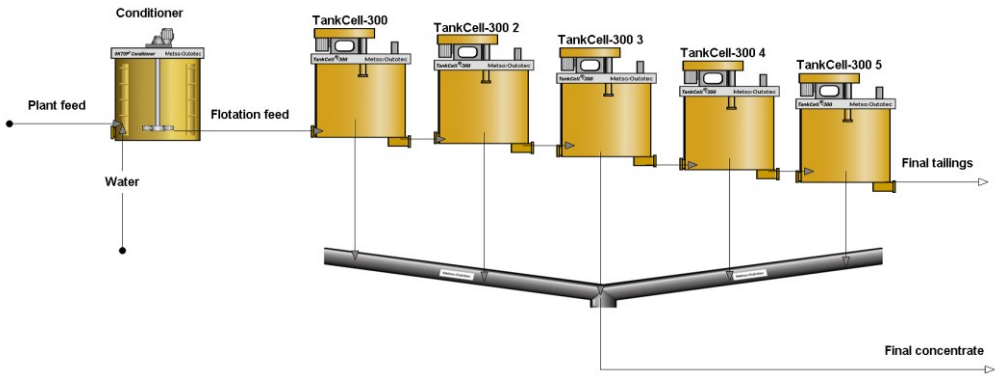

Figure 25. Simulation setup for retrofit analysis in Kennecott

The flotation kinetics were therefore adjusted based on the Row 8, before the launder retrofit, by controlling the maximum flotation rate constants of copper and molybdenum. For chalcopyrite and molybdenite, the infinite recoveries were set in a similar manner than previous simulations to 92% and 95%, respectively, whereas the infinite recovery for quartz was set to 40%. The maximum flotation rate constant of quartz was not controlled and therefore set to 0.01 like in the other case studies.

Regarding to the operational conditions, the flotation cell parameters, as well as the solids percentage of the flotation feed was adjusted in a similar manner than previous cases. The solids percentage for flotation feed was assumed to stay in 40%, bubble size (d32) in 1 mm, and airflow rate in 25

m^3/min in each cell. As both lines consists of 5 flotation cells, the froth thickness was set to the level of 400mm in first two cells, 250mm in the last three cells without center launder installed, and 350mm after the retrofit.

Based on the same operational conditions, the additional research was conducted to study the variance between the measured and simulated recovery improvements after the upgrade installation. The used methodology in this simulation part is similar compared to the Bagdad and Constancia, to validate the used methodology, but also to show the consistency of the results. The selected datapoints are presented in **Table 13**, while the ranges for selected data points are presented in **Table 14** below. The criteria for the selection were that the Proflote system was turned on, the feed flow rates remained within 90–110% of the measured average, and the grades of both metals remained within 70–130% of the average head grade.

Table 13. Selected data point for retrofit analysis in Kennecott

	Row 7			**Row 8**		
Test	Milled ore, t/h	Cu feed grade, %	Mo feed grade, %	Milled ore, t/h	Cu feed grade, %	Mo feed grade, %
1	1485	0.397	0.145	1670	0.334	0.113
2	1288	0.349	0.106	1697	0.381	0.107
3	1475	0.354	0.104	1618	0.327	0.094
4	1395	0.345	0.141	1689	0.356	0.145
5	1414	0.390	0.112	1402	0.387	0.102
6	1404	0.393	0.105	1725	0.382	0.104
7	1382	0.322	0.107	1764	0.295	0.094
8	1273	0.465	0.136	1879	0.419	0.118
9	1299	0.314	0.106	1532	0.285	0.098
10	1402	0.435	0.131	1768	0.406	0.115
11	1268	0.372	0.146	1578	0.378	0.129
12	1340	0.464	0.153	1724	0.438	0.125
13	1383	0.383	0.146	1677	0.324	0.131

Table 14. Criteria for data selection in Kennecott case study

Row	**Parameter**	**Average**	**Min limit**	**Max limit**
7	Feed, t/h	1394	1268	1485
7	Feed grade of Cu, %	0.382	0.314	0.465
7	Feed grade of Mo, %	0.124	0.104	0.094
8	Feed, t/h	1546	1402	1879
8	Feed grade of Cu, %	0.341	0.285	0.438
8	Feed grade of Mo, %	0.112	0.153	0.145

Compared to the other simulation work conducted, the range of the selected datapoints in terms of feed was selected to be wider, due to the needed amount of datapoints. The results of this research work are presented in section 6.4.

5.5 Sustainability assessment

This section outlines the research procedure used in the sustainability assessment, covering both the Life Cycle Assessment and the CO_2 emission reduction calculations. Section 5.5.1 provides a detailed explanation of the simulation parameters and assumptions, including information on the flow mapping specifications and their selection criteria, as well as the chosen impact categories and the justification behind their use. Section 5.5.2 presents the methodology applied in the CO_2 emission reduction calculations, defining the parameters and assumptions used in the analysis.

5.5.1 Life Cycle Assessment

As the simulation work of LCA was conducted to study on how the center launder retrofit will affect the Life Cycle Assessment for flotation, the setup for the conducted test work was created based on the comparison between the baseline and the upgraded line. The selected baseline scenario used in this research was created with six flotation cells, each with a volume of 300 m^3 and equipped with internal launder designs. This simulation setup is presented in **Figure 26** below.

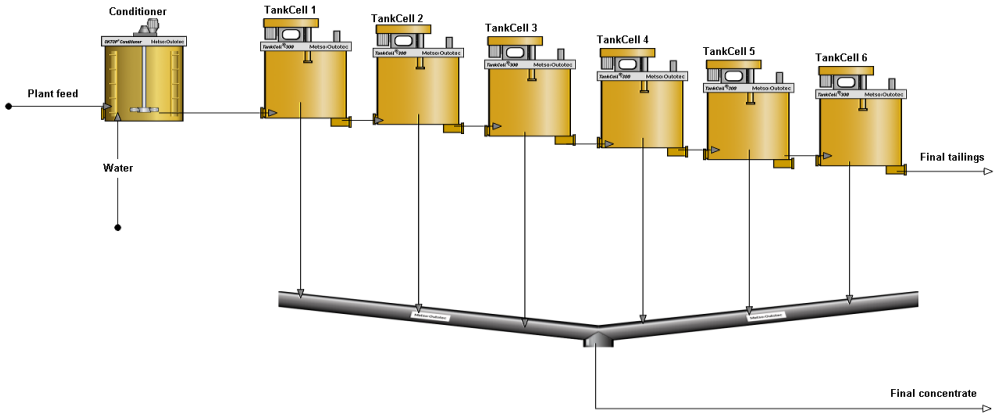

Figure 26. Simulation setup for Life Cycle Assessment

The stream setup, which was kept constant throughout all measurements, was set to 2,000 t/h with the solids content of 40%. The mineralogical composition of the feed was selected in a similar manner to the previous simulation work, consisting of chalcopyrite, molybdenite, and quartz as a gangue mineral. The copper grade in feed was set to 0.4% and molybdenum grade to 0.02%, based on the averaged shift data from the previous case studies conducted. The rest of the feed mineralogy have assumed to consist of quartz,

while all copper was assumed to come from chalcopyrite and all molybdenum from molybdenite.

The applied recovery model in this simulation part was also selected to be the rectangular distribution model, and all the simulations were completed with 50 iteration rounds. All the simulations were conducted with bulk size fraction, and the airflow rate per cell was set to 18 m^3/min. The froth thickness was set to 300 mm per cell and d32 bubble size to 1 mm, respectively.

In the base case scenario, the recovery of copper was set to 85%, and the recovery of molybdenum to 65%, based on the calculated averages from the collected shift data prior to center launder installation. The infinite recoveries were also set to 90% for chalcopyrite, 95% for molybdenite, and 40% for quartz. The upgraded scenarios were studied with three different scenarios, by upgrading two out of six cells, four out of six cells, and all six flotation cells in a bank.

Based on the set infinite recoveries for selected minerals, the maximum flotation rate constants were controlled by targeting the selected recoveries in base scenarios, and by applying the same kinetics for the upgraded simulation scenarios correspondingly. The maximum flotation rate constant for quartz was not controlled, and it was set to 0.01, like in the other case studies conducted. Based on the set controls, the applied maximum flotation rate constants for all simulations were defined to be 1.340 for chalcopyrite and 0.309 for molybdenite.

To assess the Life Cycle Assessment with HSC Simulation, the LCA tool was opened for the applied simulation. The information from the flowsheet was then transferred to the LCA tool automatically, by defining the unit area, stream, and flowrate. To map the environmental impact of the process, the flowtype for the input stream can be selected from the following options: Product flow, Elementary flow, and Reference flow, whereas the flow type for the output streams can be selected from follows: Elementary flow, Reference flow, and Waste flow.

To ensure the consistency and comparability between the conducted test work, the flow mapping was conducted in a similar manner in each simulation part. The used water and ore in the feed, as well as the total electricity were considered as product flows, while the final concentrate as a reference flow. The Ecoinvent 3.10 database was applied in flow mapping, while the used water was selected to be harvested from rainwater, fed ore to be milled (loose) quicklime, and the used electricity consumption was selected as high voltage. The providers and the criteria for the selection of them are defined in **Table 15** below.

Table 15. Description of input stream mapping in LCA

	Water	Ore feed	Total electricity
Provider	water, harvested from rainwater	quicklime, milled, loose	electricity, high voltage
Location	GLO	RoW	GLO
Details	Water is collected from the rainwater, and has not been purified or processed before the operational use	Ore has gone through the milling phase, as well as the separation phase through the cyclone	High voltage electricity, produced as a global average

The selected impact method in this Life Cycle Assessment was ReCiPe 2016 v1.03, midpoint (H), and the categories were selected to include Climate change, Water use, and Energy resources: non-renewable, fossil. Since the final concentrate was selected to be a reference flow in this calculation, the results were calculated based on the final concentrate t/h as a normalized amount. Therefore, the calculation model presents the required amount of ore, electricity, and water to produce 1 ton of concentrate per hour. The selected impact method calculates the amount of CO_2 equivalent emissions per t/h of final concentrate, based on the used product flows and the emissions associated with their production. These results where then further normalized based on the ton of copper produced, to provide more realistic values when studying the positive impact of an increase in copper recovery.

5.5.2 CO_2 emission reduction potential

As explained previously, to compare these two calculation methods, the simulated recovery improvements were used to calculate the reduced CO_2 emissions based on the Equation 31. This calculation applies copper as a reference metal, while the copper grade was set equal to that in the first part of the assessment (0.4%), and the applied throughput to be 2000 tons per hour.

The recovery improvements used were based on the simulated improvements described in section 5.5.1 above. The calculation was applied to all three different retrofit scenarios: 2 center launders installed, 4 centre launders installed, and 6 centre launders installed. Energy intensity per processed ton was set to 25 GJ/ton of copper equivalent, based on the commodity value for copper (Allen, M., 2021). Since the used locations were selected to be either global, or rest of the world in the previous Life Cycle Assessment, the emission factor was calculated as an average based on the potential emission factors presented by country, presented in **Table 16** below (Allen, M., 2021).

Table 16. Potential emission factors by country, adapted from Allen, M., 2021

Country	Emission factor, CO_2 eq. / MWh
Australia	0.80 t
Brazil	0.54 t
Canada	0.14 t
China	0.92 t
South Africa	1.02 t
USA	0.45 t
Average	0.65 t

6 Results

This section of the thesis presents the results from the simulated research work and visualizes them with graphs and tables. The section is divided into four parts. The first part (6.1) presents the results from the simulations that examined the effect of different parameters, whereas the second, third, and fourth parts present the simulated recovery improvements based on the site data from Bagdad, Constancia, and Kennecott respectively (6.2, 6.3, 6.4). The final part of this section presents the results from the conducted Life Cycle Assessment for the rougher flotation line after the center launder retrofit, as well as the results from the CO_2 reduction calculation.

6.1 Effect of different parameters

As the aim of this research was to analyse the dependence of the simulation results on the stream setup, flotation cell parameters, and the flotation kinetics, the simulations were conducted in a similar manner by controlling different parameters. **Table 17** below summarizes the operational conditions, that were assumed to stay constant throughout all three parts of the research, whereas **Table 18** details which of the parameters were kept constant, and which of them were changed in each simulated setup.

Table 17. Constant operational conditions

Cell size, m³	300
Feed, t/h	2000
Mineralogy	Cu wt-%: 0.3, Mo wt-%: 0.03

Table 18. Summary of fixed and changed parameters in each part of the sensitivity analysis

	Test 1: Stream setup	**Test 2: Cell parameters**	**Test 3: Kinetics**
Size distribution for feed	**Changed**	Constant	Constant
Solids-% for feed	**Changed**	Constant	Constant
Froth thickness	Constant	**Changed**	Constant
Bubble size	Constant	**Changed**	Constant
Airflow rate	Constant	**Changed**	Constant
Launder type	Constant	**Changed**	Constant
k_{max} (Ccp/Mlb/Qtz)	Constant	Constant	**Changed**
R_∞ (Ccp/Mlb/Qtz)	Constant	Constant	**Changed**

6.1.1 Effect of stream setup

By defining the particle size distribution of the feed, HSC Sim can calculate metal recovery by size class. Based on the simulations conducted, a clear trend was observed between the defined P80 of the feed and the resulting recovery, with higher P80 values leading to lower metal recoveries. This indicates that finer particle size distributions are associated with improved estimated recoveries. These results from the conducted research have been presented and visualized in Table 19 and **Figure 27** below.

Table 19: Recovery of Copper and Molybdenum as a function of P80

P80 (µm)	Cu recovery (%)	Mo recovery (%)
150	77.17	71.96
175	76.18	70.76
200	75.28	69.66

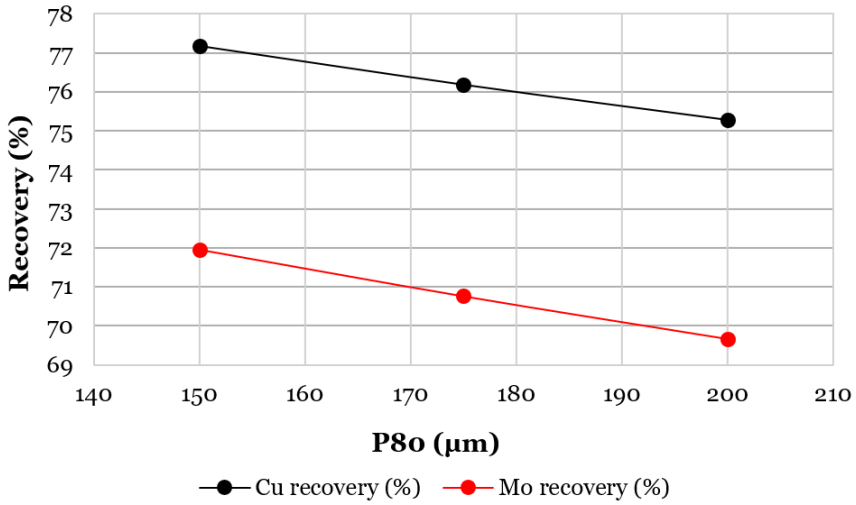

Figure 27. Simulated recovery as a function of P80

Based on these results, a smaller particle size distribution tends to increase the recovery of metal during the operation. When comparing the results of sized and unsized flotation feed characteristics, a clear difference can be observed between these two setups in terms of the outcomes achieved. This difference is presented in **Table 20** below.

Table 20. Metal recoveries with sized and unsized flotation feed

Composition	Total solids (t/h)	Cu recovery (%)	Mo recovery (%)
Sized	49.50	76.18	70.76
Bulk	60.60	81.83	77.79

Table 21 below represents the difference in copper and molybdenum recoveries and concentrate grades with different feed solids percentage. Based on these results it can be noted that the lower solids percentage correlates with the lower preliminary recovery of metals, whereas the grade of the concentrate can be seen to remain higher.

Table 21. Metal recoveries and grades as a function of feed solids content

	Cu recovery (%)	Mo recovery (%)	Cu grade (%)	Mo grade (%)
solids-% 30	77.55	72.16	10.06	0.94
solids-% 35	79.98	75.32	9.01	0.85
solids-% 40	81.83	77.79	8.10	0.77
solids-% 45	83.28	79.76	7.31	0.70

This recovery increase in copper and molybdenum as a function of solids percentage in the feed is presented in **Figure 28** below. Based on this figure, the recovery rates of both metals clearly increase with higher solid percentages in the slurry.

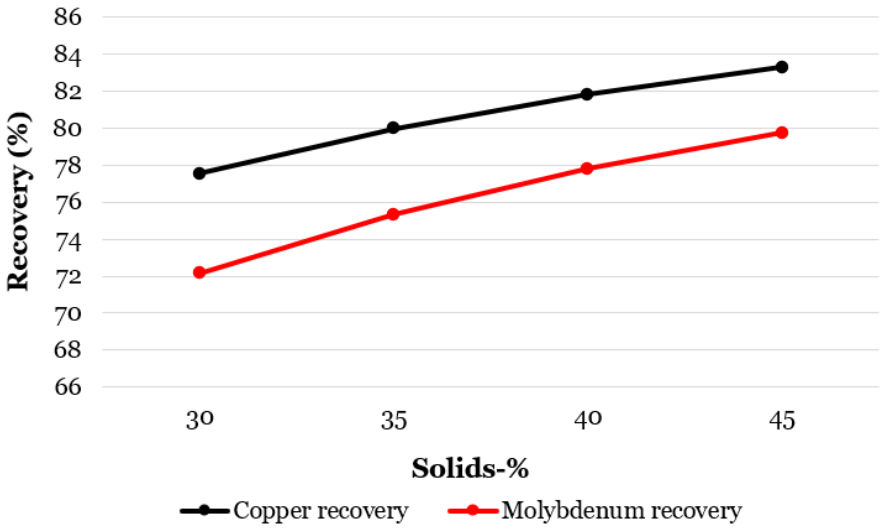

Figure 28. Recovery as a function of feed solids content

6.1.2 Effect of flotation cell parameters

This section presents the results from the research work studying the impact of flotation cell parameters on the gained results. The results from these simulations conducted have been detailed in **Table 22**, and the gained recoveries have been visualized as a function of launder arrangement in **Figure 29**.

Table 22. Effect of different launder arrangements on the final concentrate

Variable	Unit	6 x IL	3 x IL + 3x IL+R	6x IL+R	3 x IL + 3x CL	6 x CL
Total Solids Flow	t/h	49.51	54.92	60.40	61.95	74.44
Total Liquid Flow	t/h	25.47	37.03	48.58	53.95	82.42
Total Gas Flow	t/h	0.00	0.00	0.00	0.00	0.00
Pulp Mass Flow	t/h	74.98	91.95	108.99	115.90	156.86
Pulp Volumetric Flow	m3/h	42.14	55.74	69.37	75.33	108.55
Solids SG	-	2.98	2.95	2.93	2.92	2.88
Liquid SG	-	1.00	1.00	1.00	1.00	1.00
Pulp SG	-	1.78	1.65	1.57	1.54	1.45
% Solids	wt-%	66.03	59.73	55.42	53.45	47.45
Solids Fraction	vol-%	39.39	33.37	29.75	28.17	23.84
Solids Recovery	Rec-%	2.48	2.75	3.02	3.10	3.72
Liquid Recovery	Rec-%	0.85	1.23	1.62	1.80	2.75
Ore	t/h	49.51	54.92	60.40	61.95	74.44
Ore	wt-%	100.00	100.00	100.00	100.00	100.00
Ore	Rec-%	2.48	2.75	3.02	3.10	3.72
Cu	wt-%	9.23	8.47	7.82	7.63	6.52
Mo	wt-%	0.86	0.79	0.74	0.72	0.62
Ccp	wt-%	26.66	24.46	22.59	22.03	18.82
Mlb	wt-%	1.43	1.32	1.23	1.20	1.03
Qtz	wt-%	71.91	74.22	76.18	76.77	80.15
Cu	Rec-%	76.18	77.53	78.76	78.76	80.84
Mo	Rec-%	70.76	72.44	74.00	74.01	76.68
Ccp	Rec-%	76.18	77.53	78.76	78.76	80,84
Mlb	Rec-%	70.76	72.44	74.00	74.01	76.68
Qtz	Rec-%	1.80	2.06	2.32	2.40	3.01
P80	µm	118.74	115.63	113.03	110.93	104.97
P50	µm	43.48	41.66	40.26	39.55	37.74
H2O	t/h	25.47	37.03	48.58	53.95	82.42

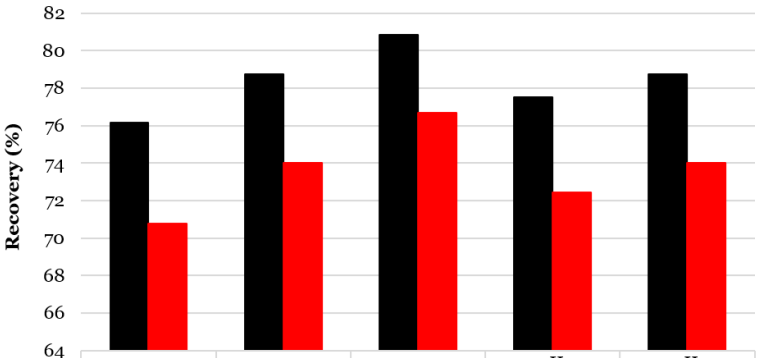

	6 x IL	6 x IL+R	6 x CL	3 x IL + 3x IL+R	3 x IL + 3x CL
Cu recovery (%)	76,18	78,76	80,84	77,53	78,76
Mo recovery (%)	70,76	74	76,68	72,44	74,01

Figure 29. Recovery of Cu and Mo with different launder arrangements

The collected results show a clear difference in the simulated metal recovery after different launder arrangements, showing the highest recovery with center launders, and lowest with internal launders. Therefore, the obtained results support the hypothesis of center launder upgrade to increase the recovery of valuables, based on the improved froth surface parameters, as well as the increased net volume to improve the performance of the cell.

However, as presented in **Table 8** above, the selection between the launder designs affects only the froth surface area, lip length, froth transport distance, and slightly the net volume of the cell. Based on the conducted test work, it was noted that the effect of froth surface area was the only parameter that significantly influenced the final results. The changes in net volume were so small that their effect was almost negligible, whereas changes in FTD and LL had no effect at all. Additionally, the selection of an internal launder installed together with radial launders limited the number of radial launders that could be used. For example, 8 for a cell volume of 300 m^3 and 6 for a cell volume of 200 m^3. Since the number of installed radial launders affects the froth surface area, these assumptions also have a significant impact on the results obtained.

The results from the conducted test work with different froth bed thicknesses, presented in **Table 23**, also show a clear trend: higher froth thickness is associated with a lower solids flow in the concentrate. This trend appears to influence the recovery and grade of the final concentrate decreasing the recovery while increasing the concentrate grade. This phenomenon is also consistent with findings reported in the literature (Wang et al., 2014; Yianatos et al., 2008). The corresponding simulated results are shown in **Figure 30** and **Figure 31** below.

Table 23. Simulation results as a function of froth bed thickness

Froth thickness	Solids (t/h)	Cu recovery (%)	Mo recovery (%)	Cu grade (%)	Mo grade (%)
300 mm	49.50	76.18	70.76	9.23	0.86
350 mm	45.90	74.94	69.23	9.80	0.91
400 mm	43.00	73.78	67.81	10.29	0.95

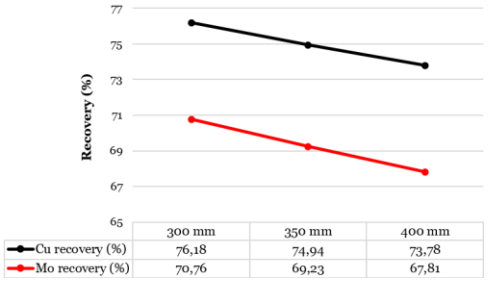

Figure 30. Recovery of Cu and Mo as a function of froth thickness

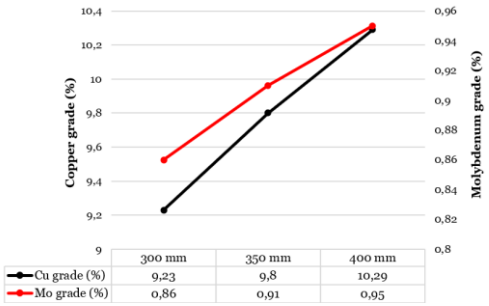

Figure 31. Grade increase of Cu and Mo as a function of froth thickness

The results from the conducted simulations after the change in operational airflow rate are presented in **Table 24** below. These results show a correlation between a higher airflow rate and the resulting recovery and concentrate grade. An increased airflow rate enhances particle entrainment into a concentrate, thereby increasing metal recovery while decreasing the concentrate grade. The simulated results are illustrated in **Figure 32** and **Figure 33**.

Table 24. Effect of airflow rate on the simulation results

Airflow rate (m^3/s)	Solids (t/h)	Cu recovery (%)	Mo recovery (%)	Cu grade (%)	Mo grade (%)
16	31.20	66.12	58.86	12.73	1.13
17	43.00	73.83	67.86	10.30	0.95
18	49.50	76.18	70.76	9.23	0.86
19	59.40	78.34	73.47	7.92	0.74
20	59.40	78.34	73.47	7.92	0.74

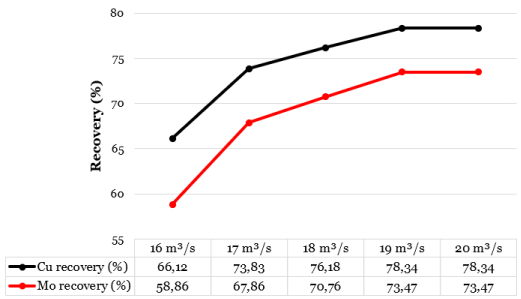

Figure 32. Recovery of Cu and Mo as a function of airflow rate

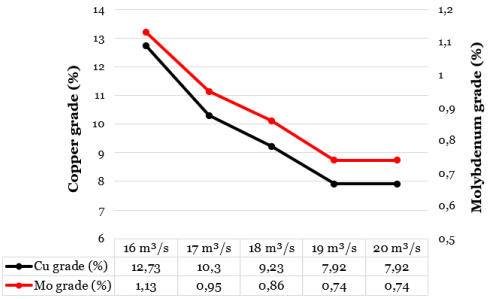

Figure 33. Grade decrease of Cu and Mo as a function of airflow rate

The results from the conducted simulations studying the effect of bubble size with a bulk size fraction of feed are presented in **Table 25** below. The simulations indicate that an increase in bubble Sauter diameter leads to higher solids recovery, thereby increasing the recovery of valuable metals, but also decreasing the concentrate grade. These results are illustrated in **Figure 34** and **Figure 35**.

Table 25. Effect of bubble size on the simulation results

d32 (mm)	Solids (t/h)	Cu recovery (%)	Mo recovery (%)	Cu grade (%)	Mo grade (%)
1	49.50	76.18	70.76	9.23	0.86
1.25	53.30	77.85	72.85	8.76	0.82
1.5	56.60	79.07	74.40	8.38	0.79
1.75	58.60	79.70	75.21	8.17	0.77
2	62.10	80.75	76.59	7.80	0.74

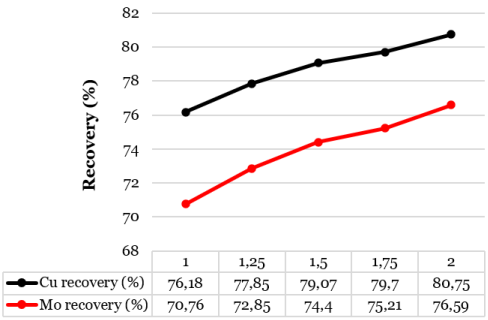

Figure 34. Recovery of Cu and Mo as a function of d32

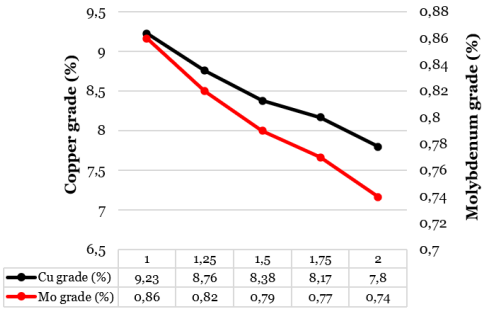

Figure 35. Grade decrease of Cu and Mo as a function of d32

In addition to conducting the simulation based on the bulk size fraction, the effect of bubble size on metal recovery was further studied by applying three different feed size fractions together with three different bubble sizes. Selected d32 bubble sizes were 1 mm, 1.25mm, and 1.5 mm, while the selected P80 values for flotation feed were 150 µm, 175 µm, and 200 µm. The results collected from the research conducted are presented in **Table 26**, with the corresponding data illustrated in **Figure 36** and **Figure 37** below.

Table 26. Effect of bubble size and P80 on the simulation results

d32 (mm) / P80 (µm)	Solids in concen-trate (t/h)	Cu recovery (%)	Mo recovery (%)	Cu grade (%)	Mo grade (%)
1/150	51.80	77.17	71.96	8.94	0.83
1/175	49.51	76.18	70.76	9.23	0.86
1/200	47.57	75.28	69.66	9.50	0.88
1.25/150	55.78	78.75	73.97	8.47	0.80
1.25/175	53.34	77.85	72.85	8.76	0.82
1.25/200	51.26	77.01	71.82	9.01	0.84
1.5/150	59.21	79.91	75.47	8.10	0.76
1.5/175	56.64	79.07	74.40	8.38	0.79
1.5/200	54.44	78.29	73.43	8.63	0.81

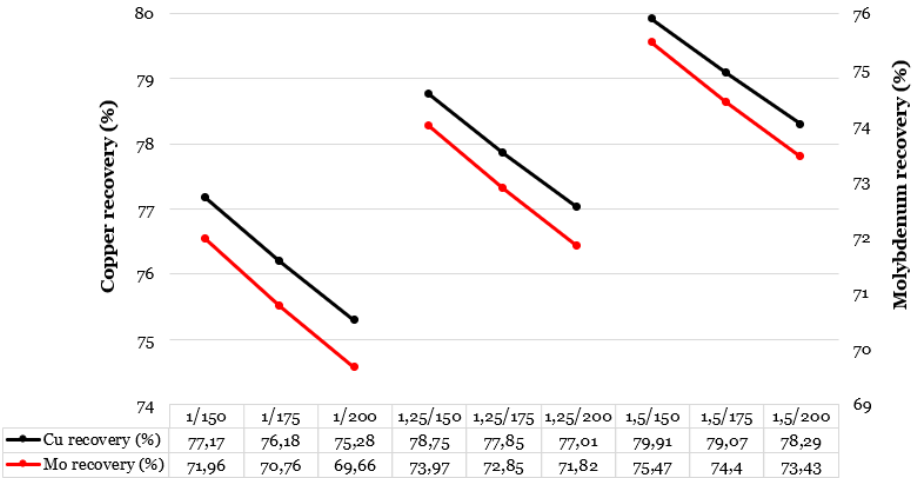

Figure 36. Copper and molybdenum recoveries as a function of bubble size and P80 for feed

The simulated results show a clear trend, with the highest metal recoveries observed for smaller particle size fractions combined with larger bubble sizes. In contrast, the effect of particle size distribution on concentrate grade is opposite, while higher metal grades are obtained with larger particle size fractions together with smaller bubble sizes.

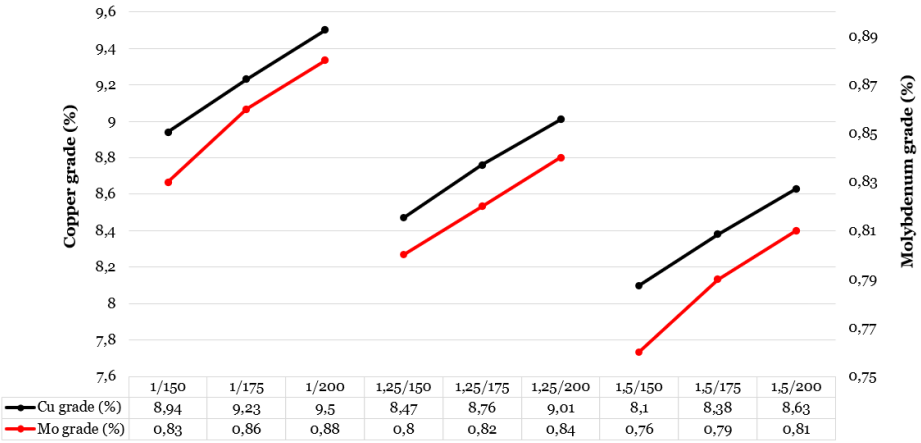

Figure 37. Copper and molybdenum grades as a function of bubble size and P80 for feed

In addition to studying the effect of different particle size distributions on flotation feed, the same parameter setup was also applied to study on how different bubble sizes in pulp phase effects on the recovery rate of copper per size fraction. **Table 27** below represents these recoveries, and particle size distributions in final concentrate with five different bubble Sauter diameters: 1 mm, 1.25 mm, 1.5 mm, 1.75 mm, and 2 mm. The gained results are visualized as a graph in **Figure 38**, showing the copper recovery per particle size fraction in final concentrate as a function of d32.

Table 27. P80, P50, and copper recovery per particle size fraction as a function of d32

	d32 1 mm	**d32 1.25mm**	**d32 1.5 mm**	**d32 1.75 mm**	**d32 2 mm**
P80	118.74	119.75	120.50	121.01	121.51
P50	43.48	44.06	44.47	44.83	45.12
833 - 1168 µm	43.57	47.25	50.17	52.54	54.53
589 - 833 µm	49.37	52.95	55.73	57.96	59.81
417 - 589 µm	55.05	58.42	60.99	63.03	64.70
295 - 417 µm	60.39	63.46	65.78	67.59	69.06
208 - 295 µm	65.29	68.02	70.05	71.62	72.89
147 - 208 µm	69.64	72.01	73.75	75.09	76.16
104 - 147 µm	73.40	75.41	76.88	78.01	78.90
74 - 104 µm	76.57	78.26	79.49	80.42	81.16
53 - 74 µm	79.19	80.60	81.61	82.39	83.00
38 - 53 µm	81.35	82.52	83.36	83.99	84.49
0 - 38 µm	84.02	84.88	85.49	85.95	86.32

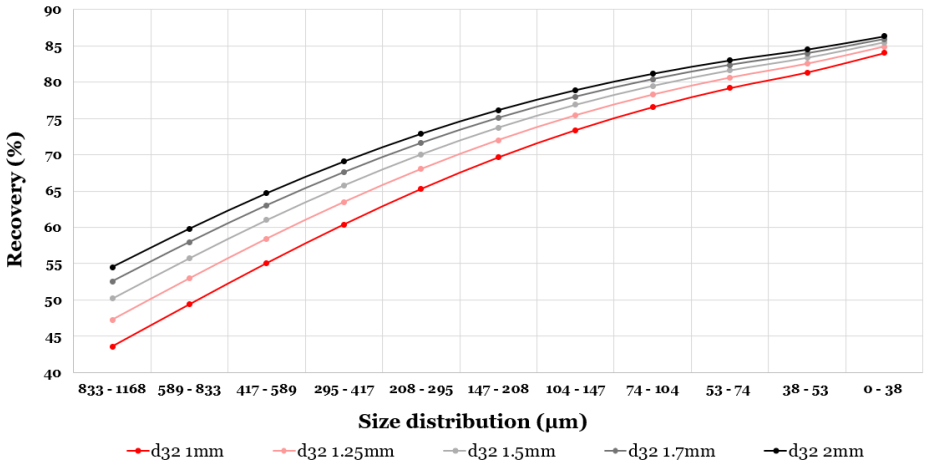

Figure 38. Copper recovery per particle size fraction as a function of d32

6.1.3 Effect of flotation kinetics

The effect of flotation kinetics on copper recovery in the concentrate is presented as a function of R_∞ and k_{max}, as described in Table 28 below. The simulations conducted show a trend of increasing copper recovery with increasing R_∞ and k_{max} values. These results are illustrated in **Figure 39** below.

Table 28. Copper recoveries as a function of R_∞ and k_{max} values

	k_{max} **for copper**				
R_∞	**0.6**	**0.7**	**0.8**	**0.9**	**1**
80	68.33	70.21	71.64	72.77	73.67
85	72.58	74.58	76.1	77.3	78.26
90	76.84	78.95	80.57	81.83	82.25
95	81.09	83.32	85.03	86.36	87.44
100	85.34	87.69	89.48	90.89	92.02

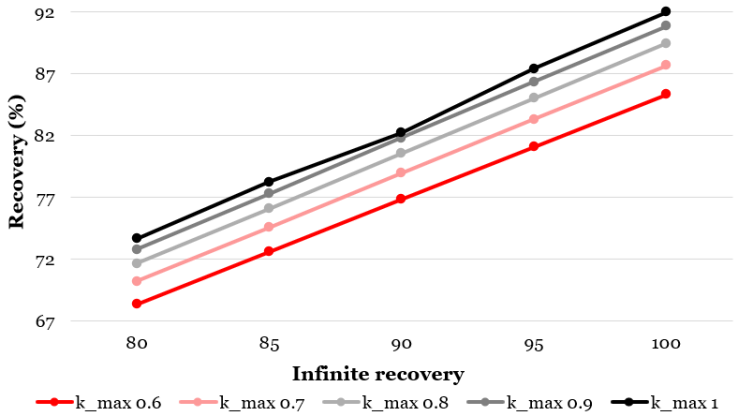

Figure 39. Dependence of recovery as a function of R_∞ and k_{max}

6.2 Simulated recovery improvements in Bagdad

This section presents the simulated results conducted to model the gained recovery improvements in Bagdad. The simulations in the first research part were conducted by using the data points detailed in **Table 9** in section 5.2. Because the operational flotation lines are parallel, the feed flowrate, and metal grades are assumed to be equal. The maximum flotation rate constants applied in the simulations for each mineral are presented in **Table 29** below. These k_{max} values have been controlled based on the set infinite recoveries for each mineral.

Table 29. Applied k_{max} values for each data point in the Bagdad case study

Test	k_{max} Ccp	k_{max} Mlb	k_{max} Qtz
1	1.16	0.47	0.01
2	0.95	0.44	0.01
3	0.96	0.36	0.01
4	0.87	0.32	0.01
5	0.66	0.36	0.01
6	1.47	0.45	0.01
7	0.83	0.53	0.01
8	0.58	0.37	0.01
9	0.51	0.35	0.01
10	0.85	0.63	0.01
11	0.76	0.75	0.01
12	0.84	0.77	0.01
13	0.48	0.41	0.01
14	0.94	0.42	0.01

Table 30 below presents the simulated recovery improvements for both copper and molybdenum, as well as the mass balanced reference values using the shift data at each selected data point.

Table 30. Simulated and mass balanced recovery improvements in the Bagdad case study

	Simulated improvements, %		Mass balanced improvements, %	
Test	Cu	Mo	Cu	Mo
1	0.38	0.82	0.24	1.23
2	0.48	1.08	1.12	3.41
3	0.49	1.28	1.12	3.66
4	0.52	1.36	0.54	0.67
5	0.69	3.27	-0.34	7.49
6	0.32	1.13	-0.04	0.60
7	0.58	0.97	0.61	-0.77
8	0.81	1.26	0.20	1.30
9	0.90	1.31	0.94	2.29
10	0.53	0.80	-1.52	2.09
11	0.64	0.71	2.29	0.33
12	0.57	0.68	1.76	0.31
13	0.97	1.20	2.51	-2.70
14	0.48	1.11	-0.02	1.39
Average	**0.60**	**1.21**	**0.67**	**1.52**

Based on the calculated averages for both metals, the simulated recovery improvements show similar trend compared to the mass balanced recovery improvements. However, it can be observed that the variation in the measured improvements is greater than that in the simulated results, which may be attributed to several factors, like operational changes. These operational changes were not considered in the simulations, as the operational conditions were assumed to remain constant.

At some time points, the measured recovery improvements were also negative, caused by the upgraded line outperforming the baseline. This outperformance may be due to ore changes, including variability in, for example, size distribution or liberation of the fed ore. These changes may significantly affect overall performance, as metal recovery is strongly influenced by the form (eg: liberated or locked) of the valuable metal within the particles, as well as by their size. Operational and ore variation requires constant optimization of airflow rates and froth thickness, while poor calibration of these parameters may also lead to underperformance.

The correlation between the improvements in each data point has been visualized in the graphs below, with **Figure 40** representing the trend observed for copper, and **Figure 41** for molybdenum respectively.

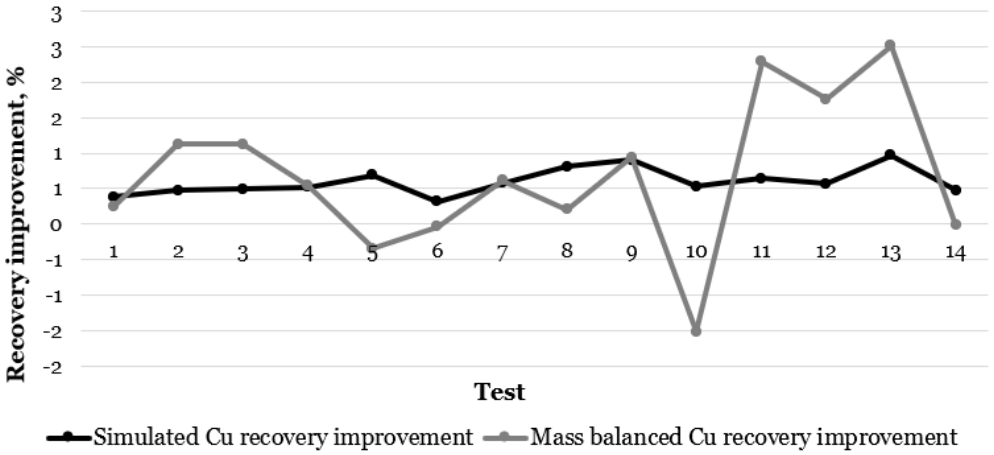

Figure 40. Correlation between the simulated and measured recovery improvements for copper in the Bagdad case study

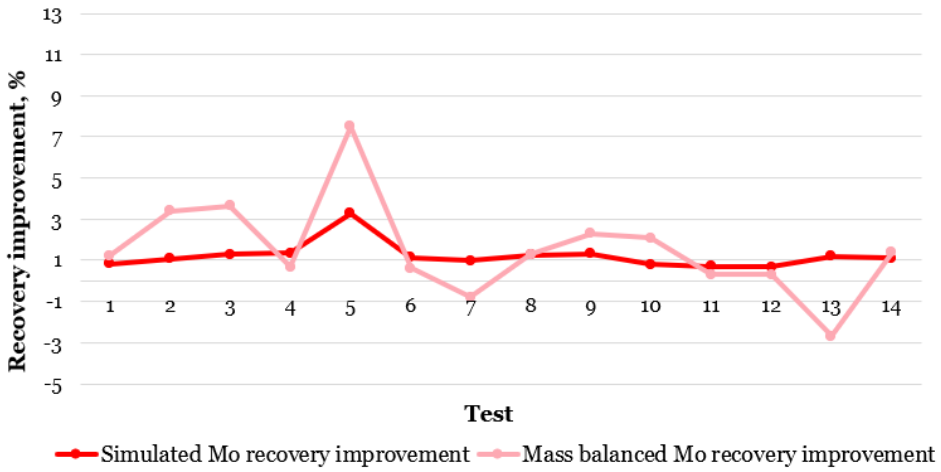

Figure 41. Correlation between the simulated and measured recovery improvements for molybdenum in the Bagdad case study

Based on these graphs, the measured recovery improvements and simulated recovery improvements can be seen to correlate with each other. The correlation between the datapoints have been calculated to be 0.40 for copper and 0.72 for molybdenum.

In comparison to the first part of the research, the second part of the study aimed to evaluate the consistency between simulated and measured overall recovery improvements. The published recovery improvements for copper and molybdenum, calculated from the shift data, were 0.93% and 3.15%, respectively (Liu et al., 2022). Based on the conducted simulation, the overall recovery improvements followed a similar trend, with copper at 0.74%, while molybdenum showed a smaller improvement of 1.36% compared to the published value. The applied flotation kinetic parameters and the simulated recovery improvements are presented in **Table 31** and **Table 32** below.

Table 31. k_{max} values applied in determination of overall recovery improvement in the Bagdad case study

k_{max} Ccp	k_{max} Mlb	k_{max} Qtz
0.63	0.33	0.01

Table 32. Simulated overall recovery improvements in the Bagdad case study

	Cu	Mo
Line A	83.48 %	74.94 %
Line B	82.74 %	73.58 %
Net recovery gain	0.74 %	1.36 %

6.3 Simulated recovery improvements in Constancia

This section presents the simulated results from the simulation conducted to model the recovery improvements of copper and molybdenum after the center launder retrofit in Constancia mine. The first part of the test work conducted was to evaluate the consistency between the measured recovery improvements and the simulated improvements by using the selected data points. The applied maximum flotation rate constants in each simulation setup are presented in **Table 33** below.

Table 33. Applied k_{max} values for each data point in the Constancia case study

Test	k_{max} Ccp	k_{max} Mlb	k_{max} Qtz
1	0.68	0.21	0.01
2	0.64	0.06	0.01
3	1.11	0.11	0.01
4	0.99	0.11	0.01
5	2.54	0.24	0.01
6	0.97	0.12	0.01
7	2.31	0.25	0.01
8	1.23	0.25	0.01
9	1.01	0.24	0.01
10	1.19	0.16	0.01
11	1.30	0.10	0.01
12	1.22	0.30	0.01
13	0.98	0.14	0.01
14	1.17	0.19	0.01

Table 34 below presents the simulated recovery improvements for both copper and molybdenum, together with the mass balanced reference values based on shift data at each selected data point.

Table 34. Simulated and mass balanced recovery improvements in the Constancia case study

	Simulated improvements (%)		Mass balanced improvements (%)	
Test	Cu	Mo	Cu	Mo
1	0.63	1.29	0.61	1.76
2	0.47	0.88	-3.42	-0.65
3	0.39	1.29	-0.24	-6.93
4	082	2.20	-1.78	-0.14
5	0.06	0.40	-0.42	-0.32
6	0.96	2.55	1.29	2.67
7	0.54	3.34	-4.27	-6.53
8	0.29	0.95	-0.09	1.79
9	0.59	1.52	1.41	1.87
10	0.45	1.54	-0.01	-9.72
11	0.90	3.25	1.13	9.50
12	1.28	3.84	1.28	-9.73
13	0.85	2.50	0.77	3.07
14	0.86	2.65	0.23	-0.93
Average	**0.65**	**2.01**	**-0.25**	**-1.02**

Similarly to the Bagdad case, when the simulated recovery improvements are compared with the mass balanced reference recoveries, the results differ considerably, due to the operational variation that is not considered in the conducted simulation work. The simulated results can be seen to show a more consistent trend, due to the equal operational parameters, whereas the mass balanced values can be seen to show also negative values, ranging from -4.27% to 1.41% for copper and from -9.73 to 9.50 for molybdenum. The studied correlation between these values have been presented as graphs in **Figure 42** and **Figure 43** below. Based on these results, the correlation for copper and molybdenum recovery improvements have calculated to be 0.38 for both.

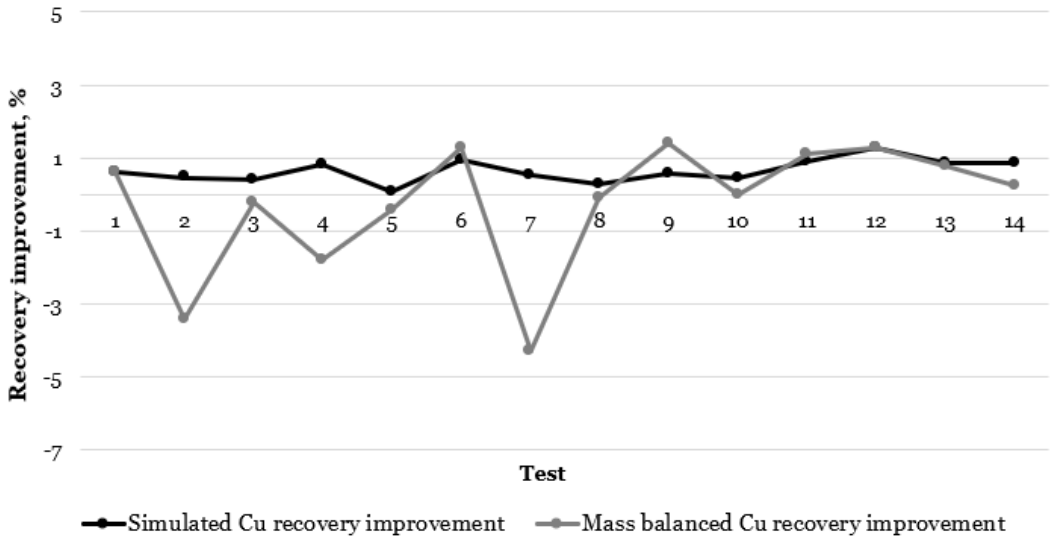

Figure 42. Correlation between the simulated and measured recovery improvements for copper in the Constancia case study

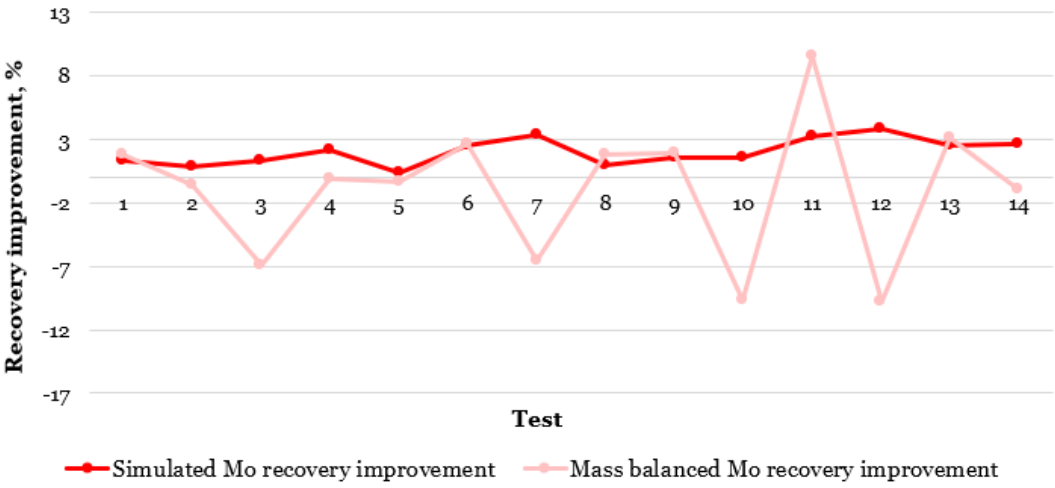

Figure 43. Correlation between the simulated and measured recovery improvements for molybdenum in the Constancia case study

The second part of the study was conducted using averaged shift data from Line 1 prior to the retrofit. According to the published recovery improvements from the retrofit case, the calculated recovery improvements over the evaluation period were 0.7% for copper and 1.4% for molybdenum (Bermudez et al., 2021). These measurements are therefore consistent with the simulation results, particularly for copper, showing recovery improvements of 0.64% and 2.10% for copper and molybdenum, respectively. Applied maximum flotation rate constants in both simulations are presented in **Table 35**, and the simulated recovery improvements in **Table 36** below.

Table 35. k_{max} values applied in determination of overall recovery improvement in the Constancia case study

k_{max} Ccp	k_{max} Mlb	k_{max} Qtz
1.2	0.21	0.01

Table 36. Simulated overall recovery improvements in the Constancia case study

	Cu	Mo
After	87.06 %	59.84 %
Before	86.42 %	57.74 %
Net recovery gain	0.64 %	2.10 %

6.4 Simulation validation results

Validation of the used simulation methodology was conducted using shift data collected from Kennecott Copperton. The results of this case study are presented in this section. As described in section 5.4, the simulation was based solely on process data prior to the retrofit installation, as the aim of this model was to assume the gained recovery improvements in the future. The used maximum flotation rate constants are presented in **Table 37**, and the simulated net recovery gains in **Table 38** below.

Table 37. k_{max} values applied in determination of overall recovery improvement in the Kennecott case study

k_{max} Ccp	k_{max} Mlb	k_{max} Qtz
0.59	0.58	0.01

Table 38. Simulated overall recovery improvements in the Kennecott case study

	Cu	Mo
After	83.98 %	85.50 %
Before	83.13 %	84.55 %
Net recovery gain	0.85 %	0.95 %

Based on the literature, the recovery improvements after the center launder retrofit in Kennecott were presented to be 0.74% for copper and 0.82% for molybdenum (Bermudez et al., 2022), which align with the simulated recovery improvements presented in **Table 38** above.

An additional part of the research was conducted to evaluate the correlation between the selected data points. The maximum flotation rate constants applied in each simulation setup are presented in **Table 39**, and the results from the research work are shown in **Table 40** below. Although there is greater variation between the mass balanced improvements, the calculated

correlations between the simulated and measured recovery values are 0.66 for copper and 0.93 for molybdenum improvements.

Table 39. Applied k_{max} values for each data point in the Kennecott case study

Test	k_{max} Ccp	k_{max} Mlb	k_{max} Qtz
1	1,04	2,09	0.01
2	1,39	1,48	0.01
3	1,67	1,84	0.01
4	1,11	1,00	0.01
5	1,06	0,27	0.01
6	0,84	0,16	0.01
7	1,05	0,29	0.01
8	6,98	1,18	0.01
9	1,89	1,99	0.01
10	1,77	11,29	0.01
11	1,25	2,83	0.01
12	2,04	5,19	0.01
13	3,92	2,70	0.01

Table 40. Simulated and mass balanced recovery improvements in the Kennecott case study

	Simulated improvements (%)		**Mass balanced improvements (%)**	
Test	Cu	Mo	Cu	Mo
1	-0.26	-0.13	1.12	0.71
2	-0.30	-0.32	-0.95	-1.33
3	-0.26	-0.27	-1.47	-1.92
4	-0.47	-0.61	-2.43	-3.55
5	0.30	1.02	-0.36	4.76
6	0.64	2.08	1.95	12.28
7	0.03	0.08	0.56	5.11
8	0.01	-0.04	-0.85	0.84
9	-0.18	-0.19	-2.02	0.65
10	-0.19	-0.01	-0.97	-1.20
11	-0.12	-0.05	1.50	0.66
12	0.38	0.02	1.72	0.82
13	-0.10	-0.25	-1.83	0.09
Average	**-0.04**	**0.10**	**-0.31**	**1.38**

The correlations between the measured recovery improvements and mass balanced improvements from the simulation work are visualized in **Figure 44** and **Figure 45** for copper and molybdenum, respectively. Regardless of the correlation between the curves, the comparison between the simulated and mass balanced results do not align. This misalignment may be due to the

stabilized operational conditions assumed in the simulations, where variation in the results occurs only because of changing feed characteristics.

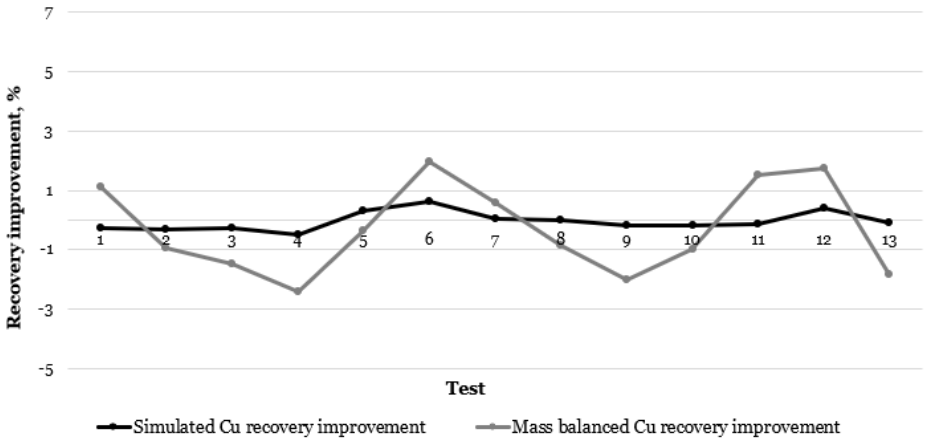

Figure 44. Correlation between the simulated and measured recovery improvements for copper in the Kennecott case study

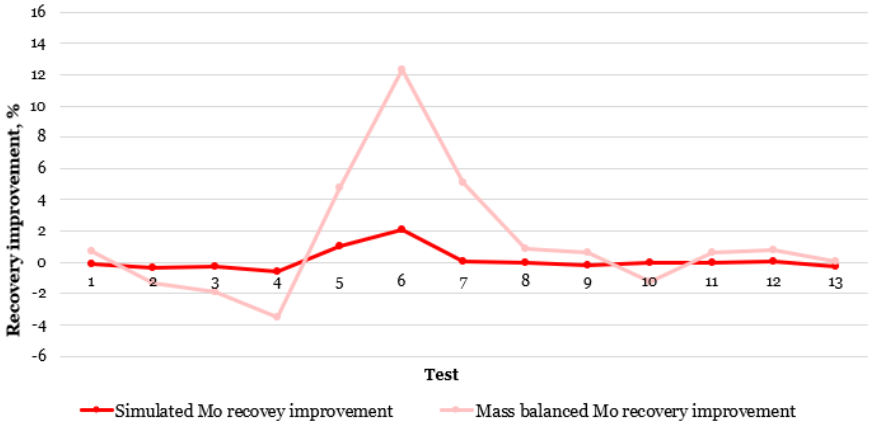

Figure 45. Correlation between the simulated and measured recovery improvements for molybdenum in the Kennecott case study

6.5 Sustainability assessment

This section combines the results of both parts of the study, the Life Cycle Assessment and the CO_2 reduction potential, to assess the sustainability of the operation. Results from the LCA study are presented in section 5.5.1, whereas section 5.5.2 presents the calculated potential for CO_2 emission reduction.

6.5.1 Life Cycle Assessment

This section presents the results obtained from the conducted Life Cycle Assessment. The simulated recovery improvements and concentrate stream

results for different scenarios with either 2, 4, or 6 center launders are shown in **Table 41**. These recovery improvements, and the stream results are not directly comparable with the case study results, as the simulation setup for them was created using hypothetical values. The purpose of these results, however, is to demonstrate the potential savings in electricity, water, and emissions under certain recovery improvements and operational conditions.

Table 41. Results of LCA simulations

	Base Case	**2 CL**	**4 CL**	**6 CL**
Copper recovery improvement (%)	0.00	0.86	1.57	2.18
Molybdenum recovery improvement (%)	0.00	3.21	6.05	8.66
Tailings (t/h)	4896.62	4862.80	4828.94	4794.80
Final concentrate (t/h)	103.37	137.19	171.05	205.20
Cu grade in tails (%)	0.06	0.06	0.06	0.05
Mo grade in tails (%)	0.01	0.01	0.01	0.01
Cu grade in concentrate (%)	8.73	7.41	6.44	5.68
Mo grade in concentrate (%)	0.33	0.29	0.26	0.24
Copper mass flow in concentrate, (t/h)	9.02	10.17	11.02	11.66

Due to the increased recovery of valuable metals, the amount of metals lost to tailings is lower compared to the base scenario without the center launder retrofit. Accordingly, the same amount of metals can be produced in fewer operational hours, saving electricity, water, and ore per processed ton of concentrate. Table 41 above illustrates this trend, showing the increase in copper mass flow in the final concentrate after the center launder retrofit, taking into account the total concentrate produced and its metal grade.

The results have been calculated based on the selected impact assessment method (ReCiPe 2016 v1.03, midpoint (H)) and the defined reference flow, which in this case is the final concentrate. Further calculations were based on the amount of copper in the final concentrate, and the results are therefore presented as equivalents per one ton per hour of produced copper. This relationship between the number of installed center launders per row and the total flow rates of fed ore and water, as well as the required amount of electricity, is illustrated in **Figure 46** below.

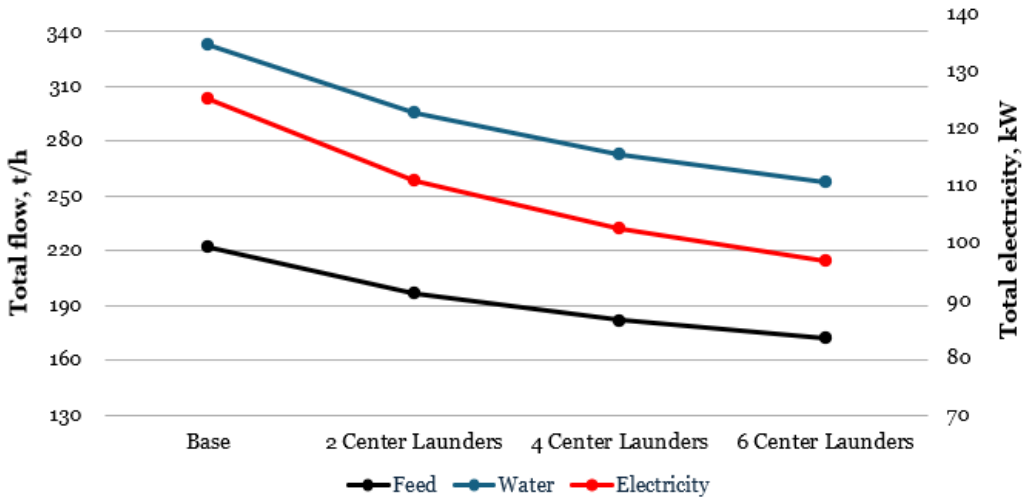

Figure 46. Trends in total electricity, and need of water and feed as a function of center launder arrangements

In all cases presented, the total feed flow rate, including both water and solids, is kept constant. The savings presented in Figure 46 above are relative values that illustrate the trend in process efficiency, showing improvements in concentrate following the increased crowding due to the center launder installation. Therefore, these results do not correspond to an actual reduction in total feed flow.

Based on the combined results, all three variables appear to be affected in a similar manner, depending on the number of center launders installed. The relative decrease between the number of upgraded cells is therefore smaller when upgrading the last two cells compared to the first two cells, depending on the total number of flotation cells in a row. This correlates with the measured recovery improvements shown in Table 41 above, where the simulated increase in copper recovery is higher after upgrading the first two cells (0.86%) compared to the last two cells (0.61%).

Figure 47 below illustrates the reduced CO_2 emission per t/h of copper produced. Based on the LCA study, majority of the produced CO_2 emissions (99.93%) originate from the fed ore, primarily due to earlier processing phases, like grinding, which requires a lot of energy. Based on these results, the center launder upgrade can be considered to have a positive impact in terms of sustainability, even if the results are not directly compared with any of the case studies conducted.

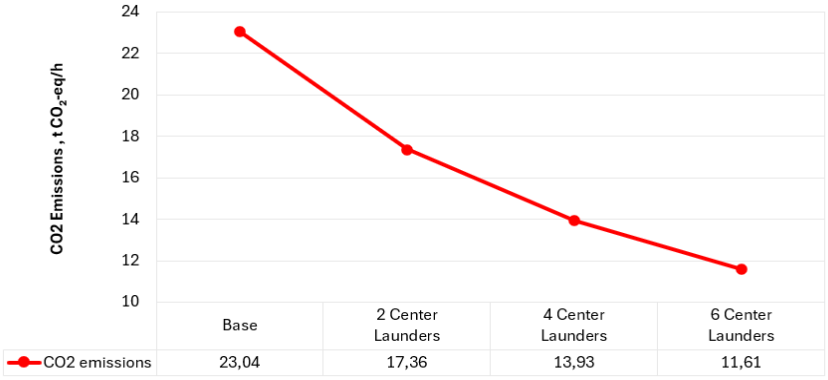

Figure 47. Tons of CO_2 equivalent per tonnage of copper produced after each simulated upgrade setup

6.5.2 CO_2 emission reduction potential

In addition to Life Cycle Assessment, the avoided CO_2 emissions can be estimated based on the achieved recovery improvements of copper. The calculation model and input parameters are presented in **Table 42** below, whereas the gained results for avoided CO_2 emissions as a function of recovery improvement per day are presented in **Table 43**.

Table 42. Input parameters for the CO_2 reduction calculations

$Avoided\ CO2 = T \cdot feed - wt\% \cdot rec\% \cdot EI \cdot U \cdot EF$	
T, tons	2000
feed-wt%, %	0.40
rec%, %	0.86 / 1.57 / 2.18
EI, MWh/ton	6.94
U, h	24.00
EF, t CO_2 eq/MWh	0.65

Table 43. Estimation of avoided CO_2 emissions for each upgrade scenario

Recovery Increase	Estimation of avoided CO_2 emissions
Cu recovery + 0.86%	= 2000 * 0.004 * 0.0086 * 6.94 * 24 * 0.65 **= 7.45 t CO_2 / day**
Cu recovery + 1.57%	= 2000 * 0.004 * 0.0157 * 6.94 * 24 * 0.65 **= 13.60 t CO_2 / day**
Cu recovery + 2.18%	= 2000 * 0.004 * 0.0218 * 6.94 * 24 * 0.65 **= 18.88 t CO_2 / day**

The results presented in Table 43 represent the savings in CO_2 emissions achieved, in contrast to the LCA results, which show the overall CO_2 emissions produced for each simulation setup. Due to the different calculation approaches, these results are not directly comparable. However, the same trend can be observed across both approaches, while the increased copper recovery directly contributes to savings in CO_2 emissions.

7 Discussion

The discussion section has been created to evaluate the gained simulation results in terms of comparability, reliability, and consistency. It will also discuss about the challenges and limitations related to the execution of the simulation work, as well as the implications for future research.

Based on the conducted retrofits, the center launder upgrade has been observed to have a positive impact on both metallurgical and operational parameters on the flotation rougher line. As a result of improved froth crowding over the launder lip, as well as the shorter froth transport distance, the probability of collecting valuable minerals has increased significantly. Additionally, optimized surface parameters have enabled the operations to achieve more stable froth layers on top of the cell, enabling better controllability, and reducing the energy consumption and footprint of the operation by lowering the power consumption of the blowers.

As operational parameters such as froth bed thickness and airflow rate were used as input variables in the conducted simulations, the impact of the center launder retrofit on them could not be directly measured. However, based on the sensitivity analyses, their effect on the simulated results was consistent with expectations from the literature. For example, a higher froth bed thickness improved concentrate grade, while the recovery of the coarser particle size fraction tended to be lower compared to finer particles in the flotation feed. Therefore, proper optimization of these parameters is critical for obtaining reliable results.

Overall, based on the available shift data and applied assumptions, the results from the conducted simulation work correlated with the measured recovery improvements. However, due to the limited availability of data, it was difficult to draw final conclusions on how the results can be reliably simulated using HSC.

7.1 Evaluation of simulation results

This part of the discussion aims to evaluate the selected recovery model based on the conducted simulations with different parameter setups. It includes the evaluation of the simulated recovery improvements from the case studies, examining how the results correlate with the hypothesis of the work, and how well the results support each other. Additionally, it discusses the environmental impact of the launder installation.

7.1.1 Importance of parameter setting

As shown by the conducted simulation work, the selection of different parameters has a significant effect on the results. This study was carried out to

examine the impact of stream setup, flotation cell parameters, and flotation kinetics. The primary objective was to provide an overall understanding of how different parameter configurations influence the outcomes, particularly in terms of metal recovery improvements. Nevertheless, the study scope was limited, and not all parameters or their potential combined effects were included in the analysis.

Throughout all simulations conducted, the operational conditions, including the amount of feed, solids percent of feed, design of operational line, as well as the copper and molybdenum grade in feed, were kept constant so that they would not affect the results. The parameters studied included particle size distribution of the feed ore, froth bed thickness, overflowing bubble size, airflow rate per cell, type of installed launder design, and flotation kinetics in terms of maximum flotation rate constant and infinite recovery for both chalcopyrite and molybdenite. Based on the collected results, the parameters that were seen to increase the gained recovery improvements of metal were:

- smaller particle size distribution (P80),
- higher solids percentage,
- larger bubble size,
- lower froth bed thickness,
- higher operational airflow rate, and
- higher kinetic values in both, R_∞ and k_{max}.

In terms of installed launder design, the highest recovery improvements were observed with center launder, whereas the internal launder design showed the lowest improvements.

Impact of froth surface parameters

Based on the **Table 8** presented in section 5.1.2, the three different launder designs: Internal launder, internal launder and radial launder, and center launder, differ in net volume, FSA, LL, and FTD, with the center launder design having the shortest FTD, smallest FSA, and highest cell volume. The effectiveness of the center launder design is based on its ability to reduce the froth surface parameters, including FSA and FTD, by similarly increasing the lip length. However, the sensitivity analysis indicated that neither the lip length nor the froth transport distance was included in the applied calculation model. Consequently, the calculated increase in metal recovery was primarily gained from the reduction of froth surface area at the top of the cell.

Overall, the findings are consistent with the literature and previous case studies, where reduced froth surface parameters have been shown to improve froth crowding and thereby enhance the recovery of valuable minerals (Brito-Parada et al., 2020). Furthermore, the results demonstrate that a decrease in

froth surface area promotes higher overall solids and water recovery by increasing pulp flow into the concentrate, as evidenced in **Table 22** presented in section 6.1.2.

Impact of feed characteristics

A similar trend was observed in simulations conducted on different particle size distributions in the flotation feed, with the smaller P80 value showing higher recoveries for both metals. This increase in recovery rate can be seen to increase quite linearly, as a function of P80 from 150 to 200. Based on the presented graph in Figure 28, higher solids content in flotation feed can be also seen to clearly increase the recovery of valuable metals. This finding is also supported by the literature, which indicates that a higher solids concentration in flotation feed may increase the collision probability between bubbles and particles, thereby improving their recovery rates (Murhula et al., 2023).

Impact of bubble size

The effect of bubble size in the pulp phase was evaluated through simulations, which showed higher metal recoveries with larger bubble Sauter diameters. According to the Equation 4 presented in section 2.2.1, the bubble surface area flux (S_b) increases as the Sauter diameter (D_{32}) decreases. Although smaller bubbles provide more surface area, several factors influence the effectiveness of bubble-particle collisions in the pulp phase, including bubble size, sliding time, hydrodynamic conditions, particle size, and optimization of flotation chemicals.

Considering these factors, coarse particles may face challenges attaching to smaller bubbles due to the limited carrying capacity, whereas the larger surface area provided by smaller bubbles may increase the collision probability and thus enhance the recovery of fine particles (Anzoom et al., 2024). The simulation results presented in Figure 38 show that larger particle size fractions showed higher copper recovery, while smaller fractions showed minimal recovery improvement. These findings therefore support the literature, indicating higher collection probability of coarser particle size fractions with increasing bubble diameter in the pulp phase.

Impact of froth thickness and air supply

Based on the conducted simulations, higher froth bed thickness was found to correlate with lower recovery but higher concentrate grade. However, in most of the other cases, increased recovery was associated with a lower concentrate grade due to the higher overall solids flow in the concentrate stream, which also led to increased recovery of gangue material.

Similarly, increasing the operational airflow rate per cell, can be seen to impact on the recovery by increasing it, as well as by decreasing the grade of metal up to certain point (Figure 32, Figure 33). The applied measurement range was from 16 m^3/min to 19 m^3/min, where the increased airflow rate per cell was seen to increase the metal recovery and decrease the concentrate grade respectively.

Impact of flotation kinetics

In addition to the conducted simulations to study the impact of operational parameters, the applied flotation kinetics parameters can be seen to have a significant impact on the gained recovery rates. The recovery model applied in this evaluation was rectangular distribution model, whereas the infinite recovery was varied between 80% to 100%, and maximum flotation rate constant between 0.6 to 1.

Based on the graph in Figure 39, the recovery of copper in final concentrate varies between 68.03% to 92.02%. This increase in recovery rates is quite linear under the constant operational conditions. On average, increasing R_∞ improved copper recovery by 4.5%, while increasing k_{max} by 0.1 resulting in a 1.5% recovery increase. These results highlight the strong dependence of recovery on kinetics and the importance of optimizing them correctly.

In conclusion, selected operational parameters, as well as the kinetics of the processed ore type greatly influence the gained results. Therefore, to obtain reliable results, all the parameters need to be considered and measured accurately.

7.1.2 Metallurgical evaluation

This section aims to evaluate how the calculated recovery improvements of both metals, copper and molybdenum, align with the simulated recovery improvements over the evaluation period. Based on the collected shift data from both operations, Bagdad and Constancia, the rougher concentrate after the center launder upgrade showed increase in average metal recoveries, as well as a decrease in average metal grade in final concentrate. In a hypothetical situation, the conducted simulation should provide similar results, to enable reliable comparison of the gained results and measured improvements.

As the research part is not capable of studying the effects of all different variables, for example: kinetic parameters, solids percentages, airflow rates, and froth thicknesses, all three case studies have been conducted in a similar manner, as the feed characteristics and operational conditions are similar between the studies. Therefore, the operational conditions between the lines

have been assumed to stay constant, and therefore the kinetics between the lines have also been kept constant.

The effect of launder type on the gained overall recovery, grade, and total amount of solids in concentrate are presented in **Table 22** presented in section 6.1.2. Based on these results, the grade of the final concentrate can be seen to decrease, while the recovery of valuable metal increase after the center launder retrofit. This decrease in grade can be assumed to be attributed to the increased total solids flow, whereas the increased crowding enhances both, recovery of valuables, as well as the recovery of gangue minerals.

The measured improvements, used as reference values in this evaluation, are based on calculated recovery improvements reported in the study publications (Bermudez et al., 2021, Bermudez et al., 2022, Liu et al., 2022). The simulated improvements are therefore the results of the research work conducted to study the reliability of the simulation in estimating the achieved overall recovery improvements, based solely on the data available from the baseline scenario. These simulated results and the measured improvements have been collected to the **Table 44** and visualised as a bar chart in **Figure 48** to allow for better comparison of them.

Table 44. Simulated and measured overall recovery improvements across all case studies

	Simulated recovery improvement		**Measured recovery improvement**	
	Cu %	**Mo %**	**Cu %**	**Mo %**
Bagdad	0.74	1.36	0.93	3.15
Constancia	0.64	2.10	0.70	1.40
Kennecott	0.85	0.95	0.74	0.82

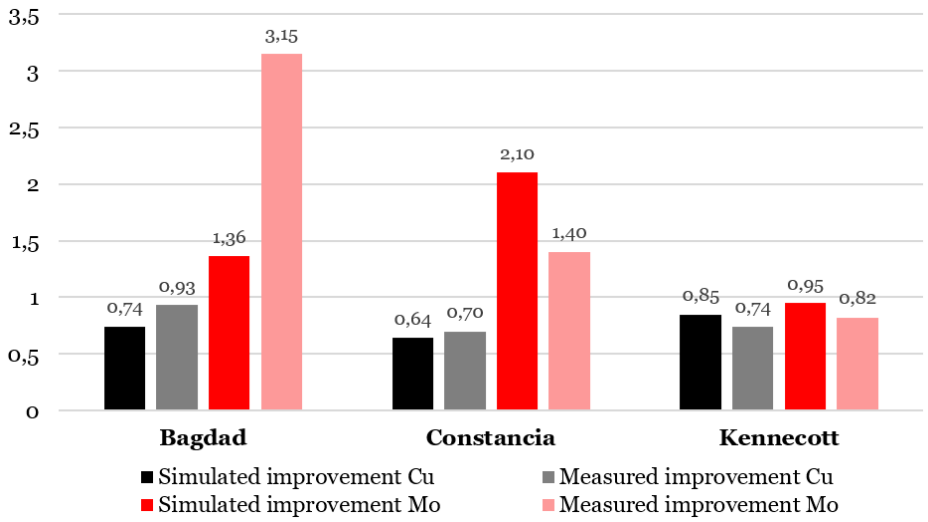

Figure 48. Comparison of simulated and measured overall recovery improvements across all case studies

When comparing the simulated recovery improvements with the measured improvements, the simulations show a similar trend. Molybdenum recovery improvement is calculated to be higher in all retrofit cases, while the simulated improvements also suggest higher recovery improvements of molybdenum compared to the copper recovery improvements. Additionally, the simulated recovery improvements for copper in all cases, and molybdenum in the case of Kennecott align well with the calculated reference values. The best results out of these three research studies conducted were seen from the Kennecott case, where the simulated values were only about 15 percent higher recovery values compared to the measured reference values.

As shown in Table 44 above, the deviation in the measured molybdenum recovery improvements is significantly higher than for copper, particularly in Constancia and Bagdad. There are many reasons for that variance of molybdenum recovery improvements between the simulated and measured values, as the simulation is based on many different assumptions, for example on the operational conditions at the mine. However, one of the potential reasons might be the significantly lower head grade of molybdenum in flotation feed, compared to copper head grades, and molybdenum head grade in Kennecott case. Head grades of both metals in each case study are presented in **Table 45** below.

Table 45. Average head grades of copper and molybdenum across all case studies

	Copper %	**Molybdenum %**
Bagdad	0.360	0.022
Constancia	0.425	0.017
Kennecott	0.338	0.108

Based on the average head grades presented above, it can be seen that the head grade of copper is quite similar between the different cases compared to molybdenum. Head grades of molybdenum in Bagdad and Constancia are on average around five to six times lower compared to Kennecott. The low head grade may cause relative error, which may lead to higher variance in calculated results.

When comparing the range on measured recovery differences between the operational lines after the retrofit, the calculated variance in molybdenum recoveries can be seen to vary a lot more in the cases of Bagdad and Constancia compared to the other measurements. These recovery differences are presented in **Table 46** below, showing both the lowest and highest recovery improvements measured between the upgraded and baseline cases for both metals.

Table 46. Recovery differences between the operational lines after the Center Launder retrofit across all case studies

	Minimum recovery difference		**Maximum recovery difference**	
	Cu	Mo	Cu	Mo
Bagdad	-4.46%	-17.15%	+8.06%	+31.71%
Constancia	-4.34%	-17.67%	+6.22%	+27.45%
Kennecott	-11.15%	-6.31%	+12.14%	+12.28%

Based on the ranges presented in Table 46 above, it is evident that the measured recovery difference for molybdenum between the baseline and the upgraded line is much higher in Bagdad and Constancia. As the measured recovery improvement is calculated as an average over the evaluation period, the calculated recovery improvement is sensitive for the high variation of the taken measurements. This can therefore cause the variation between the simulated and measured recoveries presented in Table 46 above, as the simulation does not fully capture the measurement uncertainty and process variability.

7.1.3 Sustainability evaluation

The conducted sustainability analysis included both Life Cycle Assessment (LCA) and CO_2 reduction potential calculations and aimed to study the impact of the center launder retrofit on environmental aspects. The methodologies applied in these two analyses differ slightly. The LCA study conducted was based on the environmental intensity of the process, quantifying the amounts of energy, water, and CO_2 emissions per ton of copper produced. In addition to flotation circuit, it considers the environmental impact of the entire processing chain prior to conditioning, including ore crushing, grinding, and transportation, as well as electricity production.

The CO_2 reduction calculation model was therefore based on the direct savings achieved after the launder installation due to the increased recovery of copper. Consequently, this calculation model does not consider overall CO_2 emissions but only the amount of saved consumption. The factor used to describe energy intensity was based on the average energy consumption across the entire processing chain, not only flotation. Additionally, the emissions factor was assumed based on the overall energy consumption of the mine, although this factor can vary significantly depending on the country and the energy source used, such as gas or diesel.

The limited database, as well as the assumptions made in both studies, considerably decrease the accuracy of the final results. In the LCA study, the water used was assumed to come from harvested rainwater, so consumption for processing and purification was estimated to be minimal. Examination of the LCA results shows that almost all the produced CO_2 emissions (99.93%)

originate from the fed ore, influenced by estimated emissions from previous processing steps. The high emission rate of feed is also attributed to the assumption that the energy comes solely from fossil fuels. Additionally, due to the lack of available data, no options were available for the copper-molybdenum ore type studied here. Since accurate assumptions about the ore type and energy used in previous processing steps greatly affect the results, the calculated outcomes may differ significantly.

Based on these differences between the applied models, the calculated results are not directly comparable. The assumptions made also significantly limit the reliability of the results, but the overall trend demonstrates the correct correlation. Additionally, since the results only visualize the relationship between feed and concentrate flows, they can describe trends between different upgrade scenarios with similar feed characteristics, but direct comparisons or conclusions about savings are not possible. However, overall, it can be stated that the center launder retrofit is able to reduce overall CO_2 emissions, electricity usage, and water consumption due to the achieved recovery improvements.

7.2 Reliability and consistency of the results

The research work conducted on the reliability of simulated recovery improvements was studied through two different setups to evaluate both, consistency and correlation between the simulated and measured improvements over the evaluation period, as well as the ability to estimate the improvements gained based on the baseline conditions.

This part of the discussion will evaluate the reliability and consistency of the gained results based on the statistical evaluation of them, and by analysing the method of conducting the simulation work. To ensure consistency between the conducted simulations, all of them were simulated by applying the similar methodology and by using 50 iteration rounds. Additionally, the sensitivity analysis of the parameters was conducted in stable operational conditions, while all parameters excluded from the scope of the test were stabilized, which enabled better understanding of every single parameter on gained recovery rates.

7.2.1 Correlation between simulated and measured recoveries

The consistency between the simulated and measured recovery improvements for the selected data points was examined to assess how well the simulation results correlate with real operational performance. The results from the research conducted for Bagdad, Constancia, and Kennecott are presented in **Table 30**, **Table 34**, and Table 40, respectively, and their averaged values are summarized in **Table 47** below.

Table 47. Simulated and mass balanced recovery improvements between the operational lines across all case studies

	Simulated improvements %		Mass balanced improvements %	
	Cu	**Mo**	**Cu**	**Mo**
Bagdad	0.60	1.21	0.67	1.52
Constancia	0.65	2.01	-0.25	-1.02
Kennecott	-0.04	0.10	-0.31	1.38

These results show that the average recovery improvements follow a similar overall trend for Bagdad and Kennecott, whereas the Constancia case deviates more clearly. To further evaluate the statistical similarity, t-tests were conducted for each site to determine whether there were statistical differences between the simulated and mass balanced recoveries of copper and molybdenum. Results from the conducted t-tests are presented for Bagdad, Constancia, and Kennecott, in **Table 48**, **Table 49**, and **Table 50** respectively. The data used for these tests are shown in the results section (Table 30, Table 34, and Table 40), where all the tests were conducted by assuming equal variances between the datapoints.

Table 48. Results of the t-test for the Bagdad case study

	Simulated Cu improvement	**Mass balanced**	**Simulated Mo improvement**	**Mass balanced**
Mean	0.597	0.674	1.213	1.523
Variance	0.035	1.148	0.402	5.568
Observations	14	14	14	14
Pooled Variance	0.592		2.985	
Hypothesized Mean Difference	0.000		0.000	
df	26.000		26.000	
t Stat	-0.264		-0.474	
P(T<=t) one-tail	0.397		0.320	
t Critical one-tail	1.706		1.706	
P(T<=t) two-tail	0.794		0.639	
t Critical two-tail	2.056		2.056	

Table 49. Results of the t-test for the Constancia case study

	Simulated Cu improvement	Mass balanced	Simulated Mo improvement	Mass balanced
Mean	0.649	-0.251	2.014	-1.021
Variance	0.100	3.082	1.086	29.468
Observations	14	14	14	14
Pooled Variance	1.591		15.277	
Hypothesized Mean Difference	0.000		0.000	
df	26.000		26.000	
t Stat	1.889		2.054	
P(T<=t) one-tail	0.035		0.025	
t Critical one-tail	1.706		1.706	
P(T<=t) two-tail	0.070		0.050	
t Critical two-tail	2.056		2.056	

Table 50. Results of the t-test for the Kennecott case study

	Simulated Cu improvement	Mass balanced	Simulated Mo improvement	Mass balanced
Mean	-0.040	-0.311	0.102	1.379
Variance	0.097	2.2941	0.492	16.435
Observations	13	13	13	13
Pooled Variance	1.196		8.463	
Hypothesized Mean Difference	0.000		0.000	
df	24.000		24.000	
t Stat	0.631		-1.119	
P(T<=t) one-tail	0.267		0.137	
t Critical one-tail	1.711		1.711	
P(T<=t) two-tail	0.534		0.274	
t Critical two-tail	2.064		2.064	

The t-test results confirm the visual trends observed in Table 47. For Bagdad and Kennecott, no statistically significant differences were found between simulated and mass balanced recoveries ($p > 0.05$), whereas for Constancia, the differences were statistically significant for both copper and molybdenum ($p < 0.05$). This is an important factor in future work as the validity of results favours the parallel line comparison.

The simulated datasets also represent consistently lower variance compared to the mass balanced results. This is expected, as the simulations were conducted under stabilized operational conditions, where only the ore feed rate and head grades were varied. In contrast to the conducted simulations, in real conditions the operational parameters such as airflow rate, froth

thickness, and particle size fluctuate continuously, contributing to greater variability in metal recoveries.

The calculated correlation coefficients further support these conclusions. The highest correlations were obtained for the Kennecott retrofit case, with correlation values of 0.66 for copper and 0.93 for molybdenum. The corresponding results for all sites are summarized in **Table 51**.

Table 51. Correlations between measured and simulated copper and molybdenum recoveries across all case studies

	Copper	**Molybdenum**
Bagdad	0.40	0.72
Constancia	0.38	0.38
Kennecott	0.66	0.93

These values highlight that the correlation between simulated and measured recoveries is stronger in Bagdad and Kennecott with parallel line configurations, in contrast to Constancia, where the operational lines are not directly comparable in real life, as the lines are not parallel. However, as the simulation software is not able to estimate the operational changes, either the outperformance of another line compared to another, the simulations have been assessed only based on the gained improvements after the center launder retrofit. Therefore, the simulation does not directly account for differences between the lines, which may distort the results. Additionally, the combined sampling approach hides the individual line responses and limits comparability between the lines in Constancia, which could also be one potential reason for the reduced correlation between the obtained results.

Because the simulations were performed under certain operational conditions, they do not account for the full operational variability present in industrial practice. Even when the flotation kinetics of chalcopyrite and molybdenite are controlled at each data point, variations in, operational parameters like airflow rate, froth depth, particle size distribution, and reagent dosage strongly influence cell performance and recovery, thus distorting the correlation between simulated and measured results.

Furthermore, the degree of mineral liberation plays a significant role. Free particles are more easily recovered than those coated with gangue minerals (Bahrami et al., 2019), which may contribute to the broader variance observed in mass-balanced recoveries. Since the simulations assume a constant liberation degree, deviations between simulated and measured recoveries are expected. To obtain stronger correlations, a larger dataset encompassing a wider range of operational variability would be required.

7.2.2 The importance of operational stability

Operational stability in flotation refers to the ability of the process to maintain consistent metallurgical performance despite short-term fluctuations in operating parameters such as airflow rate, froth thickness, or feed characteristics. In this study, the stability of the flotation circuits was evaluated based on the measured recoveries of copper and molybdenum before and after the center launder installation.

To assess operational stability, the collected shift data were analysed by calculating the sample standard deviation of the measured recovery differences, expressed in percentage points, between the compared lines. For Constancia and Kennecott, the deviations were calculated both before and after the retrofit, whereas for Bagdad, only post-retrofit data were available due to the lack of baseline measurements. These calculated results are summarized in **Table 52** below.

Table 52. Standard deviations of the measured copper and molybdenum recovery improvements based on collected shift data across all case studies

Case	Standard deviation for copper	Standard deviation for molybdenum
Bagdad After	1.87%	7.15%
Constancia Before	1.45%	8.41%
Constancia After	1.48%	5.39%
Kennecott Before	9.65%	10.01%
Kennecott After	2.78%	3.26%

Based on the calculated standard deviations presented in **Table 52** above, it can be observed that in the case of Kennecott, the deviations after the retrofit are much lower for both metals compared to the baseline scenario. Also, in the case of Constancia, the high standard deviation for molybdenum recovery differences were able to decrease after the retrofit installation.

When comparing the calculated standard deviations for copper and molybdenum, especially in the cases of Constancia and Bagdad, the measured deviations for molybdenum are significantly higher. This might be attributed to the lower head grade of molybdenum, as presented in Table 45. At lower feed grades, even small absolute changes in recovered mass translate into larger proportional changes in calculated recovery, leading to higher apparent variability.

Overall, the observed reduction in deviation suggests that the center launder retrofit improved the overall froth management within the flotation cells. Since the upgrade reduces the froth surface area, the retrofit enhanced froth crowding, making the process less sensitive to feed or airflow disturbances, resulting in more consistent metallurgical outcomes

7.3 Challenges and limitations

Achieving reliable simulation results involves several challenges and limitations that affect the accuracy of them. Firstly, the available shift data from the studied cases are limited, lacking detailed information on feed mineralogy, solids content, comprehensive elemental analyses, and operational conditions. Consequently, the limited data from the measurements taken at Kennecott restricted the use of the recovery model, while the absence of detailed mass flow and concentrate information reduced the reliability of the calculated recovery values.

Furthermore, the measurements taken are based on composite samples collected from multiple process streams, and complete analyses are not available for all of them. As a result, cumulative recovery across the line cannot be calculated, which makes comparing the performance between the cells difficult. In addition, the concentrate samples from the Constancia mine are composites not only from a single line but from both operational lines combined, which introduces even greater uncertainty into the assumptions.

Based on the conducted sensitivity analysis, there are several critical parameters that significantly influence the metallurgical performance, including for example froth thickness, applied airflow rate, and flotation kinetics. Therefore, when these parameters are accurately estimated, the simulation results become notably more precise. In this research work, flotation kinetics parameters were determined iteratively by adjusting them to ensure that the simulated baseline scenario aligns with actual process data. However, due to the assumptions made in defining these kinetics, some degree of variation in the results is expected.

In terms of conducted simulation work for presented case studies, the operational airflow rate has estimated to stay constant in each cell, both before and after the launder upgrade, even if the reference cases show to decrease the airflow rate after the upgrade. Air reduction is often needed in practice to control froth surface area and prevent overcrowding, but this effect is not captured by the HSC model. According to the applied recovery model, lower gas flux directly reduces bubble particle collection R_f (Equations 21-22) via decreased air recovery α (Equation 19) and superficial gas velocity J_g, while higher airflow increases recovery until a plateau. Entrainment (Equations 25–26) also depends on J_g and α, but its effect is smaller than the reduction in froth recovery. Therefore, the simulation favours maintaining or increasing air supply, even though froth stability considerations may dictate the opposite in real operation.

In addition to the constant airflow rate, the overflowing bubble Sauter diameter (d32) was also assumed to remain constant, as there was no available information on the impact of the center launder upgrade on bubble size. In contrast, the froth thickness was estimated to be higher in the cells where the

center launder was installed. Froth thickness (h_f) was taken into account, as it directly affects entrainment according to Equations 25 and 26.

When comparing the results obtained from the measured improvements based on the conducted mass balances with the simulated improvements, noticeable differences can be observed at certain data points (**Table 30**, **Table 34**, Table 40). This variation can be caused for example by the changed operational parameters like airflow rate, problems in process control, or due to changes in feed characteristics. As presented in section 6.1.1 above, the impact of both, particle size distribution and solids percentage distribution is evident in terms of gained recoveries (Figure 27, Figure 28). Since the detailed information on these operational parameters was not available, they could not be considered in the research work conducted. For this reason, direct comparison between the two operational lines shows a more consistent trend, as variability between the lines is not considered.

Furthermore, the validation of the developed simulation approach was restricted to a limited number of case studies, lacking variability in ore types and process conditions. The applied recovery model also represents a simplified approach that does not fully capture the hydrodynamic effects of process dynamics, as HSC Sim assumes steady-state operation and does not account for variations in froth stability. Therefore, while the model provides a framework for assessing metallurgical improvements, further validation will be required under broader operational conditions.

There are also several challenges and limitations regarding the conducted Life Cycle Assessment. Firstly, as described in the methodology section, a reliable LCA would require detailed information on electricity supply, type of water used, the proportion of recirculated water, and the characteristics of the fed ore. Due to the limitations of the database used, no option was available for copper–molybdenum ore feed for flotation that was already ground and ready for separation. Therefore, the feed material was chosen to be as close as possible to the actual case. As most of the calculated energy consumption and emissions are caused by blasting, grinding, and transporting the ore, while the energy source is assumed to be fossil fuels, some deviations between the results and actual values are expected. Therefore, while the obtained results provide valuable insights, they should be considered indicative rather than absolute.

7.4 Contributions and future research

The outcomes of this work are highly valuable for applying HSC simulation as part of the performance improvement estimation process. The research part of this thesis clearly defines the impact of different parameters on flotation line recoveries by analysing their sensitivities. This information is particularly useful for planning future site assessments, as it helps to identify

which parameters should be considered and how the measurements should be conducted.

This thesis focuses specifically on optimizing rougher flotation circuits after the center launder retrofit. While it provides a solid foundation for applying simulation in performance evaluation, further research is required for broader implementation, including extending model calibration to other technologies and operational conditions. Additionally, the operational design and case study conditions were limited, as only copper–molybdenum concentrators with five to seven flotation cells per rougher circuit were examined, with upgrades applied only to the last three cells in one line.

Although the similarity of the studied cases provided a good starting point for comparability, improving the reliability of the simulation methodology will require additional testing under a wider range of operational conditions, and therefore applying the model to different scales of operation, ores with varying mineralogy and particle size distributions, or retrofits with different numbers of upgraded cells would be highly beneficial.

Therefore, even if this study alone does not provide sufficient information to fully rely on the simulated results, it demonstrates the applicability of HSC simulation for recovery estimation, highlights critical process parameters, and provides a valuable framework for future research.

8 Conclusions

The primary objective of this thesis was to evaluate the consistency between simulated and measured recovery improvements after the center launder retrofit and to examine the possibility of a uniform approach for quantifying these improvements. Several previously studied retrofits were used as a basis to define assumptions on expected improvements and changes in process conditions. The main cases were Bagdad and Constancia, while the Kennecott case was used to validate the methodology under the same assumptions and approach. The analysis was further supported by a comprehensive sensitivity study to understand how the applied parameters influence the results.

In terms of reliability, both methods show challenges and limitations due to averaging and estimations based on assumed process conditions. In the research setup comparing performance differences between the two operational lines after the launder installation, the simulated differences generally correlate with the mass balanced differences. However, the simulated results are overall smoother and more averaged than the measured values, mainly because the simulations assume constant operational conditions, whereas in reality these conditions vary continuously, increasing variation in the data. Therefore, the simulation does not account for underperformance of cells or operational differences between the lines, and the difference is calculated solely based on the changed froth surface parameters, feed flow, and the head grade.

The comparison of metallurgical performance between the two operational lines indicated a clear correlation, and the estimated recovery improvements based on the baseline scenario can also appear to correlate with the published improvements, although with some limitations. The accuracy of the results may be affected by factors such as a low metal head grade, which can increase the relative error in measurements and cause greater variance in calculated metal recoveries. This may also partly explain why the accuracy of the simulation results is lower.

Based on the insights gained, it is evident that the simulation produces more averaged data and does not capture the large variations observed in the collected shift data. While a correlation between simulated and measured improvements can be seen, drawing final conclusions would require additional data and the ability to apply the methodology to further case studies. Therefore, while the developed methodology provides indicative results for launder retrofit evaluations, it should not yet be used as a standalone predictive tool until further validation has been conducted.

Future research should therefore evaluate the applied simulation methodology under broader operational ranges, including variations in particle size distribution and ore type of the flotation feed. It would also be beneficial to apply the methodology to different upgrade scenarios with varying numbers of retrofit installations, as well as to extend it to other upgrade solutions.

References

Allen, M. (2021). Mining energy consumption 2021: A high-level study into mining energy use for the key mineral commodities of the future. Engeco, for The Weir Group PLC. https://www.ceecthefuture.org/resources/mining-energy-consumption-2021

Anzoom, S. J., Bournival, G., & Ata, S. (2024). Coarse particle flotation: A review. Minerals Engineering, 206, 108499.

Aramendia, E., Brockway, P. E., Taylor, P. G., & Norman, J. (2023). Global energy consumption of the mineral mining industry: Exploring the historical perspective and future pathways to 2060. Global Environmental Change, 83, 102745.

Bahrami, A., Mirmohammadi, M., Ghorbani, Y., Kazemi, F., Abdollahi, M., & Danesh, A. (2019). Process mineralogy as a key factor affecting the flotation kinetics of copper sulfide minerals. International Journal of Minerals, Metallurgy and Materials, 26(4), 430–439.

Bergh, L., & Yianatos, J. (2011). The long way toward multivariate predictive control of flotation processes. Journal of Process Control, 21(2), 226–234.

Bermudez, G., Amelunxen, P., Medina, M., Taylor, M., & Dube, R. (2021). Copper and molybdenum recovery increased by upgrading flotation cells with center launders at Hudbay Constancia. SME Annual Meeting (pp. 1-5). Denver: SME.

Bermudez, G., Perkins, T., Sorensen, R., Smith, C., Bartsch, J., Moyo, J., Dobe, R., & Brändström, M. (2022). Froth launder modification in 300-m² flotation cells at Kennecott Copperton concentrator. SME Annual Meeting (pp. 14-24). Salt Lake City: SME.

Bermudez, G., Gallimore, M., Jalili, A., Frausto, J.J. (2023a). Decarbonizing existing flotation circuits. In Proceedings of the Past Convention 2023. Metso Outotec

Bermudez, G., Jalili, A., Cardoso, C., Gallimore, M. (2023b). Decarbonization of operative flotation cells. In Proceedings of Flotation '23. November 6–9, 2023. Cape Town, South Africa, Metso Outotec.

Bilal, M., Park, I., Hornn, V., Ito, M., Hassan, F., Jeon, S., & Hiroyoshi, N. (2022). The Challenges and Prospects of Recovering Fine Copper Sulfides from Tailings Using Different Flotation Techniques: A Review. Minerals, 12(5), 586.

Bu, X., Xie, G., Peng, Y., Ge, L., & Ni, C. (2016). Kinetics of flotation. Order of process, rate constant distribution and ultimate recovery. Physicochemical Problems of Mineral Processing, 53(1), 342–365.

Brito-Parada, P. R., Mesa, D., Karvonen, J., Grau, R., Davoise, D., & López, A. (2020). Froth zone design optimisation – the key to enhancing recovery in large flotation cells. The Southern African Institute of Mining and Metallurgy.

Çilek, E. (2004). Estimation of flotation kinetic parameters by considering interactions of the operating variables. Minerals Engineering, 17(1), 81–85.

Coleman, R. (2009). Flotation cells: selecting the correct concentrate launder design. Filtration and Separation, 46(6), 36–37.

Corona-Arroyo, M., Bermudez, G., Dube, R., & Jalili, A. (2021). Recent advances in flotation cell froth management. In Proceedings of the Canadian Institute of Mining Virtual Convention and Expo (pp. 3–6).

Dahlström, D.A. (2003). Liquid-Solid Separation. In M. C. Fuerstenau & K. N. Han (Eds.), Principles of mineral processing (pp. 307–362). SME.

Dreyer, J.P. (1976). Development of agitair flotation machines. Journal of the Southern African Institute of Mining and Metallurgy 76(11), 1–7.

Elshkaki, A., Graedel, T. E., Ciacci, L., & Reck, B. K. (2018). Resource demand scenarios for the major metals. Environmental Science & Technology, 52(5), 2491–2497.

Farrokhpay, S. (2011). The significance of froth stability in mineral flotation—A review. Advances in Colloid and Interface Science, 166(1–2), 1–7.

Fuerstenau, M.C. & Somasundaran, P. (2003). Flotation. In M. C. Fuerstenau & K. N. Han (Eds.), Principles of mineral processing (pp. 245–306). SME

Gorain, B. K., Franzidis, J. P., & Manlapig, E. V. (2000). Flotation cell design: Application of fundamental principles. Julius Kruttschnitt Mineral Research Centre. Indooroopilly. Queensland. Australia, 1502-1512.

Gorain, B. K. (2007). Design, operating principles, and optimization of mechanical flotation cells. In M. C. Fuerstenau, G. J. Jameson, & R.-H. Yoon (Eds.), Froth Flotation: A Century of Innovation (Illustrated ed., pp. 637-641). SME. ISBN: 0873352521, 9780873352529.

Gorain, B. K. (2013). Developing solutions to complex flotation problems. In Proceedings of the 45th Annual Canadian Mineral Processors Operators Conference (pp. 293-312). Canadian Minerals Prosessors.

Grau, R., Davoise, D., Yáñez, A., & López, Á. (2019). Optimizing the froth area of large mechanical flotation cell. Procemin Geomet. Santiago: Geacemin.

Harmsen, J., Roes, A., & Patel, M. (2013). The impact of copper scarcity on the efficiency of 2050 global renewable energy scenarios. Energy, 50, 62–73.

Hassanzadeh, A., Safari, M., Hoang, D. H., Khoshdast, H., Albijanic, B., & Kowalczuk, P. B. (2022). Technological assessments on recent developments in fine and coarse particle flotation systems. Minerals Engineering, 180, 104892.

Heath, J., & Runge, K. (2019). Froth Management. SME Mineral Processing and Extractive Metallurgy, Handbook; Dunne, RC, Kawatra, SK, Young, CA, Eds, 959-966.

Herbst, J. A., Lo, Y., & Flintoff, B. (2003). Size reduction and liberation. Principles of Mineral Processing, 3, 61-118.

Jera, TM., Bhondayi, C. (2021). A review of Flotation Physical Froth Flow Modifiers. Minerals 11:864.

Kortelainen, J. (2019). Utilization of digital twin in model-based control of flotation cells. Master's thesis, LUT University, Finland.

Lopez-Pacheco, A. (2021). Centering in on froth-flotation optimization. CIM Magazine, 32-33.

Loveday, B., & Brouckaert, C. (1995). An analysis of flotation circuit design principles. The Chemical Engineering Journal and the Biochemical Engineering Journal, 59(1), 15–21.

Li, C., Runge, K., Shi, F., & Farrokhpay, S. (2018). Effect of flotation conditions on froth rheology. Powder Technology, 340, 537–542.

Liu, W., Bolookhuu, O., Bermudez, G., Dube, R., Cooper, G., Hill, L., & Kashuba, D. (2022) Flotation launder upgrade effect on coarse particle recovery at Bagdad Copper and Molybdenum Concentrator. In Proceedings of the Canadian Institute of Mining, Metallurgy and Petroleum Convention 2022, Vancouver, BC. SME.

Lynch, A. J., Johnson, N. W., Manlapig, E. V., & Thorne, C. G. (1981). Mineral and coal flotation circuits: Their simulation and control. Elseiver.

Lynch, A.J., Watt, J.S., Finch, J.A., Harbort, G.J. (2007). History of flotation. Australasian Institute of Mining and Metallurgy, Carlton, Melbourne, Australia.

Magdalena, R., Valero, A., & Calvo, G. (2023). Limit of recovery: How future evolution of ore grades could influence energy consumption and prices for Nickel, Cobalt, and PGMs. Minerals Engineering, 200, 108150.

Markovic, Z. S., Jankovic, A., & Tomanec, R. (2008). Effect of particle size and liberation on flotation of a low grade porphyry copper ore. Journal of Mining and Metallurgy, Section A: Mining, 44(1), 24-30.

Marmiroli, B., Rigamonti, L., & Brito-Parada, P. R. (2022). Life Cycle Assessment in mineral processing: A review of the role of flotation. The International Journal of Life Cycle Assessment, 27(1), 62-81.

Mathe, Z., Harris, M., O'Connor, C., & Franzidis, J. (1998). Review of froth modelling in steady state flotation systems. Minerals Engineering, 11(5), 397–421.

Memary, R., Giurco, D., Mudd, G., & Mason, L. (2012). Life cycle assessment: a time-series analysis of copper. Journal of Cleaner Production, 33, 97–108.

Mesa, D., & Brito-Parada, P. R. (2019). Scale-up in froth flotation: A state-of-the-art review. Separation and Purification Technology, 210, 950–962.

Morita, K., Pal, U., Rhamdhani, M. A., & Pontikes, Y. (2025). Preface to the Journal of Sustainable Metallurgy 10th Anniversary Topical Collection. Journal of Sustainable Metallurgy.

Mudd, G. M., & Weng, Z. (2012). Base metals. In T. M. Letcher, & J. L. Scott (Eds.), Materials for a Sustainable Future (pp. 11 - 59). RSC Publishing.

Mudd, G., Weng, Z., & Jowitt, S. (2013). A detailed assessment of global Cu resource trends and endowments. Economic Geology, 108(5), 1163–1183.

Mular, A.L. (2003). Size separation. Principles of Mineral Processing, 4, 119-172.

Murhula, E., Hashan, M., & Otsuki, A. (2023). Effect of Solid Concentration and Particle Size on the Flotation Kinetics and Entrainment of Quartz and Hematite. *Metals*, *13*(1), 53.

Nagaraj, D.R., & Farinato, R.S. (2016). Evolution of flotation chemistry and chemicals: A century of innovations and the lingering challenges. Minerals Engineering, 96–97, 2–14.

Northey, S., Mohr, S., Mudd, G., Weng, Z., & Giurco, D. (2014). Modelling future copper ore grade decline based on a detailed assessment of copper resources and mining. Resources Conservation and Recycling, 83, 190–201.

Pavloudakis, F., Roumpos, C., & Spanidis, P. (2024). Sustainable mining and processing of mineral resources. Sustainability, 16(19), 8393.

Pease, J., Curry, D., & Young, M. (2006). Designing flotation circuits for high fines recovery. Minerals Engineering, 19(6–8), 831–840.

Prakash, R., Majumder, S. K., & Singh, A. (2018). Flotation technique: Its mechanisms and design parameters. Chemical Engineering and Processing - Process Intensification, 127, 249–270.

Quintanilla, P., Neethling, S. J., & Brito-Parada, P. R. (2020). Modelling for froth flotation control: A review. Minerals Engineering, 162, 106718.

Radmehr, V., Shafaei, S. Z., Noaparast, M., & Abdollahi, H. (2018). Optimizing flotation circuit recovery by effective stage arrangements: a case study. Minerals, 8(10), 417.

Richardson, J.M & Morrison, R.D. (2003). Metallurgical balances and efficiency. Principles of Mineral Processing, 10, 363-389.

Seaman, D. R., Li, K., Lamson, G., Seaman, B. A., & Adams, M. H. (2021). Overcoming rougher residence time limitations in the rougher flotation bank at Red Chris Mine. In Proceedings of the Mill Operators Conference (pp. 193–207). Brisbane, Australian Institute of Mining and Metallurgy.

Segura-Salazar, J., Lima, F. M., & Tavares, L. M. (2019). Life Cycle Assessment in the minerals industry: Current practice, harmonization efforts, and potential improvement through the integration with process simulation. Journal of Cleaner Production, 232, 174–192.

Soto-Vázquez, R. (2025). Life-cycle assessment in mining and mineral processing: A bibliometric overview. Green and Smart Mining Engineering, 2, pp. 73-83.

Tanaka, Y., Miki, H., Suyantara, G. P. W., Aoki, Y., & Hirajima, T. (2021). Mineralogical prediction on the flotation behavior of copper and molybdenum minerals from blended Cu–Mo ores in seawater. Minerals, 11(8), 869.

Tsatouhas, G., Grano, S., & Vera, M. (2005). Case studies on the performance and characterisation of the froth phase in industrial flotation circuits. Minerals Engineering, 19(6–8), 774–783.

Vallejos, P., Yianatos, J., Grau, R., & Yañez, A. (2020). Evaluation of flotation circuits design using a novel approach. Minerals Engineering, 158, 106591.

Vallejos, P., Yianatos, J., Grau, R., & Yáñez, A. (2023). The impact of froth launders design in an industrial flotation bank using novel metallurgical and hydrodynamic models. Minerals, 13(2), 169.

Wang, L., Peng, Y., Runge, K., & Bradshaw, D. (2014). A review of entrainment: Mechanisms, contributing factors and modelling in flotation. Minerals Engineering, 70, 77–91.

Watari, T., Nansai, K., & Nakajima, K. (2021). Major metals demand, supply, and environmental impacts to 2100: A critical review. Resources Conservation and Recycling, 164, 105107.

Wills, B. A., & Finch, J. A. (2016). Froth flotation. In B. A. Wills & J. A. Finch (Eds.), Wills' mineral processing technology (8th ed., pp. 265-380). Butterworth-Heinemann. https://doi.org/10.1016/B978-0-08-097053-0.00012-1

Yianatos, J., Henríquez, F., & Oroz, A. (2005). Characterization of large size flotation cells. Minerals Engineering, 19(6–8), 531–538.

Yianatos, J., Contreras, F., Díaz, F., & Villanueva, A. (2008). Direct measurement of entrainment in large flotation cells. Powder Technology, 189(1), 42–47.

Yianatos, J., Bergh, L., Pino, C., Vinnet, L., Muñoz, C., & Yañez, A. (2012). Industrial evaluation of a new flotation mechanism for large flotation cells. Minerals Engineering, 36–38, 262–271.

Yianatos, J., & Vallejos, P. (2024). Challenges in flotation scale-up: The impact of flotation kinetics and froth transport. Minerals Engineering, 207, 108541.

Zhu, H., Li, Y., Lartey, C., Li, W., & Qian, G. (2020). Flotation kinetics of molybdenite in common sulfate salt solutions. Minerals Engineering, 148, 106182.

A. Neethling parameter setting

Parameter	Value	Description
Flotation Bank		
No. Cells in Row	1	Number of cells in the bank row
No. Parallel Rows	1	Number of parallel rows
Selected Configuration	-	
Parameters Quick Set	Neethling	Custom / Neethling preset / Yianatos preset
Residence Time		
Operation Mode	Continuous	Continuous or batch flotation
Residence Time Calculation	Feed Volumetric	Method to calculate cell residence time
Lab. Residence Time (min)	-	Residence time in laboratory test (for design reference)
Scale-up Factor	1	Cell residence time is divided by scale-up factor
Cell Dimensions		
Flotation Technology	TankCell®	
Cell Model	e300	
Launder Type	CL	
Net Volume (m^3)	306,61	
Pulp Area (m^2)	50,27	
Froth Surface Area (m^2)	23,5	
Lip Height (m)	6,6	
Lip Length (m)	28,3	
Froth Transport Distance (m)	1,05	
No. Radial Launders	0	
Rotor Diameter (mm)	1 750	
Rotor Speed (rpm)	70	
Power Number	5,9	
Step to Next Cell (m)	0,8	Vertical step-down to the next cell in the bank
Selected Motor (kW)	250	Installed power of mixing mechanism
Kinetic Adjustment		
Use kinetic adjustment	-	No activation
Gas Hold-Up		
Gas Hold-up in the pulp calculation method	Simulated	Options to select with: Simulated or Fixed
d32 calculation method	Simulated	Options to select with: Simulated or Fixed
Froth Volume		

Froth Volume Calculation	Based on Froth Thickness	Options to select with: Based on Froth Thickness or Fixed Vol. %
Froth Thickness (mm)	350	
Froth Recovery		
Froth Recovery	Neethling	Options to select with: Not in Use, Fixed Value, Function of Froth Depth, Function of Froth Retention, Yianatos, or Neethling
Max Froth Thickness (mm)	400	
Entrainment		
Entrainment	Neethling	Options to select with: Neethling, Not in Use, Fixed Value, Savassi Equation, or Yianatos
Neethling parameters		
d32 (mm)	1	Bubble Sauter diameter in the pulp phase (Imperial College Model)
Bubble Size Calculation	Linear to Max	
Overflowing Froth Bubble max Diameter (mm)	10	Linear function of froth depth
Pulp-Froth Interface Area (%)	100	Percentage of Pulp Area
Surface Voidage at Maximum Loading	0.25	Bubble surface voidage
Air Recovery Calculation	Bursting rate based	Method for air recovery
Bursting Flux - Constant Term (m/s)	0.0075	Empirical correlation term
Bursting Flux - Linear Term	0.0012	Empirical correlation term
Bursting Flux - 2nd order Term (s/m)	24.5	Empirical correlation term
Representative Solids Fraction	0.2	Used in particle settling velocity calculation
fo Factor	0.5	Fraction of material detaching after coalescence at minimum bubble loading (Typical: 0.2 to 0.5)
Peclet Number	0.15	Used in axial dispersion coefficient calculation
Plateau Border Drag Coefficient	50	Used in axial dispersion coefficient calculation
Lambda Prefactor	8	Used in liquid flow rate calculation (Typical: 6 to 8)

Airflow		
Air Calculation	Calculates Jg	Calculates Jg (pulp & froth) or air consumption (based on Jg in pulp or froth)
Define airflow rate per cell	False	Jg / Airflow is common for all cells in the row
Airflow Rate (m^3/min)	25	Flotation air per cell
Dynamic Air Calculation	Airflow rate is controlled	Uses PID control or direct control on the airflow in Simulation Data I/O
Water Recovery		
Water Recovery	Neethling	
Sb Scaling		
Sb in use	False	
Dynamic Parameters		
Max Airflow Rate	25	
Level Sensor		
Measurement Method (mm)	positive	Method how the level is measured in mm or % (in dynamic calculation)
Measurement Range (mm)	500	Maximum measurement range of the froth depth